UNIVERSIDADE DE BRASÍLIA -UNB
INSTITUTO DE GEOCIÊNCIAS - IG

GEOLOGIA, PETROLOGIA E ESTUDOS ISOTÓPICOS DOS DEPÓSITOS DE NÍQUEL-COBRE SULFETADOS SANTA RITA E PERI-PERI, NORDESTE DO BRASIL

FAUSTO DE ALMEIDA LAZARIN

DISSERTAÇÃO DE MESTRADO Nº 285

Brasília
2011

UNIVERSIDADE DE BRASÍLIA -UNB
INSTITUTO DE GEOCIÊNCIAS - IG

GEOLOGIA, PETROLOGIA E ESTUDOS ISOTÓPICOS DOS DEPÓSITOS DE NÍQUEL-COBRE SULFETADOS SANTA RITA E PERI-PERI, NORDESTE DO BRASIL

FAUSTO DE ALMEIDA LAZARIN

Dissertação de Mestrado Nº 285

Orientador: Prof. Elton Luiz Dantas (UnB)
Co-orientador: Prof. César F. Ferreira Filho (UnB)

Banca Examinadora:
Examinador: Prof. Elton Luiz Dantas (UnB)
Examinador: Profª. Maria Emilia Schutesky Della Giustina (UnB)
Examinador: Profª. Maria da Glória da Silva (UFBA)

Brasília
2011

AGRADECIMENTOS

- Aos meus pais pelo apoio e incentivo durante todo o período de minha formação acadêmica e profissional.
- À minha namorada Mariana, pelo companheirismo e amor durante todos os momentos desta etapa de minha vida.
- À Constança e Vitor, e toda minha família Almeida e Lazarin.
- À minha avó Márcia Almeida, grande exemplo de sucesso na vida.
- Aos meus GeoAmigos, que sempre estarão presentes em minha vida geológica.
- Aos professores da UnB, em especial Cesar Ferreira Filho e Elton Dantas, que proporcionaram o desenvolvimento do meu conhecimento geológico.
- Aos amigos por onde andei e andarei em minhas caminhadas e marteladas, seja na neve, cerrado, floresta ou praia, todos contribuíram e são importantes.
- Ao CNPq e CAPES pelo suporte contínuo de campo e laboratório durante todo o projeto.
- Ao staff do Laboratório de Geocronologia da Universidade de Brasília. Aos geólogos João Gualberto, Bruno Figueredo, Vitor Hugo, Ana Santana e Carolina Reis (CPRM-BA), por todo suporte, assistência e discussões geológicas.
- Ao geólogo Ricardo Lopes, companheiro de discussões geológicas na exploração mineral.
- À empresa Mirabela Mineração do Brasil Ltda. que proporcionou e viabilizou este projeto.
- Ao geólogo Douglas Cook, que acompanhou e auxiliou os trabalhos de campo nos depósitos da Mirabela Mineração do Brasil Ltda.

RESUMO

O Complexo Máfico-Ultramáfico Fazenda Mirabela é uma intrusão Paleoproterozóica localizada no sudeste do Estado da Bahia, próximo à cidade de Ipiaú. Caracteriza-se por mineralizações de Ni-Cu associadas às rochas máficas e ultramáficas, cujos depósitos são denominados de Santa Rita e Peri-Peri.

Geologicamente, Mirabela situa-se no sudeste do Cráton do São Francisco, intrusiva em rochas arqueanas na porção sul do Cinturão Itabuna-Salvador-Curaçá. A intrusão acamadada tem filiação basalto-toleítica, que consiste em uma associação máfica-ultramáfica diferenciada na base sobreposta por uma fase gabronorítica. O Complexo Mirabela foi subdividido de acordo com parâmetros litológicos e petrográficos em cinco zonas: Grupo de Borda Inferior - gabronoritos e ortopiroxenitos; Zona Inferior – dunitos; Zona Intermediária – harzburgitos, olivina ortopiroxenitos, ortopiroxenitos e websteritos; Zona Superior - gabronoritos; e Grupo de Borda Superior - websteritos, ortopiroxenitos, harzburgitos e gabronoritos.

Análises geoquímicas em furos de sondagem do depósito Peri-Peri demonstram que a distribuição dos conteúdos de Ni, Cu, Pt e Pd está associada aos horizontes máficos-ultramáficos com predominância de sulfetos disseminados.

Estudos petrográficos da Intrusão Mirabela indicam que os agregados policristalinos de sulfetos de Ni-Cu ocorrem disseminados associados a um forte controle litoestratigráfico, dos harzburgitos até os websteritos em Santa Rita, e websteritos aos harzburgitos em Peri-Peri, sugerindo a ocorrência de rochas mais primitivas no topo da câmara magmática.

Análises isotópicas $\delta^{34}S$ na Intrusão Mirabela indicam uma sulfetação associada a um magmatismo mantélico mineralizado, entretanto, os resultados Sm-Nd para o complexo máfico-ultramáfico corroboram com uma contaminação crustal do magma por rochas encaixantes, e a ocorrência de um pulso magmático que fracionou e originou o corpo acamadado.

As datações geocronológicas U-Pb obtidas pelas análises em zircões definiram idades Paleoproterozóicas para o Complexo Mirabela (1990 ±28 Ma) e a Intrusão Palestina (2079 ±14 Ma), e Arqueana para a rocha encaixante (2541 ±15 Ma) à Intrusão Mirabela. Dados consistentes com a geologia regional da porção sul do Cinturão Itabuna-Salvador-Curaçá.

As mineralizações sulfetadas de Ni-Cu dos depósitos Santa Rita e Peri-Peri têm origem mantélica e ocorrem em concentrações econômicas associadas aos horizontes ultramáficos da intrusão, abrindo novas possibilidades de estudos de outros corpos máficos-ultramáficos intrusivos com características semelhantes ao longo do Cinturão Itabuna-Salvador-Curaçá.

ABSTRACT

The Fazenda Mirabela Mafic-Ultramafic Complex is a Paleoproterozoic intrusion located in the southeast of the Bahia State, near of the Ipiaú town. It is characterized by Ni-Cu mineralization associated with mafic and ultramafic rocks, whose deposits are called Santa Rita and Peri-Peri.

Geologically, Mirabela is located in southeastern of São Francisco Craton, intrusive in archean rocks in the southern portion of the Itabuna-Salvador-Curaçá Belt. The layered intrusion has a basalt-tholeiitic filiation, which consists in a differentiated mafic-ultramafic association in the base superimposed for a gabbronoritic phase. The Mirabela Complex was subdivided according with lithological and petrographical parameters in five zones: Lower Border Group – gabbronorites and orthopyroxenites; Lower Zone – dunites; Intermediate Zone: harzburgites, olivine orthopyroxenites, orthopyroxenites and websterites; Upper Zone: gabbronorites; and Upper Border Group: websterites, orthopyroxenites, harzburgites and gabbronorites.

Geochemical analyses in Peri-Peri diamond drill holes show that the distribution of Ni, Cu, Pt and Pd contents is associated with the mafic-ultramafic horizons with predominance of disseminated sulfides.

Petrographic studies of the Mirabela Intrusion indicate occurrences of polycrystalline aggregates of Ni-Cu disseminated sulfides associated with a strong lithostratigraphic control, from the harzburgites to websterites in Santa Rita, and the websterites to harzburgites in Peri-Peri, suggesting the occurrence of primitive rocks on the top of the magmatic camara.

$\delta^{34}S$ isotopic analyses in the Mirabela Intrusion indicate a magmatic sulfidation associated with a mineralized mantle magmatism, however, the Sm-Nd results for the mafic-ultramafic complex corroborate with a crustal contamination of the magma for the country rocks, and the occurrence of a magmatic pulse that was fractionated and originated the layered body.

The U-Pb geochronological ages obtained by the zircon analyses defined the Paloproterozoic ages for the Mirabela Complex (1990 ±28 Ma) and the Palestina Intrusion (2079 ±14 Ma), and Archean for the country rock (2541 ±15Ma) of the Mirabela Intrusion. Consistent data with the regional geology of the southern portion of the Itabuna-Salvador-Curaçá Belt.

The Ni-Cu sulfides mineralizations of the Santa Rita and Peri-Peri deposits have mantle origin and occur in economic concentrations associated with the ultramafic horizons of the intrusion, opening up new possibilities for studies of other mafic-ultramafic intrusive bodies with similar characteristics along the Itabuna-Salvador-Curaçá Belt.

SUMÁRIO

ÍNDICE DE FIGURAS

ÍNDICE DE TABELAS

1. INTRODUÇÃO

1.1. Apresentação e objetivos

Este trabalho é resultado de pesquisa realizada nos depósitos de Ni-Cu do Complexo Máfico-Ultramáfico Fazenda Mirabela, no município de Itagibá (BA).

Os depósitos de sulfetos de Ni (Cu-EGP) são considerados como de origem magmática e formados pela segregação e concentração de líquidos imiscíveis de sulfetos a partir de magmas de composição máfica-ultramáfica (Whitney and Naldrett 1989; Naldrett 2004). A evolução magmática dos complexos acamadados é fator condicionante do posicionamento estratigráfico e petrológico dos depósitos de níquel sulfetado, pois permite definir as principais causas responsáveis pela mineralização sulfetada. Estas podem indicar as zonas estratigráficas mais favoráveis às novas mineralizações, sendo portanto de grande importância para trabalhos exploratórios desenvolvidos pelas empresas de mineração.

O Complexo Fazenda Mirabela é caracterizado por mineralizações de Ni-Cu associadas às rochas máficas e ultramáficas, cujos depósitos são denominados como Santa Rita e Peri-Peri, em zonas de minério sulfetado, e Serra Azul, em área de mineralização laterítica. Estes depósitos pertencem à empresa Mirabela Mineração do Brasil Ltda, que produz concentrado de Ni à partir do minério de Santa Rita desde janeiro de 2010. A mina de Santa Rita é a terceira maior mina de Ni sulfetado a céu aberto do mundo, com capacidade instalada para produção de 18,5 kt de Ni em concentrado (www.mirabela.com.br).

O escopo deste trabalho foi o estudo da geologia, petrologia, geologia isotópica e geocronologia dos depósitos Santa Rita e Peri-Peri. Para a realização desta pesquisa, a empresa Mirabela disponibilizou uma visita de campo na área da Intrusão Mirabela, testemunhos de sondagem, para descrições e análises petrológicas, isotópicas e geocronológicas, e dados geoquímicos.

Esta dissertação de mestrado está em sua maior parte organizada em um artigo a ser submetido para publicação na revista Mineralium Deposita (Capítulo 4). Os capítulos iniciais da dissertação apresentam o contexto geológico do Complexo Mirabela (Capítulo 2) e os métodos utilizados neste estudo (Capítulo 3), enquanto os capítulos finais discutem os resultados dos estudos geocronológicos desenvolvidos nos

complexos máfico-ultramáficos e suas encaixantes (Capítulo 5) e apresenta os principais resultados desta dissertação (Capítulo 6).

1.2. Localização e Fisiografia

A área de trabalho corresponde ao Complexo Fazenda Mirabela, o qual localiza-se no sudeste do estado da Bahia, no município de Itagibá, a 6km da cidade de Ipiaú. Regionalmente a área tem aproximadamente 47km^2 e limita-se entre as coordenadas UTM de vértices noroeste 417450N e 8433100E, e sudeste 426110N e 8427660E, Datum SAD 69 – Zona 24S.

Os acessos à cidade de Ipiaú podem ser feitos através de rodovias federais e estaduais apartir de Salvador e Ilhéus, distantes aproximadamente 230km e 120km, respectivamente (Figura 1.1). O Complexo Mirabela situa-se adjacente à rodovia BA-650, aproximadamente 2km a sul da BR-330.

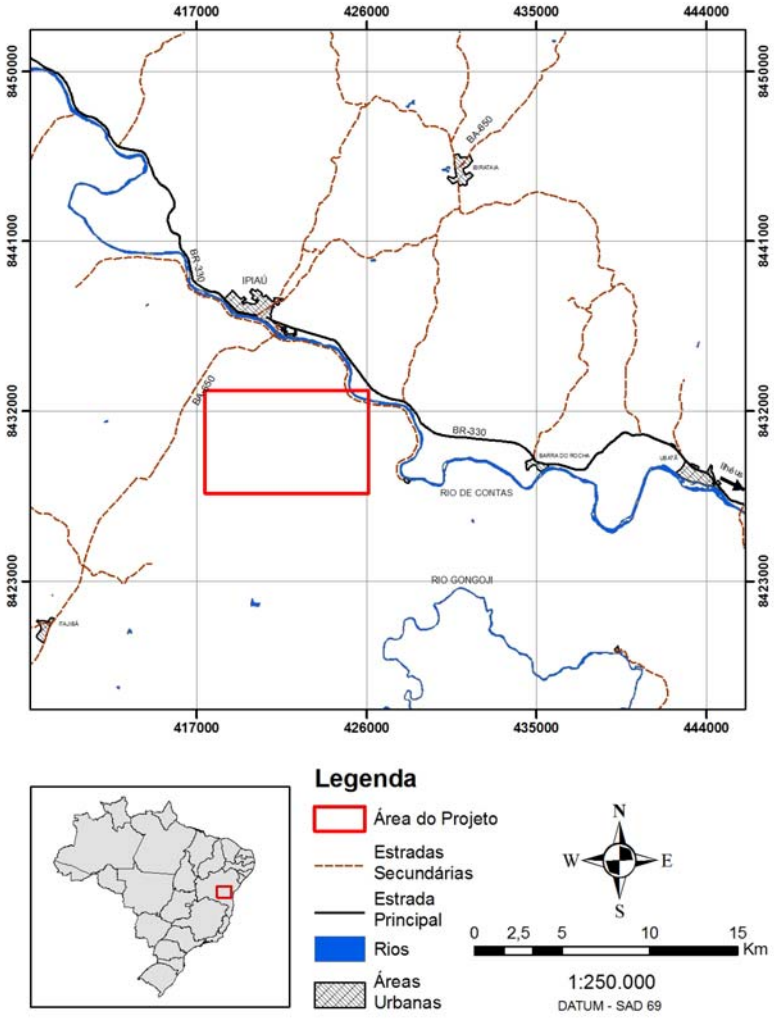

Figura 1.1 – Mapa de localização da área referente a este estudo, demarcada pelo retângulo em vermelho.

Fisiograficamente a região está inserida em um domínio de floresta sub-tropical. A bacia hidrográfica é composta por uma rede de drenagens afluentes do Rio de Contas. A topografia local é caracterizada por relevos planos a suavemente ondulados com coberturas de solos. As altitudes são de aproximadamente 150m com elevações topográficas arredondadas de 350 a 400m, compostas por litologias resistentes inseridas em terrenos metamórficos, tais como Formações Ferríferas Bandadas (BIFs) e os Complexos Máfico-Ultramáficos Mirabela e Palestina.

1.3. Justificativa e objetivos

Corpos máfico-ultramáficos têm sido largamente descritos na literatura geológica devido ao potencial metalogenético para mineralizações de Ni, Cu, EGP, Fe, Ti, V, Cr, Co e Au. Estas intrusões hospedam depósitos de origem magmática formados em decorrência de processos de fracionamento ígneo e de imiscibilidade de líquidos sulfetados imiscíveis. Estes corpos têm um importante potencial econômico e são indicadores da ambiência geotectônica do terreno durante a época de formação.

No Estado da Bahia, porção sul-sudeste do Cráton do São Francisco, ocorrem várias intrusões máfica-ultramáficas encaixadas em terrenos metamórficos de alto grau do embasamento. Algumas destas intrusões detêm mineralizações sulfetadas.

O Complexo Fazenda Mirabela foi escolhido para a realização de estudos geológicos, petrológicos, isotópicos e geocronológicos, destacando-se os depósitos Santa Rita e Peri-Peri, objetos da pesquisa em questão.

Este trabalho propiciará o entendimento dos seguintes aspectos do depósito e suas encaixantes:

- O posicionamento estratigráfico e condicionamento petrológico dos depósitos de Ni-Cu sulfetados, no contexto da evolução magmática da Intrusão Mirabela, com uso de petrografia sistemática e geoquímica de furos de sondagem.

- A origem do enxofre do minério sulfetado de Ni-Cu, com base nos estudos isotópicos de S.

- A definição do período no qual o magma foi extraído do manto e a ocorrência de possível contaminação por rochas encaixantes durante a ascensão magmática, através da análise de isótopos Sm-Nd em rochas do Complexo Mirabela e suas encaixantes.

- A idade de cristalização do Complexo Mirabela e suas encaixantes, com base em datações geocronológicas U-Pb.

Estes estudos têm importância acadêmica e em trabalhos exploratórios desenvolvidos pelas empresas de mineração, pois estabelecem parâmetros metalogenéticos mais robustos para os depósitos de Ni-Cu sulfetado do Complexo Mirabela e contribuem para o entendimento da geologia regional do sul do estado da Bahia.

2. CONTEXTO GEOLÓGICO REGIONAL

O Complexo Máfico-Ultramáfico Fazenda Mirabela é uma intrusão Paleoproterozóica relacionada ao Cráton do São Francisco, o qual é definido por Almeida (1977) como uma unidade geotectônica estabilizada no final do evento Orogênico Paleoproterozóico (2.0-1.8 Ga). Durante este evento desenvolveu-se o lineamento estrutural Contendas-Jacobina, o qual foi testemunho do evento colisional Paleoproterozóico que deu origem ao cráton, e amalgamou blocos arqueanos consolidando o cráton do São Francisco-Congo. Esta grande placa posteriormente foi dividida no Mesozóico, formando o oceano Atlântico.

Na porção sul-sudeste do Cráton do São Francisco, o Bloco Jequié compreende granulitos heterogêneos ortoderivados com inclusões de granulitos básicos e paraderivados (3.0 Ga; Wilson 1987), e granulitos enderbíticos, charnockitos e charno-enderbíticos de 2.7-2.8 Ga (Alibert and Barbosa 1992).

A porção sudeste é definida pelo Cinturão Itabuna-Salvador-Curaçá de idade Paleoproterozóica e Arqueana, segmento mais jovem exposto do Cráton do São Francisco que se estende do sudeste da Bahia ao longo da costa atlântica até a cidade de Salvador, e depois de norte para nordeste, separando os Blocos Gavião e Jequié do Bloco Serrinha.

A porção norte do Cinturão Itabuna-Salvador-Curaçá é composta por rochas granulíticas e anfibolíticas (Melo et al 1995), representadas por Tonalitos-Trondhjemitos-Granodioritos (TTG) e rochas supracrustais (Teixeira 1997) em contato oeste com rochas máficas-ultramáficas (Melo 1991; Loureiro 1991). O sul é caracterizado por granulitos tonalíticos-trondhjemíticos paleoproterozóicos a arqueanos, granulitos charnoquíticos arqueanos (2.6 Ga; Silva et al 1997), rochas metassedimentares, gabros e basaltos de fundo oceânico e/ou de bacias *back-arc*, e monzonitos shoshoníticos, e pelas intrusões máfica-ultramáficas Fazenda Mirabela e Palestina (Barbosa et al 2007). As idades T_{DM} de protólitos magmáticos da parte sul do bloco estão entre 2.46-2.28 e 2.81-2.6 Ga (Alibert and Barbosa 1992; Sato 1998).

Durante a Orogenia Paleoproterozóica (2.3-2.0 Ga), os Blocos Jequié, Serrinha e Gavião e o Cinturão Itabuna-Salvador-Curaçá colidiram resultando na formação de importante cadeia de montanhas denominada Orógeno Itabuna-Salvador-Curaçá. O início da colisão resultou em uma superposição tectônica do Cinturão Itabuna-Salvador-

Curaçá acima do Bloco Jequié, e ambos sobre o Bloco Gavião (Figura 2.1 e 2.2) (Barbosa and Sabaté 2002).

Dados Pb-Pb de corpos plutônicos do Sudeste da Bahia no limite Orógeno Araçuaí/Cráton do São Francisco resultaram em idades de 2089 a 2079 Ma, e T_{DM} entre 2562 e 2542 Ma, indicando geração dos magmas parentais apartir de protólitos Arqueanos (Corrêa-Gomes and Oliveira 2002).

O metamorfismo de alto grau Paleoproterozóico na porção central do Orogéno Itabuna-Salvador-Curaçá foi de fácies granulito sob condições de 5-7 kbar e 850ºC, e anfibolito e xisto verde nas bordas (Barbosa and Sabaté 2003). Dados geocronológicos indicaram que o metamorfismo regional é resultante de um espessamento crustal associado com uma colisão por volta de 2.0 Ga (Barbosa and Sabaté 2004).

Peucat et al (2011) estabelece a idade do metamorfismo granulítico do sul do Cinturão Itabuna-Salvador-Curaçá entre 2086 ± 7 Ma e 2087 ± 11, e na porção central em 2082 ± 5 Ma. Estes dados demonstram que o evento de alto grau metamórfico ocorreu no mesmo momento em toda a extensão do Cinturão Itabuna-Salvador-Curaçá (Peucat et al 2011).

Uma estreita faixa em condições metamórficas de fácies anfibolito, definida por Banda de Ipiaú, está entre os Blocos Itabuna-Salvador-Curaçá e Jequié. Esta banda também é denominada por Complexo Ibicuí-Ipiaú (Barbosa et al 2007). A Banda de Ipiaú é composta por rochas anfibolíticas, graníticas e migmatíticas em fácies anfibolito (Barbosa et al 2007), com direção SSW-NNE de Nova Canaã para Aratuípe (Silva et al 1992; Misi and Silva 1992).

A parte sul do Cinturão Itabuna-Salvador-Curaçá assemelha-se a modernos arcos vulcânicos ou associações de margem continental ativa magmática (Barbosa 1990). Arcos de ilhas, bacias *back-arc* e zonas de subducção são ambientes predominantes durante o desenvolvimento deste bloco (Barbosa and Sabaté 2002).

O alojamento das intrusões acamadadas Mirabela e Palestina durante a deformação Paleoproterozóica está subordinado a um regime transpressivo sin a tardi tectônico associado a um espessamento crustal (Abram and Silva 1992) (Figura 2.233). Estas rochas são intrusivas ao longo de um lineamento estrutural que se estende por mais de 100 km adjacente à margem oeste do Cinturão Itabuna-Salvador-Curaçá (Silva et al 1992). Abram (1993) correlaciona o Complexo Fazenda Mirabela e outros corpos máfico-ultramáficos ao longo da faixa Aratuípe-Nova Canaã ao mesmo regime transpressivo sin a tardi tectônico.

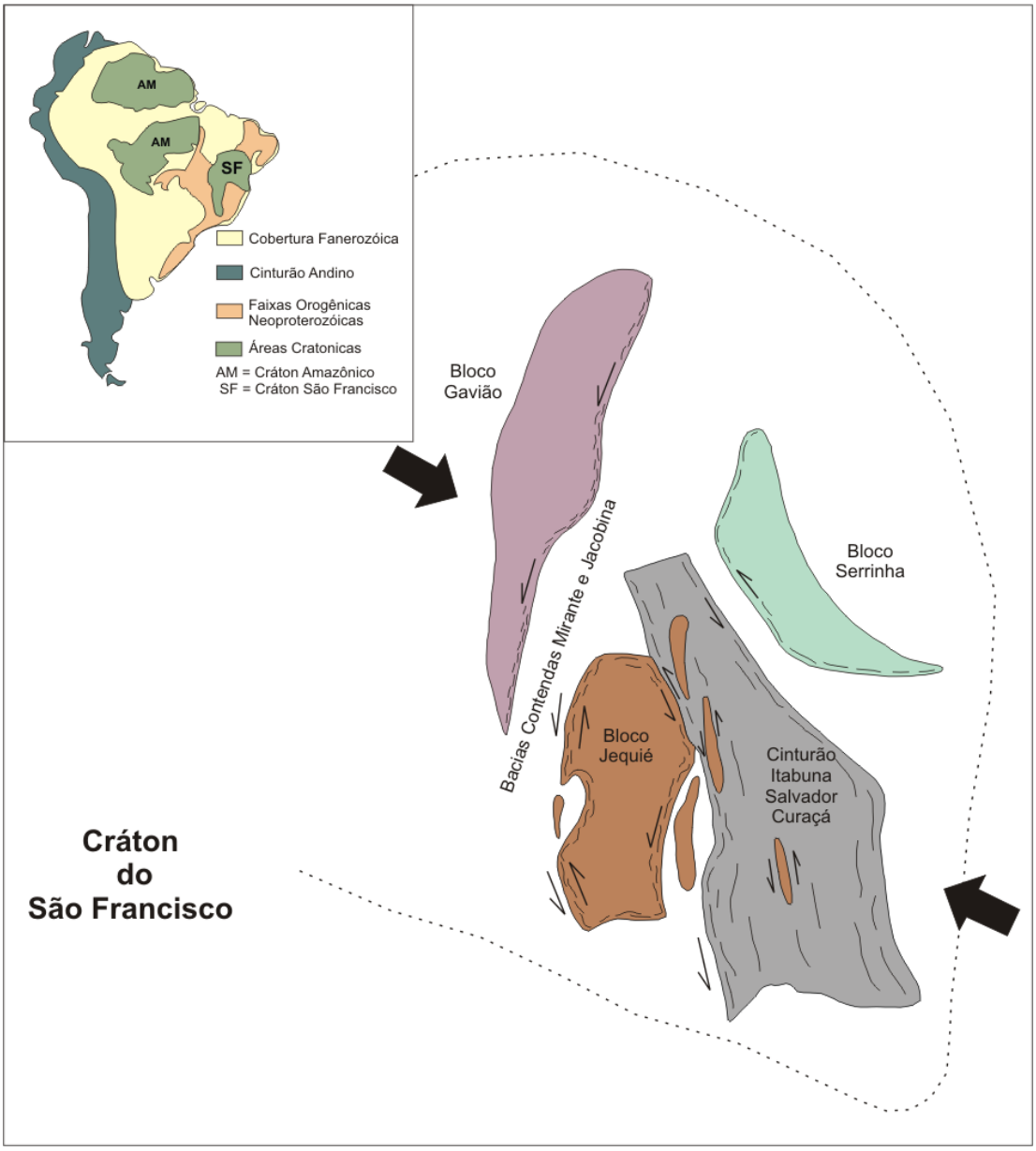

Figura 2.1 – Colisão dos Blocos Gavião, Jequié, Itabuna-Salvador-Curaçá e Serrinha durante a Orogenia Paleoproterozóica em 2.3-2.0 Ga (modificado de Barbosa and Sabaté 2002).

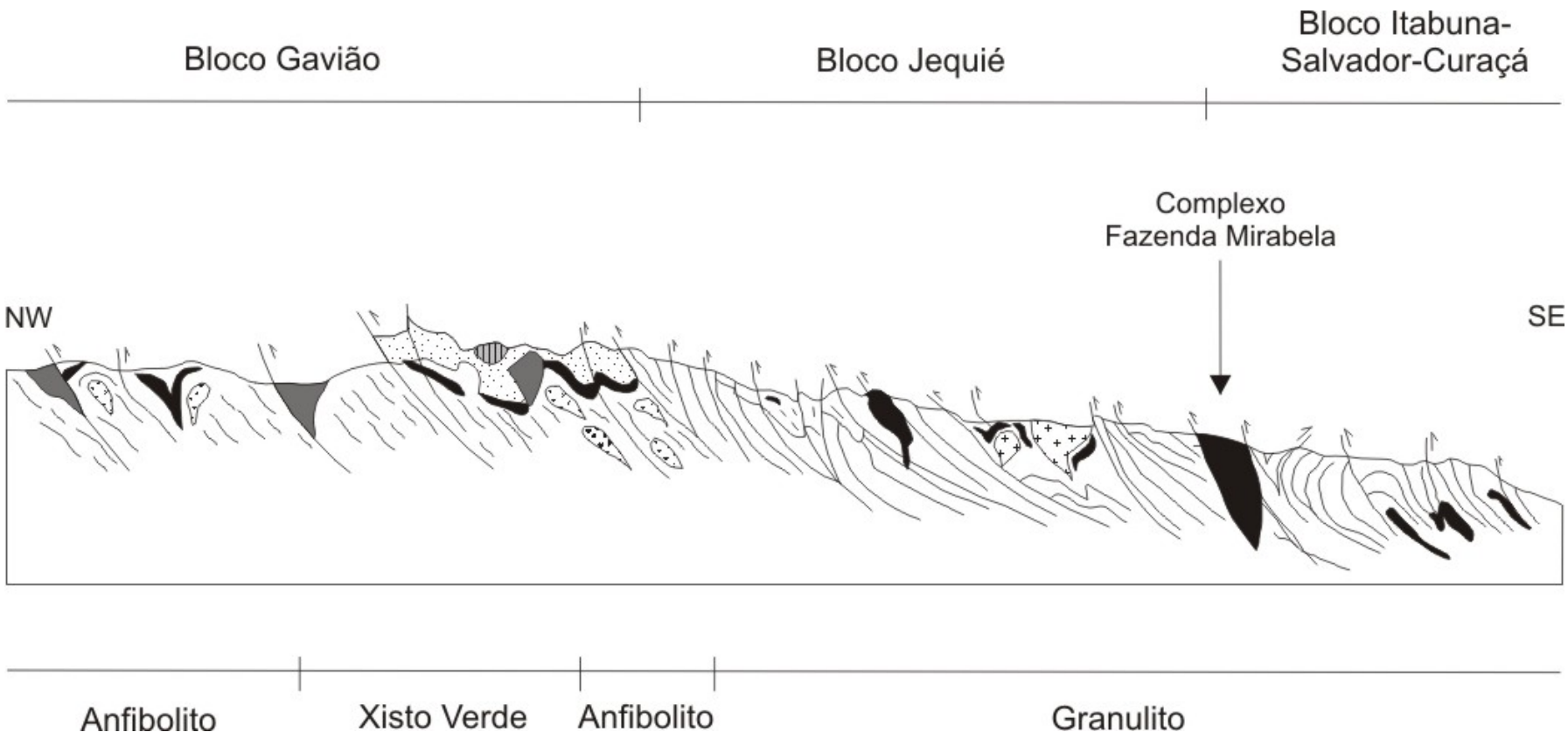

Figura 2.2 – Reconstrução geotectônica da porção sul do Cinturão Itabuna-Salvador-Curaçá. Situação atual do bloco (modificado de Barbosa and Sabaté 2004)

As rochas encaixantes à Intrusão Mirabela correspondem a sucessões de ortognaisses e rochas supracrustais equilibradas em fácies granulito (Figura 2.3). Os ortognaisses constituem charnockitos e enderbitos deformados, e as rochas supracrustais gnaisses quartzo-feldspáticos, horizontes de meta-vulcânicas máficas com granulação fina, *sills* meta-gabronoríticos, formações ferríferas bandadas e serpentinitos; representando metassedimentos intercalados, e gabros e basaltos de fundo oceânico e/ou de bacias *back-arc* (Barbosa and Sabaté 2004).

O Complexo Mirabela é deformado em suas bordas, visto que foi alojado ao final do processo colisional, e parcialmente reequilibrado em fácies granulito, com provável temperatura magmática acima de 1.000°C e reequilíbrio *sub-solidus* em 850°C. A composição da intrusão é essencialmente basalto-toleítica, que consiste em uma associação máfica-ultramáfica diferenciada na base sobreposta por uma fase gabronorítica. O fracionamento regular e contínuo da intrusão sugere um sistema magmático sem reversões significativas ocasionadas por novos pulsos de magma parental. Barnes et al (2011) baseado em análises dos sulfetos e dos cumulatos silicatados, sugere que a sulfetação do Complexo Mirabela está associada à mistura de magmas, proveniente de um influxo de magma fracionado sulfetado em um magma primitivo ultramáfico insaturado em sulfetos.

A área exposta da Intrusão Mirabela tem um formato oval de 4km de comprimento por 3km de largura, e área aflorante de aproximadamente 7km^2 encaixada em terrenos metamórficos de alto grau (Figura 2.4).

Cunha and Fróes (1992) dividem o Complexo Fazenda Mirabela em duas sequências litoestratigráficas distintas: uma ocidental máfica-ultramáfica e outra oriental essencialmente gabróica. Esta subdivisão é baseada nas mudanças de fases *cumulus*, texturas e proporções cumuláticas entre as duas sequências. Abram (1993) combinando limites litológicos (Cunha and Froés 1992), com feições petrográficas e geoquímicas dividiu o Complexo Fazenda Mirabela em quatro zonas litoestratigráficas distintas.

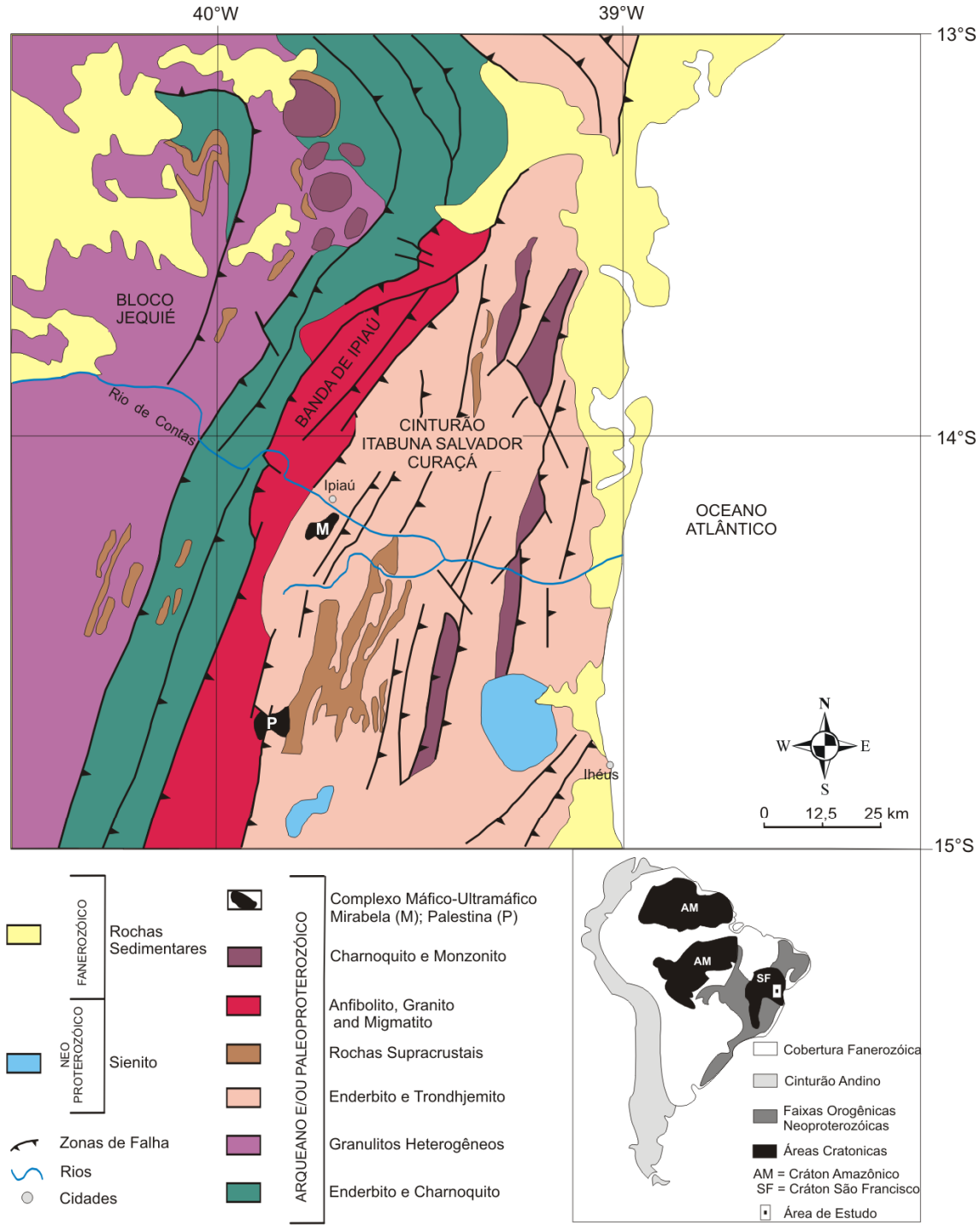

Figura 2.3 – Mapa geológico da porção sul-sudeste do Cráton do São Francisco (modificado de Barbosa et al 2003). Destacam-se no mapa as intrusões máficas-ultramáficas Mirabela e Palestina em rochas Arqueanas.

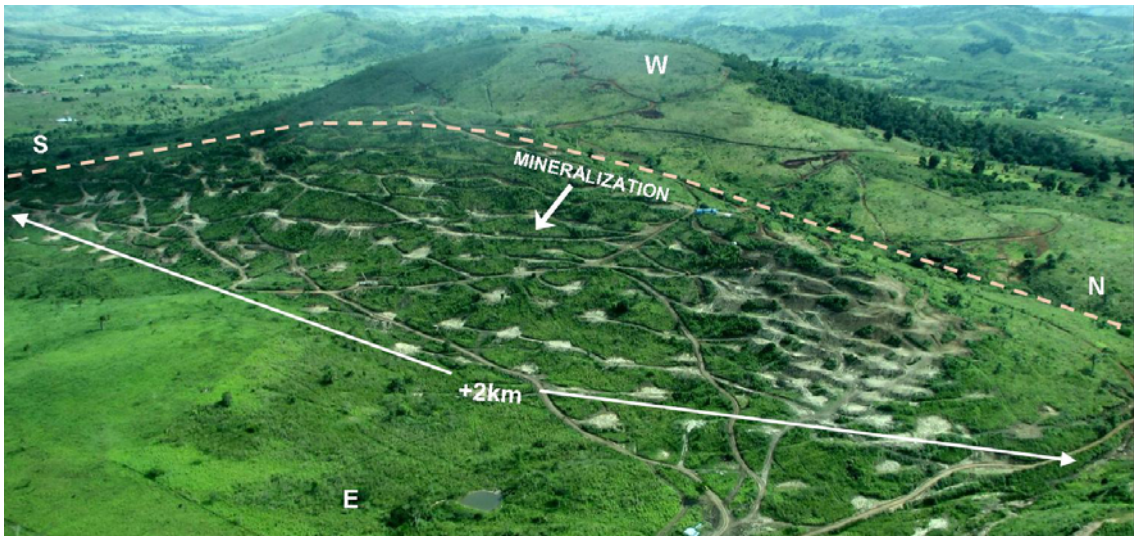

Figura 2.4 – Foto aérea do Complexo Fazenda Mirabela durante a fase de sondagem. Dimensões do corpo e orientação do *plunge* do corpo de minério (Fonte: Mirabela Mineração do Brasil).

Figura 2.5 – A. Camada de dunito na Zona Inferior. B. Dunito (detalhe). C. Cava sul da Mina de Santa Rita. Zona Intermediária - olivina ortopiroxenitos, ortopiroxenitos e websteritos. D. Contato Zona Intermediária (piroxenitos) – Zona Superior (gabronoritos). Legendas: Dn – dunito, CFM – Complexo Fazenda Mirabela, Gn – gnaisse, GbN – gabronorito, Pyx + sulf – piroxenito com sulfetos.

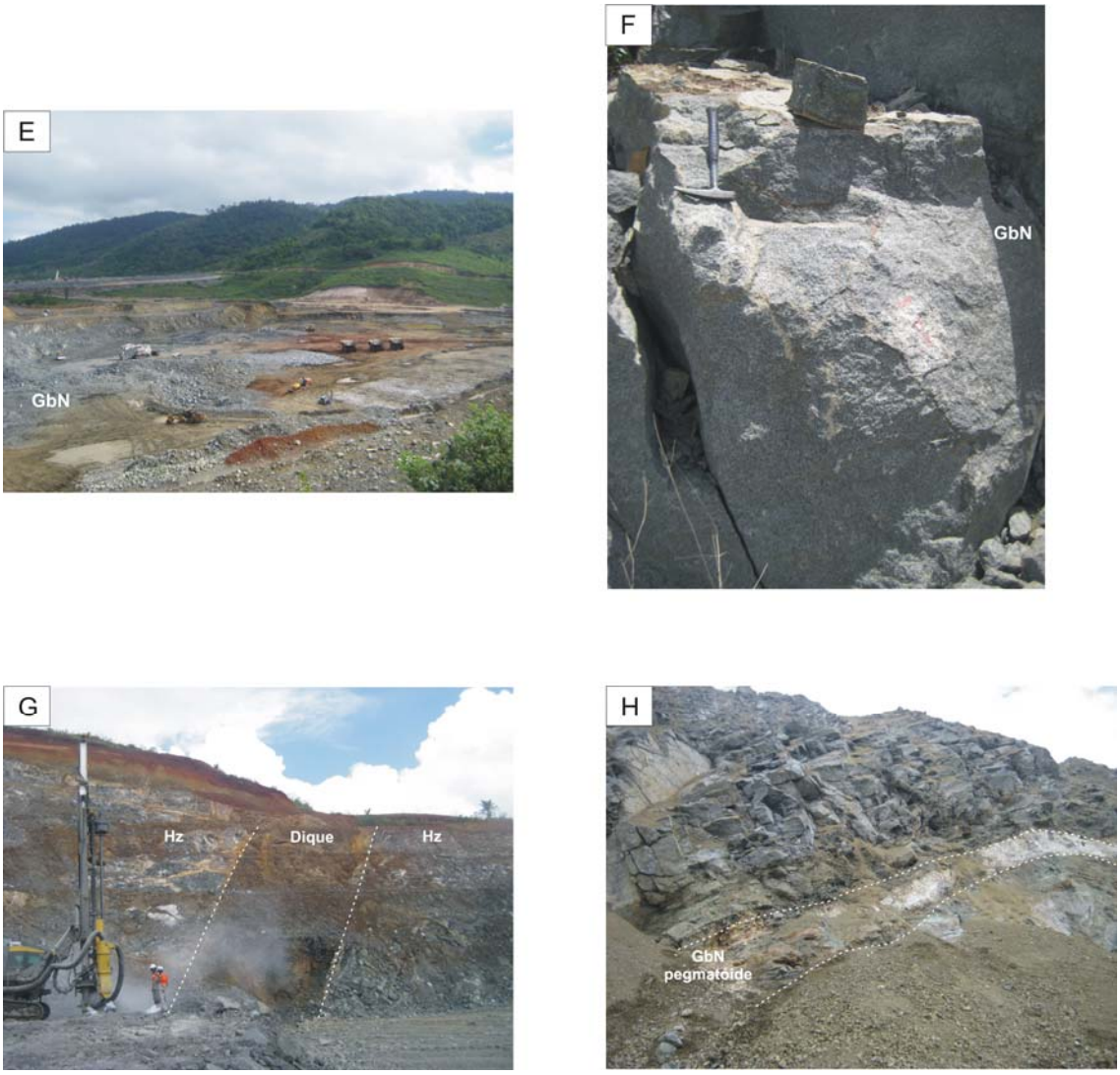

Figura 2.6 – E. Visão leste da Mina de Santa Rita - Zona Superior – gabronoritos. F. Gabronorito da Zona Superior. G. Dique de dolerito cortando a Intrusão Mirabela. H. Gabronorito Pegmatóide utilizado para datação geocronológica do Complexo Fazenda Mirabela (FM-03). Legendas: GbN – gabronorito, Hz – harzburgito.

3. ATIVIDADES E MÉTODOS

O trabalho de pesquisa iniciou-se com o levantamento bibliográfico de toda a porção leste do Cráton do São Francisco, com ênfase nas ocorrências de intrusões máficas-ultramáficas e rochas encaixantes arqueanas do Cinturão Itabuna-Salvador-Curaçá.

A etapa de campo foi realizada durante o mês de março de 2010 na mina Santa Rita, com a colaboração dos orientadores César F. Ferreira Filho e Elton Luiz Dantas, e o geólogo da empresa Mirabela Mineração do Brasil, Douglas Cook. Durante o período de campo realizaram-se reconhecimentos geológicos e amostragens em toda a extensão da área do Complexo Mirabela, posteriormente foram selecionados testemunhos de sondagem para descrição e coleta de amostras para análises petrográficas, isotópicas e geocronológicas. A amostragem totalizou a coleta de 57 amostras, sendo 53 correspondentes aos testemunhos de sondagem e 04 de afloramentos rochosos descritos durante o reconhecimento geológico. Posteriormente à etapa de campo, procederam-se as análises petrográficas, isotópicas (S e Sm-Nd) e geocronológicas (U-Pb) das amostras selecionadas.

A empresa Mirabela cedeu os resultados geoquímicos referentes a dois furos de sondagem do depósito Peri-Peri e algumas seções geológicas.

3.1 Petrografia

Foram confeccionadas 33 lâminas delgadas utilizando-se amostras coletadas em testemunhos de sondagem do Complexo Fazenda Mirabela, sendo que 16 amostras são correspondentes ao depósito Santa Rita e 17 ao Peri-Peri. O estudo foi realizado em um microscópio petrográfico acoplado à câmera fotográfica digital no Laboratório de Mineralogia do Instituto de Geociências da Universidade de Brasília.

O objetivo das descrições petrográficas neste estudo visou a compreensão de todo o processo de fracionamento magmático do Complexo Mirabela, descrevendo as assembléias mineralógicas de cada unidade estratigráfica e as ocorrências de sulfetos associados. As concentrações econômicas de sulfetos de Ni e Cu estão subordinadas aos horizontes de rochas ultramáficas sob a forma de disseminações, blebs e vênulas.

As abreviaturas dos nomes dos minerais utilizados na pesquisa são propostas por Whitney & Evans (2010).

3.2 Análise Isotópica de S

Análises de isótopos de S são amplamente utilizadas para identificar processos e/ou condições físico-químicas de fluidos mineralizantes. Este procedimento é bastante difundido em trabalhos sobre depósitos magmáticos e assimilação de fontes externas de enxofre por magmas básicos na formação de grandes depósitos de Ni-Cu-EGP (Naldrett 1966, Keays 1995 e Li et al 2001).

Foram coletadas 15 amostras de rochas dos depósitos Santa Rita e Peri-Peri para estudos isotópicos de S em pentlanditas, calcopiritas, piritas e pirrotitas, coletadas manualmente e dispostas em pipetas com resina líquida (Anexo 2). As análises foram realizadas no Laboratório de Geocronologia do Instituto de Geociências da Universidade de Brasília sob a supervisão do Prof. Berhard Bühn.

Depósitos de sulfetos de Ni-Cu tipo *intrusion related* são relacionados a regimes tectônicos extensionais na crosta, podendo estar associados à contaminação do magma máfico-ultramáfico por rochas crustais enriquecidas em enxofre. Ocorrências mundiais são representadas pelos depósitos de Noril'sk e Pechenga, na Rússia, Duluth, nos Estados Unidos, Voisey's Bay, no Canadá, Jinchuan, na China, Uitkomst na África do Sul, entre outros. Processos de contaminação do magma por rochas crustais podem contribuir para a formação de depósitos de Ni-Cu sulfetados, mas não são condicionantes obrigatórios, visto que existem exemplos de depósitos estritamente magmáticos, sem assimilação de rochas encaixantes, tais como Nebo-Babel na Austrália (Seat et al 2009) e Americano do Brasil, no Brasil (Mota e Silva et al 2010). Estudos sistemáticos de isótopos de S em depósitos máfico-ultramáficos sulfetados são ferramentas decisivas para o entendimento da gênese das mineralizações, pois caracterizam a origem e formas de ocorrência, e contribuem para o desenvolvimento de trabalhos minerais exploratórios.

3.3 Análise Isotópica Sm-Nd

Para este trabalho foram realizadas 15 análises isotópicas Sm–Nd segundo método descrito por Gioia & Pimentel (2000) no Laboratório de Geocronologia da Universidade de Brasília (Anexo 3).

A análise Sm-Nd baseia-se no decaimento do isótopo ^{147}Sm para ^{143}Nd com emissão de uma partícula α. A aplicação do método Sm-Nd atribui às rochas máficas e

ultramáficas a possibilidade de obter as idades isocrônicas através da longa meia-vida, a qual é resultante do acúmulo muito lento de ^{143}Nd (Faure 1986, De Paolo 1988).

3.4 Geocronologia U-Pb

Para este estudo a escolha do mineral a ser datado levou em consideração a quantidade de Pb comum incorporado no momento de sua cristalização e os teores de U, e aplicação do método U-Pb para datação de eventos máficos e ultramáficos, caso seja possível a cristalização de zircão magmático.

No Complexo Mirabela foram utilizados zircões magmáticos extraídos de um gabronorito pegmatóide para determinar a idade de cristalização do complexo acamadado. Trabalho semelhante foi desenvolvido na intrusão acamadada de Great Dyke, cujos zircões foram extraídos de um websterito pegmatóide, e definiram a idade de cristalização da sequência ultramáfica, contribuindo para o conhecimento da evolução crustal Arqueana do Zimbabwe (Armstrong & Wilson 2000).

4. GEOLOGICAL, PETROLOGICAL AND ISOTOPIC (SULFUR AND SM-ND) CONSTRAINTS FOR THE ORIGIN OF THE SANTA RITA AND PERI-PERI NI-CU SULFIDE DEPOSITS, NORTHEASTERN BRAZIL.

4.1. Abstract

The Fazenda Mirabela Mafic-Ultramafic Complex is a Paleoproterozoic intrusion in southeastern of São Francisco Craton, intrusive in archean rocks in the southern portion of the Itabuna-Salvador-Curaçá Belt. The layered intrusion has a basalt-tholeiitic filiation, which consists in a differentiated mafic-ultramafic association in the base superimposed for a gabbronoritic phase. The Mirabela Complex is characterized by Ni-Cu mineralization associated with mafic and ultramafic rocks, whose deposits are called Santa Rita and Peri-Peri.

Petrographic studies of the Mirabela Intrusion suggest the occurrence of primitive rocks on the top of the magmatic camara. Isotopic analyses of $\delta^{34}S$ in the Mirabela Complex indicate a magmatic sulfidation associated with a mineralized mantle magmatism and the Sm-Nd results indicate a crustal contamination of the magma for the country rocks, and the occurrence of a magmatic pulse that was fractionated and originated the layered body.

4.2. Introduction

The Ni-Cu sulfide deposits are considered to be of magmatic origin and formed by segregation and concentration of immiscible sulfide liquid from magmas of mafic-ultramafic composition (Whitney & Naldrett 1989; Naldrett 2004) or volcanic flows. The magmatic evolution of the layered complex is determinant for the stratigraphic and petrologic emplacement of the deposits.

Magmatic Ni-Cu deposits usually occur as sulfide concentrations toward the base of the magmatic host bodies. The sulfide minerals consist mainly of pyrrhotite-pentlandite-chalcopyrite-pyrite, with massive, matrix or disseminated concentration. Nickel is the main economic commodity, copper may be either a co-product or by-product, and platinum group elements (PGEs) are usual by-products. These metals are associated with sulfides, which generally make up more than 10% of the ore (Eckstrand 1996).

The intrusion-related Ni-Cu sulfide deposits are typically associated with extensional tectonics in the crust, including rifted continental crust or continental margin, represented by the occurrences of Noril'sk and Pechenga, in Russia, Duluth, in United States, Voisey's Bay, in Canada and Jinchuan, in China (Naldrett 2004). These Ni-Cu sulfide deposits are generally considered to be associated with contamination of the mafic-ultramafic magma by the crust (Barnes and Lightfoot 2005).

The stable and radiogenic isotopic systems have been applied to the studies of magma origin and contamination. The interaction between siliceous country rocks and mafic magma has also been suggested as an important pre-requisite for the generation of large sulfide-rich magmatic Ni-Cu-PGE deposits.

The Fazenda Mirabela Complex is a layered body hosted in metamorphic high-grade terrains in the south-southeast portion of the São Francisco Craton. The Complex consists of a differentiated mafic-ultramafic association of rocks at the base, overlain by a gabbronoritic zone. Associated to the Mirabela intrusion, the lateritic deposit Serra Azul is located in the ultramafic unit, and the deposits Santa Rita and Peri-Peri are emplaced in the mafic-ultramafic units.

The Santa Rita deposit is on the base of the layered intrusion, associated with harzburgites, olivine orthopyroxenites and orthopyroxenites (Abram 1994; Cunha & Fróes 1992), although the unusual Peri-Peri deposit is on the top of the intrusion, possibly on the superior zone of the magmatic system, uncommon position for Ni-Cu-PGE mineralizations associated to layered intrusions.

This paper presents the results of petrological and isotopic studies in the Fazenda Mirabela Complex, with focus in the study of the origin of the Ni-Cu sulfide mineralization and the petrological evolution of the mafic-ultramafic body.

The results provide new insights for the formation of the Ni-Cu sulfide deposits associated with layered intrusions, particularly for Santa Rita and Peri-Peri deposits.

4.2.1. Exploration Review

The company Mineração Nhambú Ltda, a joint venture between BP Minerals and RTZ, detected the possibility of mafic-ultramafic intrusive complexes following regional aeromagnetic surveys by the CPRM in the Itaberaba-Belmonte area, south of Bahia State, in 1976. Mineração Nhambú conducted a regional exploration program for base and precious metals between 1979 and 1981, starting with stream sediments and

soil sampling program, followed for ground geophysical (induced polarization and magnetic) and geochemical (soil) surveys, geological mapping and two diamond drill holes.

Caraíba Metais S.A. worked in the Fazenda Mirabela region to explore copper, nickel and PGEs during 1985 to 1989. The company carried out with detailed geological mapping, soil geochemistry, geophysical surveying (gravity, magnetic and induced polarization) and five diamond drill holes.

The Companhia Baiana de Pesquisa Mineral (CBPM) claimed the Mirabela and Palestina areas during 1989 to 2002. The initial CBPM exploration was executed for the "Projeto Verificações Minerais no Estado da Bahia, Prospecto Fazenda Mirabela" (Cunha et al 1998), comprising the re-evaluation of the previous exploration work by Mineração Nhambú and Caraíba Metais S.A., a detailed geological mapping, profiles of ground geophysics (magnetic and very low frequency-electromagnetic), density and magnetic susceptibility measurements for the five diamond drill holes executed by Caraíba Metais S.A.

CBPM in 1998 flew an airborne magnetic and QuesTEM surveys, with a ground magnetic, electromagnetic and induced polarization geophysical surveys. In 2000, the exploration was conducted for the "Projeto Avaliação de Ni-Cu-Platinóides na Faixa Ipiaú" (Ferreira et al 2000), with five diamond drill holes on the primary mineralization (sulfide ore) obtained by Caraíba Metais S.A. (Fróes & Moraes 2000), and auger (101 holes) and diamond drilling (36 holes) program on the secondary mineralization (lateritic ore).

In 2003, Mirabela Mineração do Brasil Ltda was selected in a public tender by CBPM to develop the nickel resources of the Mirabela Lateritic and Sulfide Ni-Cu-PGE Target. The diamond drilling program began in 2004, and in September 2008, the measured and indicated open pit optimized resource was 130.3 Mt @ 0.60% Ni, 0.16% Cu and 0.09g/t Pt, for 781.800 t of contained Ni metal (Figure 4.1). In September 2009, the production of the open pit mine Santa Rita started.

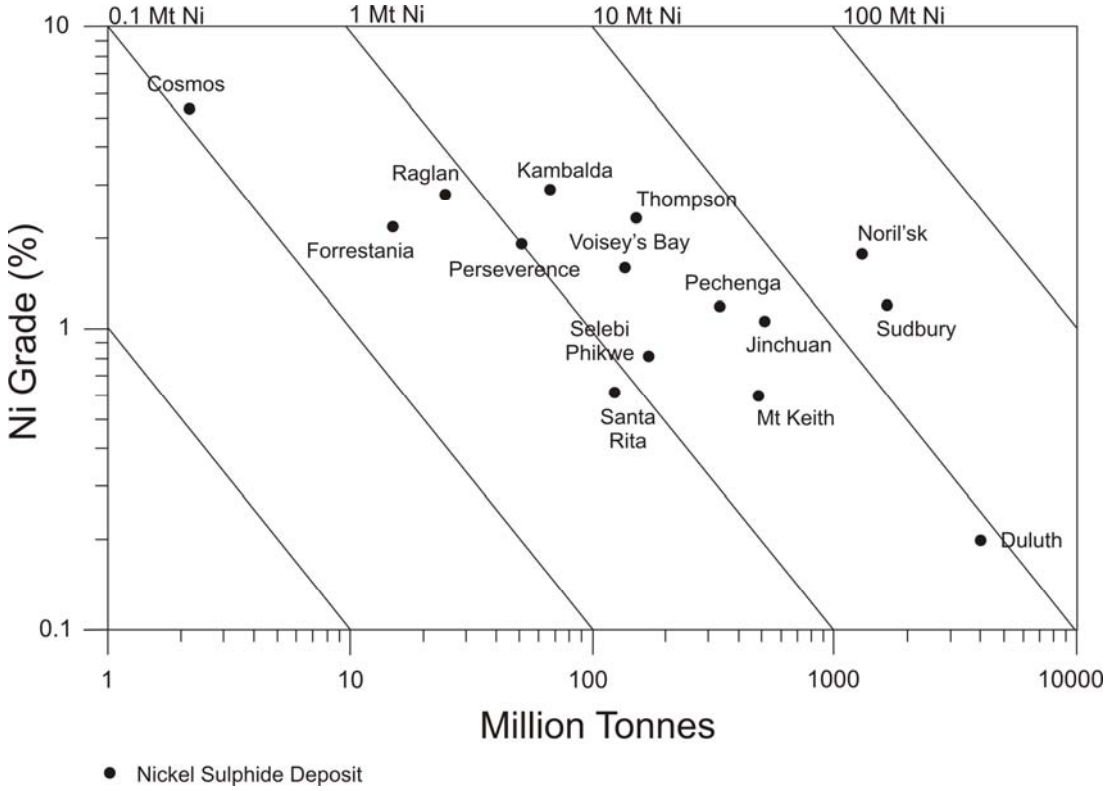

Figure 4.1 – Major nickel sulfide deposits of the world (modified from Naldrett 2004).

4.3. Regional Setting

The Fazenda Mirabela Complex is a Paleoproterozoic intrusion related to the São Francisco Craton, defined by Almeida (1977) as an established geotectonic unit in the end of the Paleoproterozoic Orogenic event (2.0-1.8 Ga). During this event the Contendas-Jacobina structural lineament was developed, which was testimony of the Paleoproterozoic collisional event giving rise to the craton and amalgamated the Archean blocks, consolidating the San Francisco-Congo craton. This large plate was subsequently divided in the Mesozoic, forming the Atlantic Ocean.

In the south-southeast portion of the São Francisco Craton, the Jequié Block comprises heterogeneous orthoderived granulites with inclusions of basic and paraderived granulites (3.0 Ga; Wilson 1987) and enderbitic, charnockite and charno-enderbitic granulites of 2.7 - 2.8 Ga (Alibert & Barbosa 1992).

The southeast portion is the Paleoproterozoic and Archean age Itabuna-Salvador-Curaçá Belt, the youngest segment exposed of São Francisco Craton, extending from southeast of the Bahia state along the atlantic coast to the Salvador city,

then northwards into northeast, separating the Gavião and Jequié Blocks from the Serrinha Block (Figure 4.2).

The north portion of the Itabuna-Salvador-Curaçá Belt is composed for granulitic and anfibolitic rocks (Melo et al 1995), represented by TTGs and supracrustal rocks (Teixeira 1997) in west contact with mafic-ultramafic rocks (Melo 1991; Loureiro 1991). The south is caracterized for Paleoproterozoic to Archean tonalitic-trondhjemitic granulites, charnockitic granulites (2.6 Ga; Silva et al 1997), metassedimentary rocks, ocean floor gabbros and basalts and/or back-arc basins, and shoshonitic monzonites. The T_{DM} ages for the magmatic protolites of the south portion of the block are in 2.46-2.28 and 2.81-2.6 Ga (Alibert & Barbosa 1992; Sato 1998).

During the Paleoproterozoic Orogeny (2.3-2.0 Ga), the Jequié, Serrinha and Gavião Blocks and the Itabuna-Salvador-Curaçá Belt collided resulting in the formation of an important mountain belt called Itabuna-Salvador-Curaçá Orogen. The beginning of the collision resulted in a tectonic superposition of the Itabuna-Salvador-Curaçá Belt above the Jequié Block, and both upon the Gavião Block (Barbosa & Sabaté 2002).

Pb-Pb data of plutonic bodies of the Southeast of Bahia in the limit of Araçuaí Orogen/São Francisco Craton resulted in ages from 2089 to 2079 Ma, and TDM between 2562 and 2542 Ma, indicating generation of parental magmas starting from Archean protolith (Corrêa-Gomes & Oliveira 2002).

The Paleoproterozoic high grade metamorphism in the central portion of Itabuna-Salvador-Curaçá Orogen was granulite facies under conditons of 5–7 kbar and 850˚C, and amphibolite and green-schist facies on the borders (Barbosa & Sabaté 2003). Geochronological constraints indicate that the regional metamorphism resulting from crustal thickening associated with the collision process took place around 2.0 Ga (Barbosa & Sabaté 2004).

Peucat et al (2011) establishes the age of the granulitic metamorphism of the southern Itabuna-Salvador-Curaçá Belt between 2086 ±7 and 2087 ±11 Ma, and in the central portion 2082 ± 5 Ma. These data demonstrate that the high-grade metamorphic event occurred in same moment in the entire Itabuna-Salvador-Curaçá Belt (Peucat et al 2011).

A narrow belt of amphibolite facies metamorphic rocks, defined as the Ipiaú Band, is accomodated between the Itabuna-Salvador-Curaçá Belt and Jequié Block. This band, also called Ibicuí-Ipiaú Complex (Barbosa et al 2007), is composed of amphibolitic, granitic and migmatitic rocks in amphibolite facies (Barbosa et al 2007),

with SSW-NNE trend from Nova Canaã to Aratuípe (Silva et al 1992; Misi & Silva 1992).

The southern part of the Itabuna-Salvador-Curaçá Belt resembles modern volcanic arc or magmatic active continental margin associations (Barbosa 1990). Island arcs, back-arc basins and subduction zones were the predominant environments during the original construction of this belt (Barbosa & Sabaté 2002).

The emplacement of the Mirabela and Palestina layered intrusions during the Paleoproterozoic deformation is subordinated to a sin to late tectonical system associated with a crustal thickening (Abram & Silva 1992). These rocks are intrusive along a structural lineament that extends for more than 100 km adjacent to the west side of the Itabuna-Salvador-Curaçá Belt (Silva et al 1992). Abram (1993) correlates the Fazenda Mirabela Complex and other mafic-ultramafic bodies along the Aratuípe-Nova Canaã Belt to the same sin to late tectonic transpression.

The country rocks of the Mirabela Complex include a supracrustal succession and orthogneisses, which have equilibrated at granulite facies (Figura 4.2). The orthogneisses represent deformed charnockites and enderbites, and the supracrustals rocks are quartz-feldspathic gneisses, horizons of fine-grained meta-mafic volcanics, meta-gabbronoritic sills, silicate-oxide facies banded iron formations and rare serpentinites. This succession represents intercalated metasediments, and ocean floor/back-arc basin gabbros and basalts (Barbosa & Sabaté 2004).

The Mirabela Complex is deformed on the borders, due to the emplacement of the body at the end of the collisional process, and partly reequilibrated at granulite facies, displaying magmatic temperature above 1.000°C and sub-solidus reequilibration at 850°C (Barbosa & Sapucaia 1996). The intrusion is a layered body originally of tholeitic basalt composition, consisting in a differentiated mafic-ultramafic association of rocks at the base, overlain by a gabbronoritic zone. This regular fractionation trend suggests that the magmatic system was closed without replenishment by new magma pulses (Abram 1993). Barnes et al (2011) based on analysis of the sulfides and cumulus silicate, suggests that the Mirabela Complex sulphidation is associated with magma-mixing mechanism, from an influx of sulfide fractionated magma into a primitive and sulfide-unsaturated ultramafic magma.

The exposed area of the Mirabela intrusion is an ovoid shape of 4km long by 3km wide with an outcropping area of approximately 7km^2 hosted in high-grade metamorphic terrains.

Cunha & Fróes (1992) divide the Mirabela Intrusion in two distinct lithostratigraphic sequences: a mafic-ultramafic western and other eastern essentially gabbroic. This subdivision is based on changes of *cumulus* phases, textures and cumulate proportions between the two sequences. Abram (1993) combining lithological boundaries (Cunha & Fróes 1992) with petrographical and geochemical features divided the Fazenda Mirabela Complex into four distinct lithostratigraphic zones.

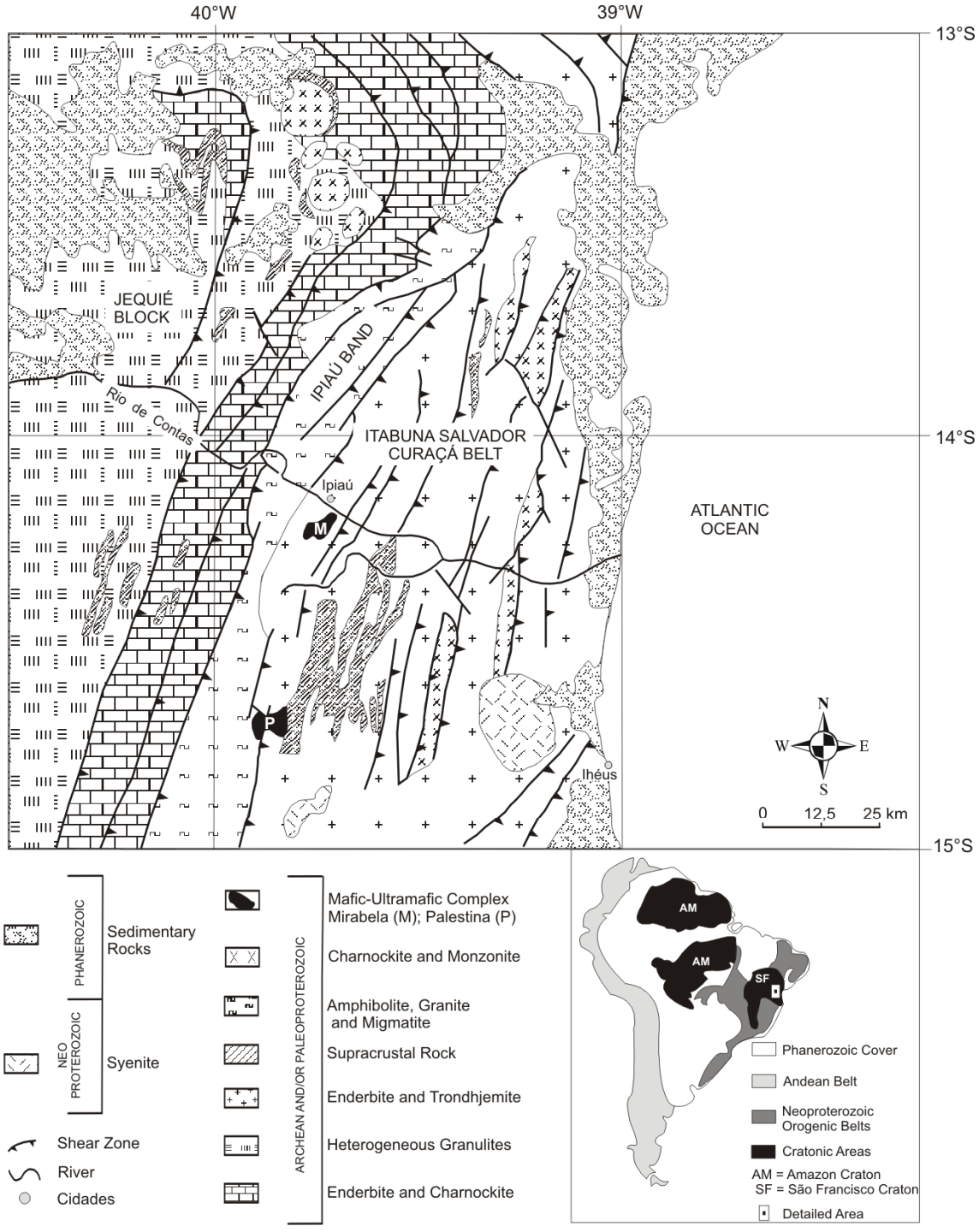

Figure 4.2 – Geological sketch map of the south/south-eastern São Francisco Craton (Barbosa et al 2003).

4.4. The Fazenda Mirabela Intrusion

4.4.1. Previous studies

Two previous extensive studies of the Fazenda Mirabela Complex were developed. The Companhia Baiana de Pesquisa Mineral (CBPM) supported an MSc study of the petrology, geochemistry and Ni-Cu-PGE of the Fazenda Mirabela Complex, under the supervision of the Professor A. J. Naldrett at the University of Toronto (Fróes 1993). The Brazilian Geological Survey (CPRM) supported an MSc study of the Fazenda Mirabela mafic-ultramafic body, petrographical, geochemical and typological characterization, and metalogenetic implications, under the supervision of the Professor M. G. da Silva at the University of Bahia (Abram 1993). These studies provided the broad understanding of the stratigraphy and petrography of the Mirabela mafic-ultramafic intrusion and its Ni-Cu sulfide mineralization used in this study.

4.4.2. Geology and stratigraphy of the layered intrusion

The Mirabela intrusion evolved from a parental magma of tholeiitic composition, which has differentiated into ultramafic lithologies at the base, overlain by a gabbronoritic zone, crosscut by dolerite and pegmatite dykes. It has an ovoid exposed area of 4km long by 3km wide, with a total area of 7km^2, subdivided in five different petrological zones (Figure 4.3).

The Mirabela Complex was investigated through detailed descriptions of diamond drill holes across the intersected extension of the stratigraphy, where the body is continuously exposed to geological descriptions and core sampling.

The sampling for the petrographic and isotopic studies was performed along drill holes of the Santa Rita and Peri-Peri deposits. The geological map of the Mirabela Complex used in this study was based on public reports provided by Mirabela Nickel Ltd.

After the field work, the drill holes descriptions and the detailed petrographic studies of the Mirabela Complex, it was chosen to subdivide the intrusion in five zones (Figure 4.4).

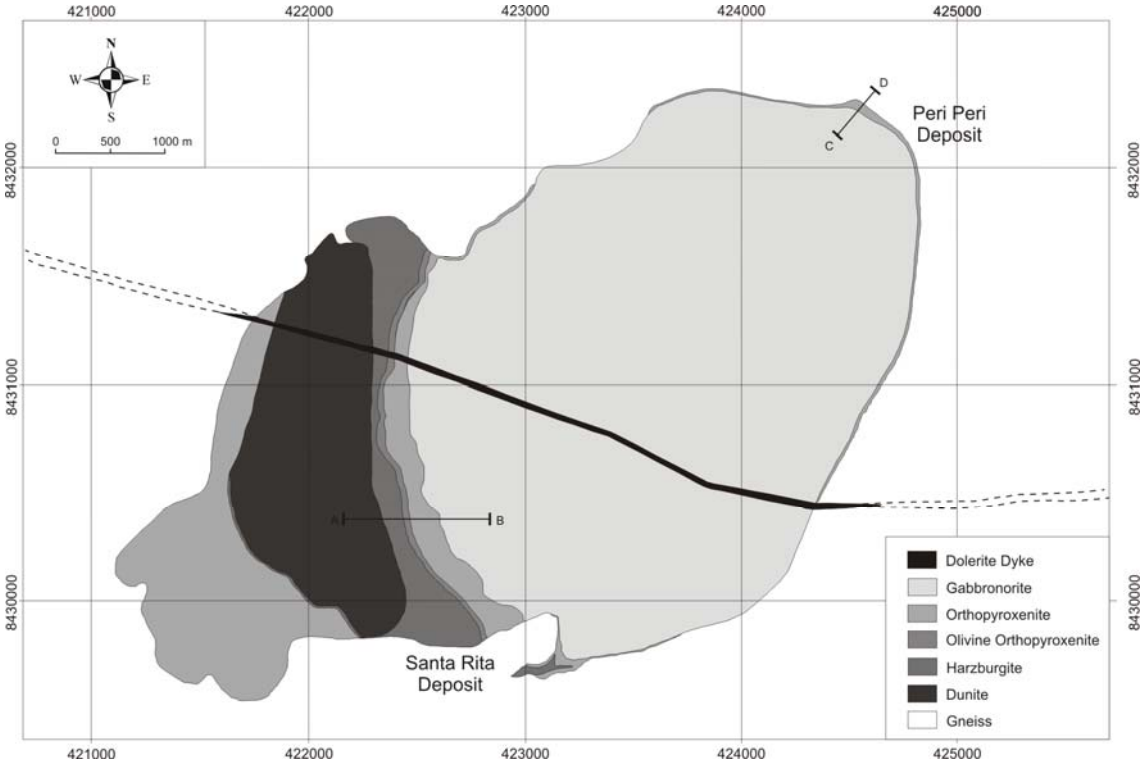

Figure 4.3 – Fazenda Mirabela mafic-ultramafic body and Ni-Cu deposits (modified of Cunha et al 1991).

(i) Lower Border Group – This unit is on the base of the stratigraphy of the Mirabela Intrusion, composed of orthopyroxenites and gabbronorites in contact with the country rocks.

(ii) Lower Zone - This topographically elevated zone occupies about one-third of the total area of the intrusion on the western side. It is composed by partially serpentinized dunites. The dunites have medium-grained mesocumulate texture (cumulus olivine + chromite) and interstitial clinopyroxene, orthopyroxene, phlogopite and fine-grained disseminated sulfides. The olivine shows weak to intense serpentinization along micro-fractures, the chromites are small to large euhedral crystals (up to 0.5 mm) occurring in interstitial aggregates to olivine, whereas tiny crystals (usually <0.1 mm) are enclosed in cumulus olivine.

(iii) Intermediate Zone – This zone host most of the Santa Rita deposit and is characterized for harzburgite, olivine orthopyroxenite, orthopyroxenite and websterite. The harzburgites host the base of the Santa Rita deposit with a medium to coarse grained mesocumulate and orthocumulate texture composed of serpentinized olivine,

orthopyroxene and clinopyroxene cumulus, and interstitial chromite, amphibole and sulfides (pentlandite + chalcopyrite + pyrrhotite + pyrite). This unit host about 35% of the total mineral resource of the intrusion, with highest nickel and copper grades and anomalous PGE contents.

The pyroxenites have gray brownish color, with mesocumulate medium to coarse-grained texture, mostly of orthopyroxene cumulates, and subordinate clinopyroxene. These rocks have post-cumulates amphiboles (hornblende), plagioclase, chromite and interstitial sulfides, represented by pentlandite, chalcopyrite, pyrite and pyrrhotite.

A thin (< 5 m) but continuous layer of websterite occurs at the boundary of the ultramafic and mafic zones. These rocks have brownish color and consist of medium to coarse-grained cumulus orthopyroxenes and/or clinopyroxenes, and high modal proportion of intercumulus plagioclase.

(iv) Upper Zone – Zone with mafic composition that occurs at the east of the ultramafic rocks and occupies two-thirds of the intrusion area. It defines the broad oval shape of the Fazenda Mirabela Intrusion and represents a low and flat region. It comprises mainly gabbronorite and leucogabbronorite with medium-grained mesocumulatic texture. They consist of plagioclase, orthopyroxene, clinopyroxene, amphibole (hornblende), biotite, magnetite and traces of sulfides (pentlandite + chalcopyrite + pyrite + pyrrhotite). The lower part of this zone forms the hanging wall of the Santa Rita deposit.

(v) Upper Border Group - This border group is located on the top of the stratigraphy of the Mirabela Intrusion, and consists of websterite, orthopyroxenite, harzburgite and gabbronorite. The ultramafic lithotypes host the Peri-Peri Ni-Cu deposit and occurrences of pentlandite, chalcopyrite, pyrrhotite and pyrite. A narrow zone of gabbronorite is in contact with the country rocks, with light gray color and fine-grained equigranular and granoblastic texture composed by plagioclase, orthopyroxene, clinopyroxene, amphibole (hornblende), biotite, Fe-Ti oxides (magnetite/ilmenite) and rare occurrences of quartz and apatite.

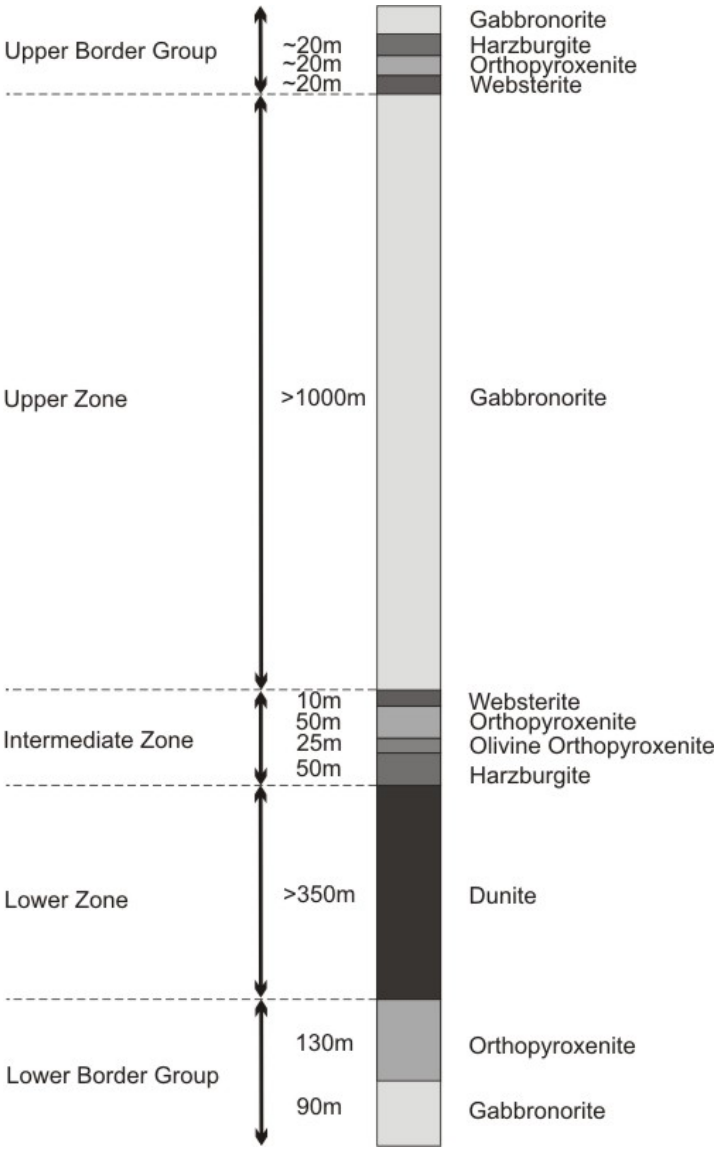

Figure 4.4 – Stratigraphic sequence of the Mirabela Complex (modified of Froés 1993).

At least two sets of dolerite dykes cut the Fazenda Mirabela Intrusion in an east-west orientation. One set of dykes is approximately 10m to 15m thick, dips steeply to the south, and consists of plagioclase, clinopyroxene, titanomagnetite, with traces of apatite, biotite and hornblende. Another set of dykes is granoblastic mafic lithology of plagioclase, clinopyroxene, orthopyroxene, hornblende and traces of biotite, apatite, quartz and sulfide on fractures (Mirabela Nickel Ltd 2007).

The grade of the Ni-Cu sulfide mineralization increases in the contact with these dykes.

The intrusion of pegmatite dykes are common within the peridotite unit, characterized by large euhedral crystals of plagioclase up to 3cm long in a fine grained matrix of polygonal plagioclase, oriented phlogopite and chlorite, zircon, apatite,

masses of monazite in the mica matrix, and veinlets and disseminations of chalcopyrite and pyrite (Fróes 1993).

4.4.3. Characteristics of the country rocks

The country rocks are granulite facies orthogneisses (charnockites and enderbites) and supracrustal rocks. The charnockites are associated with the northwest portion of the Mirabela Complex, gray color, fine-grained and massive. They consist of microcline, quartz, plagioclase, orthopyroxene, biotite, apatite and zircon accessories. The charnockitic texture is inequigranular xenoblastic with grain size ranging from 0.1 to 5.0 mm long.

The supracrustal rocks occur in the east and south parts of the Mirabela Complex, and they are characterized for quartz-feldspathic gneisses with a hornblende charno-enderbitic composition and a grano-nematoblastic texture, fine grained meta-mafics, meta-gabbronorites, BIFs and rare serpentinites.

Sulfides in the country rocks are disseminated and/or locally in veinlets and blebs. The assemblage of sulfides is composed of variable proportions of chalcopyrite, pyrrhotite and pyrite, which vary with rock type.

4.5. Ni-Cu sulfide deposits

Magmatic Nickel-Copper-PGE sulfide deposits form as the result of the segregation and concentration of liquid sulfide droplets from mafic or ultramafic magma, and the preferential partitioning of chalcophile elements into the sulfide liquid (Naldrett 2004). Ni and Cu in magmatic deposits are hosted in base metal sulfides, usually consisting of an intergrowth of pyrrhotite (Fe_7S_8), pentlandite ($[FeNi]_9S_8$), and chalcopyrite ($FeCuS_2$). The PGE are generally present as platinum group minerals in the form of small grains closely associated with sulfides.

The highest concentrations of sulfides tend to occur either at the base of the host body or in the immediate footwall. At most Ni sulfide deposits the sulfide ore may be divided into disseminated, matrix or net textured, and massive, based on a combination of the sulfide content of the rock and the silicate texture (Barnes & Lightfoot 2005).

4.5.1. Santa Rita and Peri-Peri deposits

The Santa Rita deposit is a stratiform body of disseminated nickel and cooper sulfides, located on the harzburgite, through the olivine orthopyroxenite and into the base of the orthopyroxenite units. The mineralized zone extends for 1.5km along strike with an average 35m thick and up to 500m deep (Figure 4.5).

The Peri-Peri deposit is located in the uppermost zone of the Mirabela Layered Complex. It was discovered by Mirabela Nickel Ltd. during a drilling program in this area. The drill holes revealed a mafic-ultramafic zone characterized by gabbronorites in contact with orthopyroxenite and websterites, and the gneissic host rocks (Figure 4.6). This sequence of rocks host disseminated Ni-Cu sulfides associated with minor massive and stringer Ni-Cu sulfides.

The sulfur saturation appears to have post-dated olivine precipitation, and the sulfide mineralization shows strong lithostratigraphic control, concentrated within the peridotite and upwards into the pyroxenite. The sulfide mineralization of the deposits is constituted by interstitial post-cumulate phase to the cumulate silicates, characterized by pentlandite, chalcopyrite, pyrite, and pyrrhotite. Sulfides occur as fine-grained disseminations, interstitial blebs, veinlets and fine filaments in micro-fractures.

The Santa Rita and Peri-Peri deposits are classified based on petro-tectonic setting as NC-5 (according to Naldrett 2004), which comprises a miscellaneous group of deposits that are all associated with magmas ranging from picritic to tholeiitic composition and orogenic tectonical setting. This classification includes another three important deposits, the Moxie intrusion of Northern Main (Thompson & Naldrett 1984), the Caledonian intrusions of north-eastern Scotland (Fletcher 1987), and the Rona intrusion near of Narvik, Norway (Boyd & Mathiesen 1979). These deposits are small (2Mt to 8Mt) and are emplaced in intrusions less than 3km thick with basal accumulations of massive to semi-massive sulfides close to the magma feeder conduit.

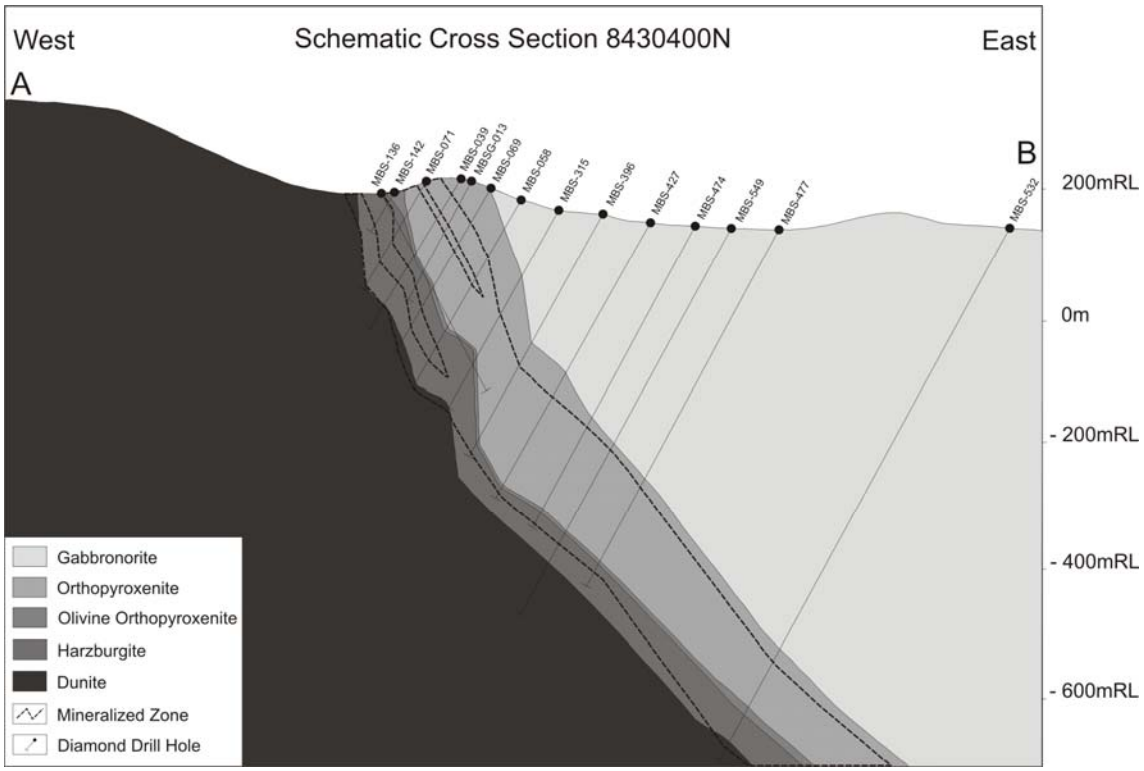

Figure 4.5 – Geological section of Santa Rita deposit (Mirabela Nickel Ltd). See Figure 4.3 the section plotted on the Geological Map of the Mirabela Intrusion.

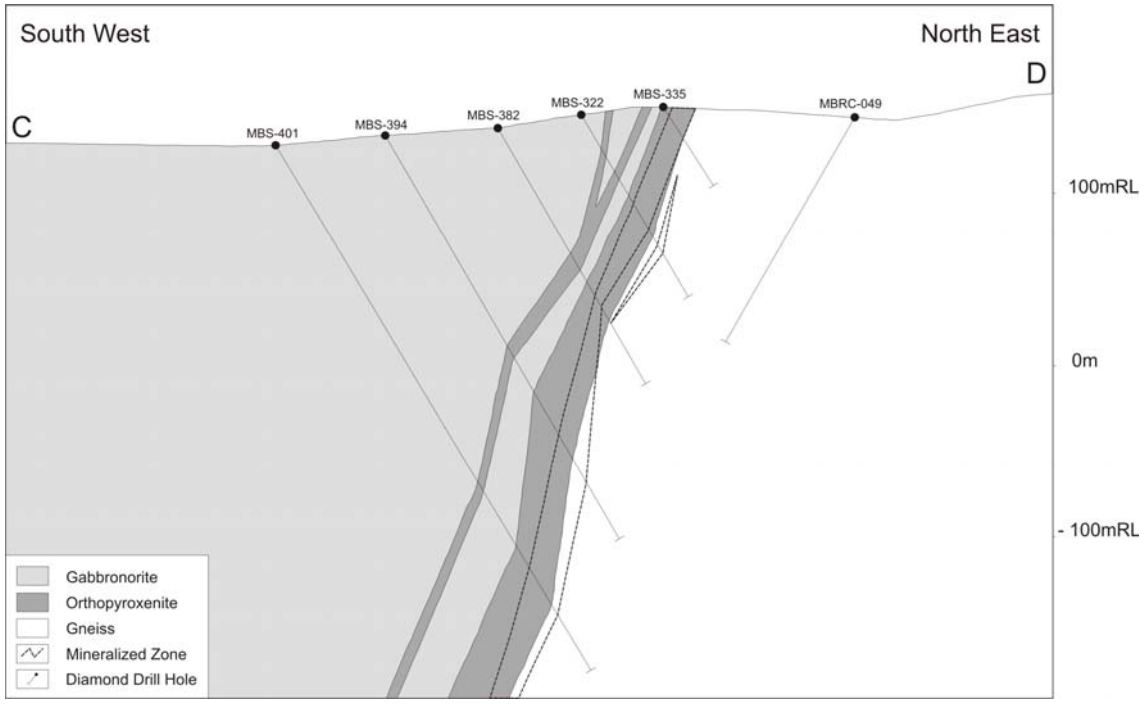

Figure 4.6 – Geological section of Peri-Peri deposit (Mirabela Nickel Ltd). See Figure 4.3 the section plotted on the Geological Map of the Mirabela Intrusion.

4.5.2. Stratigraphic units and sulfides

The rocks of the Fazenda Mirabela Complex are associated with occurrences of disseminated sulfides in all stratigraphic horizons, with variations in concentrations and mineral assemblages (Figure 4.7). The relations of the sulfides textures and the stratigraphic units of the Mirabela Intrusion are described below:

Dunite – Sulfides occur in very fine-grained disseminated crystals of 50-300μm and <1.0 % vol. The major nickel mineral is pentlandite associated with traces of chalcopyrite as fine-grained inclusions in olivine.

Harzburgite - Sulfides (mostly pentlandite and minor chalcopyrite) occur as blebs (30-400μm) and veinlets (200 x 10μm) intergrown with olivine relics and disseminated grains (5-60μm) in serpentine. Traces constituents in harzburgite include pyrite and pyrrhotite. Pentlandite occurs as relative simple intergrowths with chalcopyrite and as discrete mono-mineralic blebs.

Olivine Orthopyroxenite - Sulfides occur as poly-mineral aggregates (0.1-1.5mm) at triple junctions of silicates and fine-grained disseminated particles (<1-100μm) enclosed by pyroxenes. The major sulfide is pentlandite with subordinated chalcopyrite, pyrrhotite and pyrite. The sulfides occur as interstitial blebs to the pyroxenes and the pentlandite is also found as typical flames (5-50μm) within pyrrhotite.

Orthopyroxenite – Pentlandite, chalcopyrite and pyrite occur as interstitial blebs to the pyroxenes. Pentlandite is also found as discrete grains (<100μm) included in pyroxenes. Fine-grained pentlandite blebs (<15μm) intergrown with pyrrhotite also occur within pyroxenes. Pyrite commonly forms a very complex intergrowth pattern with pentlandite.

Websterite – Very fine blebs (0.1-1.5mm) of pentlandite, chalcopyrite, pyrrhotite and pyrite, interstitial to the medium-grained anhedral crystals of pyroxenes.

Gabbronorite - Traces of very fine sulfides (0.1-1.5mm) interstitial to the pyroxenes and plagioclase with medium-grained faneritic texture.

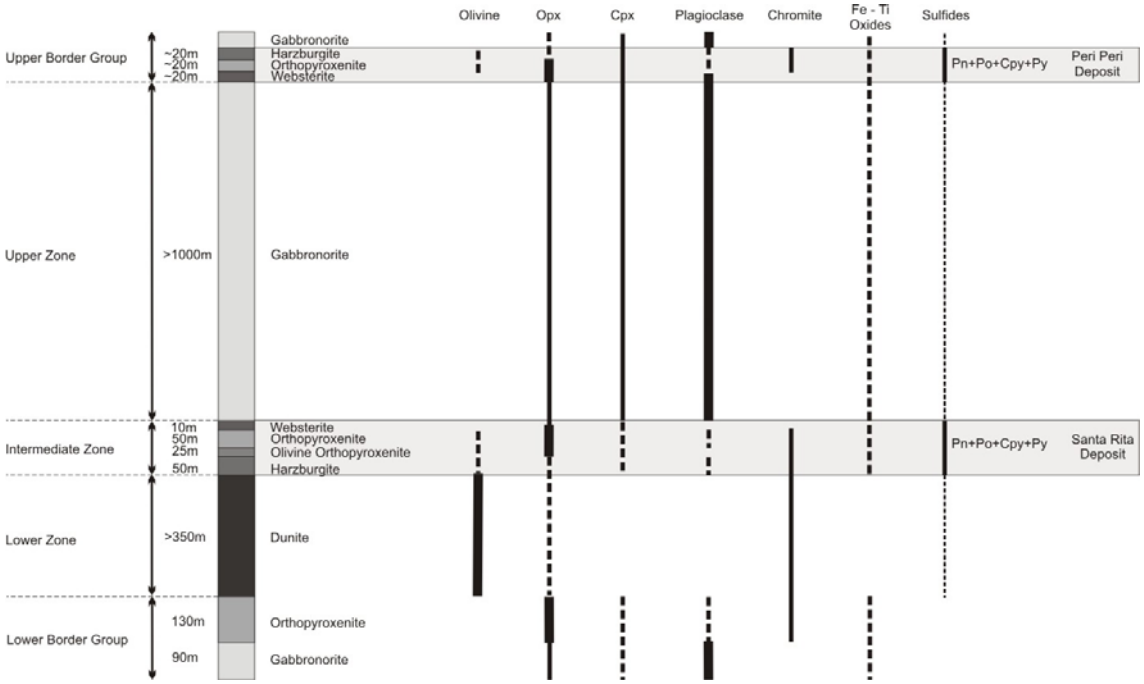

Figure 4.7 – Fazenda Mirabela Complex Stratigraphy (modified of Fróes 1993 and Mirabela Nickel Ltd 2007).

4.6. Sampling and Analytical Procedures

4.6.1. Bulk rock analyses

ALS Chemex Ltd has been used as the principal analytical laboratory company. The sample preparation has been completed in Brazil and the pulps assayed in analytical laboratories in Perth, Australia, and Vancouver, Canada. Assays checks were also completed by ACME Analytical Laboratory Ltd in Vancouver and Ultra Trace Analytical Laboratories in Perth.

The majority of the Ni assaying has been completed using Inductively Coupled Plasma Atomic Emission Spectroscopy (ICP-AES) on dissolved lithium metaborate fusion disks, and Inductively Coupled Plasma Mass Spectroscopy (ICP-MS) of dissolved samples fused with lithium metaborate.

Mirabela has a quality control data to validate the analytical performance of the assay laboratories. The sampling methods, the chain of custody procedures and sample preparation, and the analytical techniques are all appropriate and compatible with industry standards.

The geochemical study of the Peri-Peri deposit is mainly based in two representative diamond drill holes from the mine database. The holes MBS-391 and

MBS-401 were analyzed for major and minor elements. They have northeast direction and crosscut the deposit rock types.

The Peri-Peri deposit consists of portions of mafic and ultramafic cumulate rocks that control the occurrence of the major and minor elements. The highest geochemical values for Mg, S, Cr, Ni, Pt+Pd, Cu and Ba are associated with the ultramafic rocks of the drill holes, suggesting a stratigraphic control for the Peri-Peri deposit.

4.6.2. Petrographical analyses

The detailed petrology was performed in 33 thin sections of the Mirabela intrusion, including 16 and 17 samples of the Santa Rita and Peri-Peri deposits respectively. The thin sections came from two diamond drill holes of Mirabela Company, one of Santa Rita and another of Peri-Peri. The petrographic study was developed in optical microscopes of the Mineralogy Laboratory of the Geosciences Institute, University of Brasília (Brazil).

The abbreviations for the mineral names used in this research were provided by Whitney & Evans (2010).

4.6.3. S isotopic analyses

Sulfur isotopic analyses were carried out at the Geochronology Laboratory of the Geosciences Institute of the University of Brasília. A total of 15 rocks were collected from the Santa Rita and Peri-Peri deposits for sulfur isotopic study. The sulfides analyzed were interstitial blebs and veinlets of pentlandites, chalcopyrites, pyrites and pyrrhotites collected with hand-picking techniques and with individual mounts prepared.

4.6.4. Sm-Nd isotopic analyses

Sm–Nd isotopic analyses in 27 rock samples followed the method described by Gioia & Pimentel (2000) and were carried out at the Geochronology Laboratory of the University of Brasília. The TDM values were calculated using DePaolo's model (1981).

4.7. Results

4.7.1. Distribution of Ni-Cu-PGE-S through the orebody

The Ni, Cu and PGE distribution of the Peri-Peri deposit is mainly based on geochemical analyses in two representative drill cores from the Mirabela Nickel Ltd database. Because the Fazenda Mirabela Complex consists of mafic-ultramafic cumulate rocks, major and minor elements contents are controlled by the type and relative proportion of cumulus minerals.

The plot of Mg versus Cr and Ca (Figure 4.8) indicates the predominance of samples with high Mg and Cr contents associated to the mafic-ultramafic rocks.

The plot of Mg, S, Cr, Ni, Pt + Pd, Cu and Ba versus the depth (Figure 4.9 and 4.10) show the concentration of elements along the drill holes stratigraphy, these elements are associated with mafic-ultramafic rocks defining a stratigraphic control for the Peri-Peri deposit. This relationship occurs for both boreholes, but in different concentrations, because the hole MBS-401 is located in an area with a higher occurrence of ultramafic rocks than MBS-391, and therefore enriched in Mg, Ni and Cr.

The study of the chalcophile elements in Ni-Cu sulfides based on the drill holes show the distribution of the Ni, Cu and Pt + Pd versus S for Peri-Peri deposit (Figure 4.11). The sulfur contents reflect the amount of sulfides, and the Ni, Cu and Pt+Pd the sulfide types.

The occurrences of Ni, Cu, Pt + Pd and S are associated with mafic-ultramafic rocks, and may have a rectilinear distribution (Ni and Cu) or random (Pt + Pd) along the stratigraphy of the deposit. The contents of Ni, Cu and Pt + Pd of the Peri-Peri deposit indicate the predominance of disseminated sulfides on mafic-ultramafic horizons. The Ni and Cu contents have a low variation and a medium to high correlation (Figure 4.12). The Pt + Pd contents for the deposit are lower than 1800 ppb.

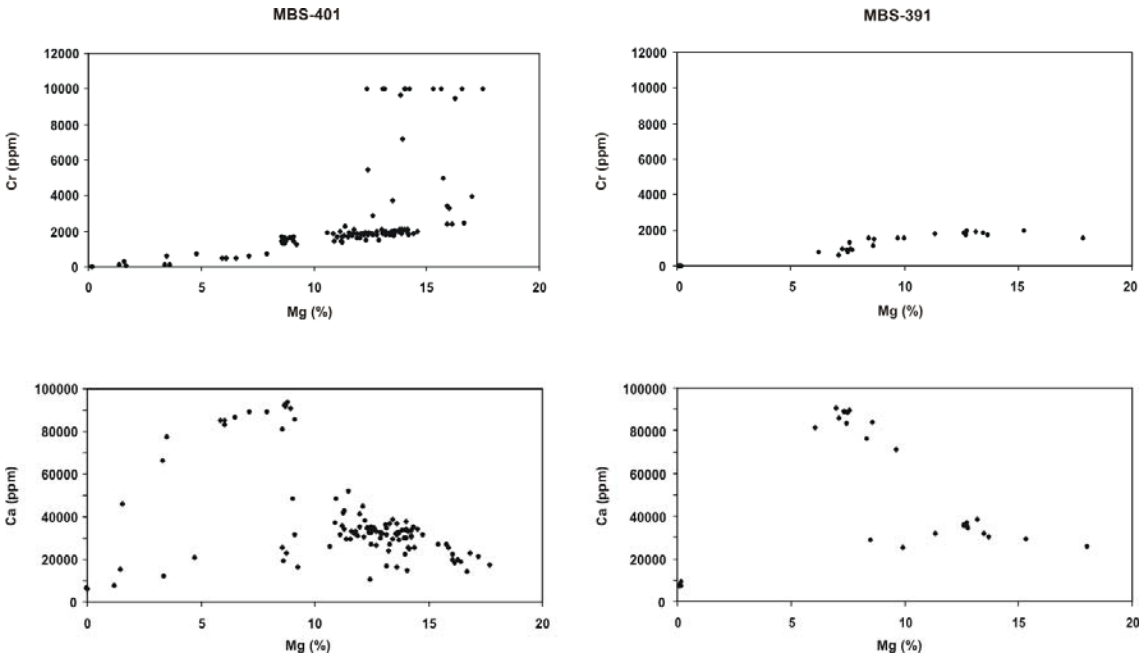

Figure 4.8 – Mg (%) versus Cr (ppm) and Ca graphics for two diamond drill holes of the Peri-Peri deposit. Geochemical database from Mirabela Nickel Ltd.

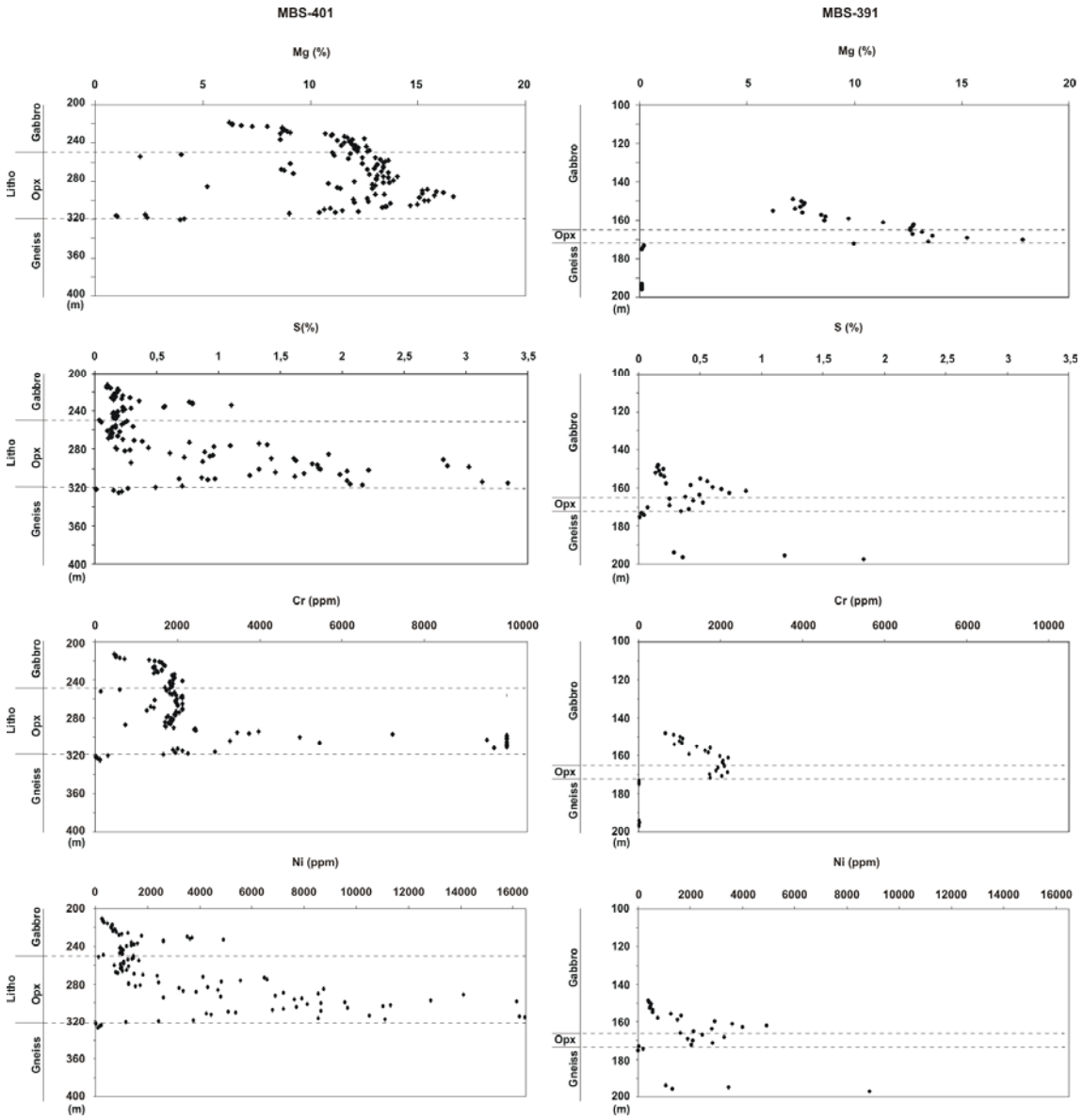

Figure 4.9 - Variation of Mg (%), S (%), Cr (ppm), Ni (ppm) throughout the stratigraphic interval of the holes MBS-401 and MBS-391. Geochemical database from Mirabela Nickel Ltd.

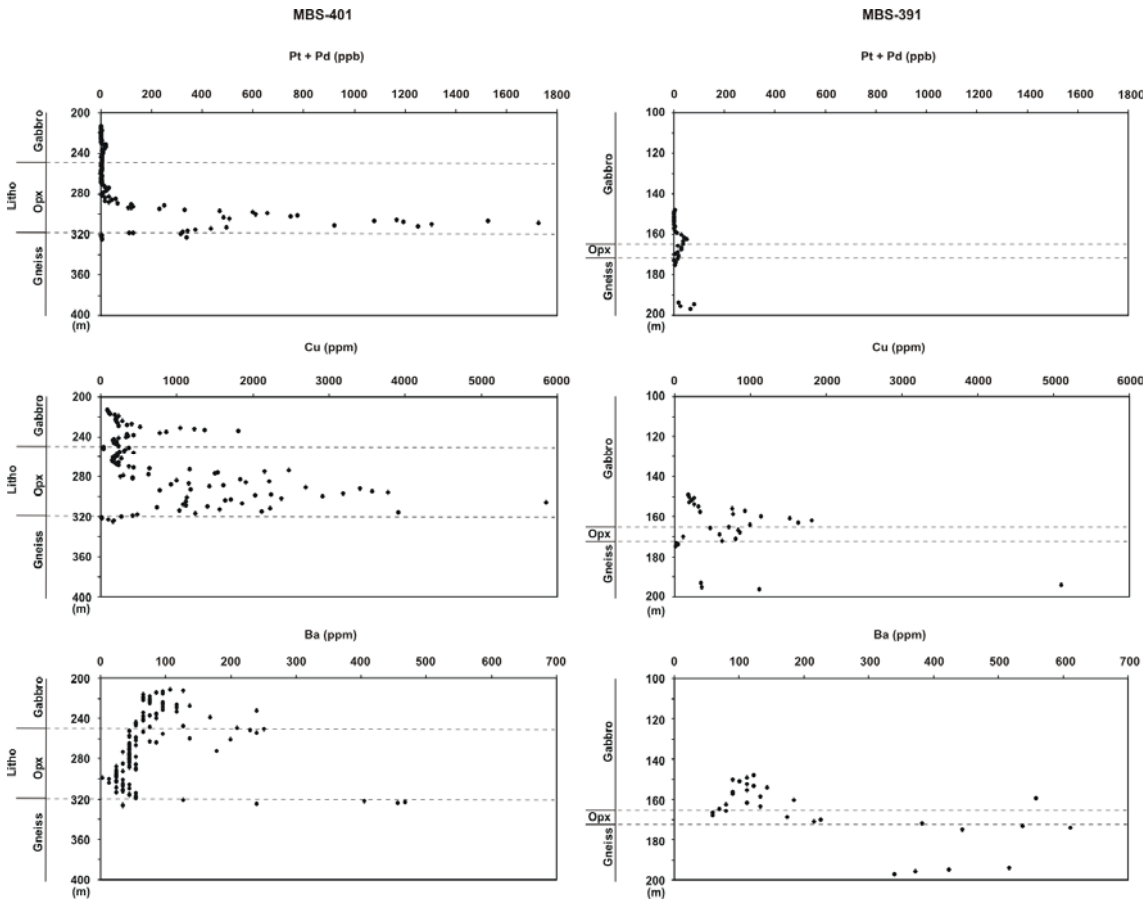

Figure 4.10 - Variation of Pt + Pd (ppb), Cu (ppm) and Ba (ppm) throughout the stratigraphic interval of the holes MBS-401 and MBS-391. Geochemical database from Mirabela Nickel Ltd.

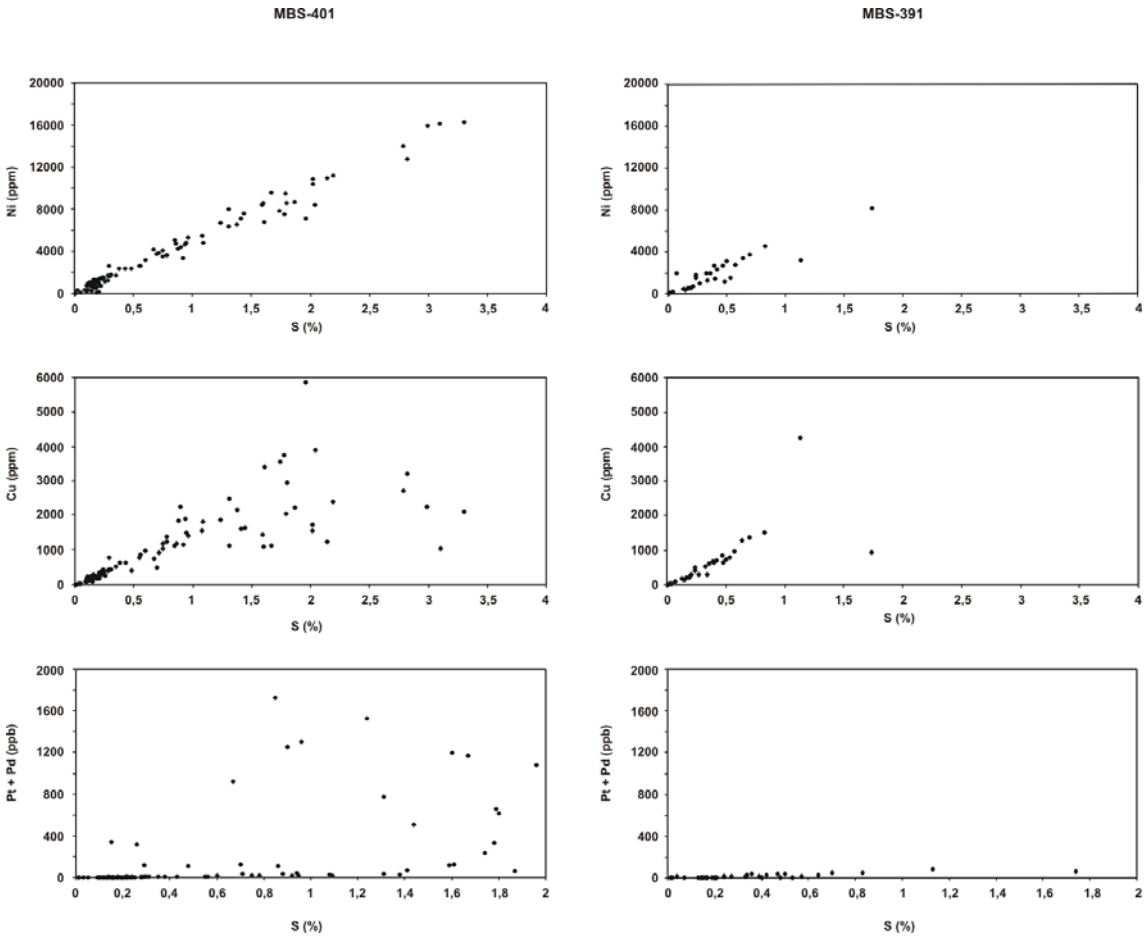

Figure 4.11 – Ni (ppm), Cu (ppm) and Pt+Pd (ppb) versus S (%) graphic for two diamond drill holes of the Peri-Peri deposit. Geochemical database from Mirabela Nickel Ltd.

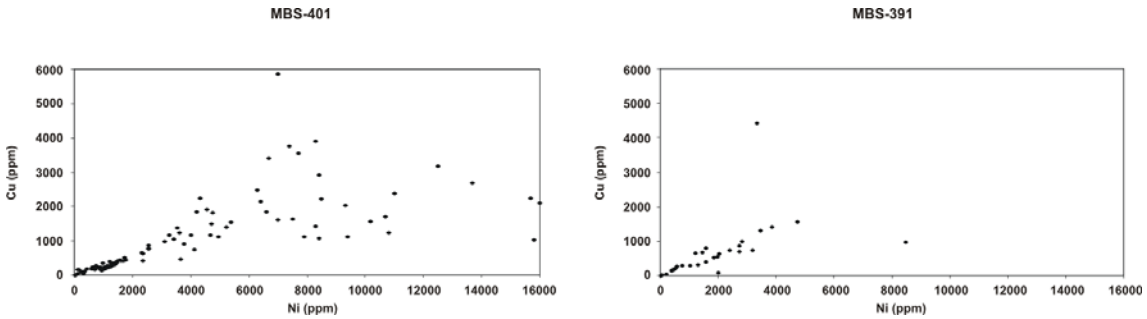

Figure 4.12 - Ni (ppm) versus Cu (ppm) graphic for two diamond drill holes of the Peri-Peri deposit. Geochemical database from Mirabela Nickel Ltd.

4.7.2. Sulfide mineralogy

Magmatic Ni-Cu sulfides associated with mafic-ultramafic magmas are generally considered to have formed as a result of the separation of an immiscible sulfide-oxide melt from a sulfur-saturated silicate melt shortly before, during or after the emplacement at temperature of about 900º C (Naldrett 2004). This process implies that the silicate melt and the sulfide liquid were in chemical equilibrium at high temperatures when sulfides segregated, resulting in geochemical constraints for the composition of the sulfide melt (Naldrett 2004).

The disseminated Ni-Cu sulfides show strong lithostratigraphic control in the Fazenda Mirabel intrusion. The stratiform ore body follows the stratigraphic contacts extending upwards from the harzburgite to websterite in Santa Rita Deposit and from websterite to harzburgite in Peri-Peri Deposit.

The mineralization of Fazenda Mirabela Complex has a primary disseminated nature, originated from accumulation of sulfide liquid within the cumulate silicate phase as interstitial sulfides in ultramafic rocks (Figure 4.13) and comprises predominantly pentlandite associated with chalcopyrite, pyrite and pyrrhotite.

The mode of occurrence of the sulfides is as polycrystalline granular aggregates of pentlandite, chalcopyrite, pyrrhotite and pyrite (Figure 4.14). They are usually fine-grained and with 0.1 to 1.0mm in size, however larger lenses occur locally with sulfide aggregates. The granular aggregates are intergrown to the silicates and in disseminated grains (5-60μm) (Figure 4.15). Chalcopyrite also occurs in veinlets (0.01 x 1.0mm) and fine filaments in micro-fractures. Pentlandite is the primary nickel-bearing phase, characterized for polycrystalline aggregates and eventually as exsolution lamellae (flames) within pyrrhotite or as exsolution rims bordering pyrrhotite crystals.

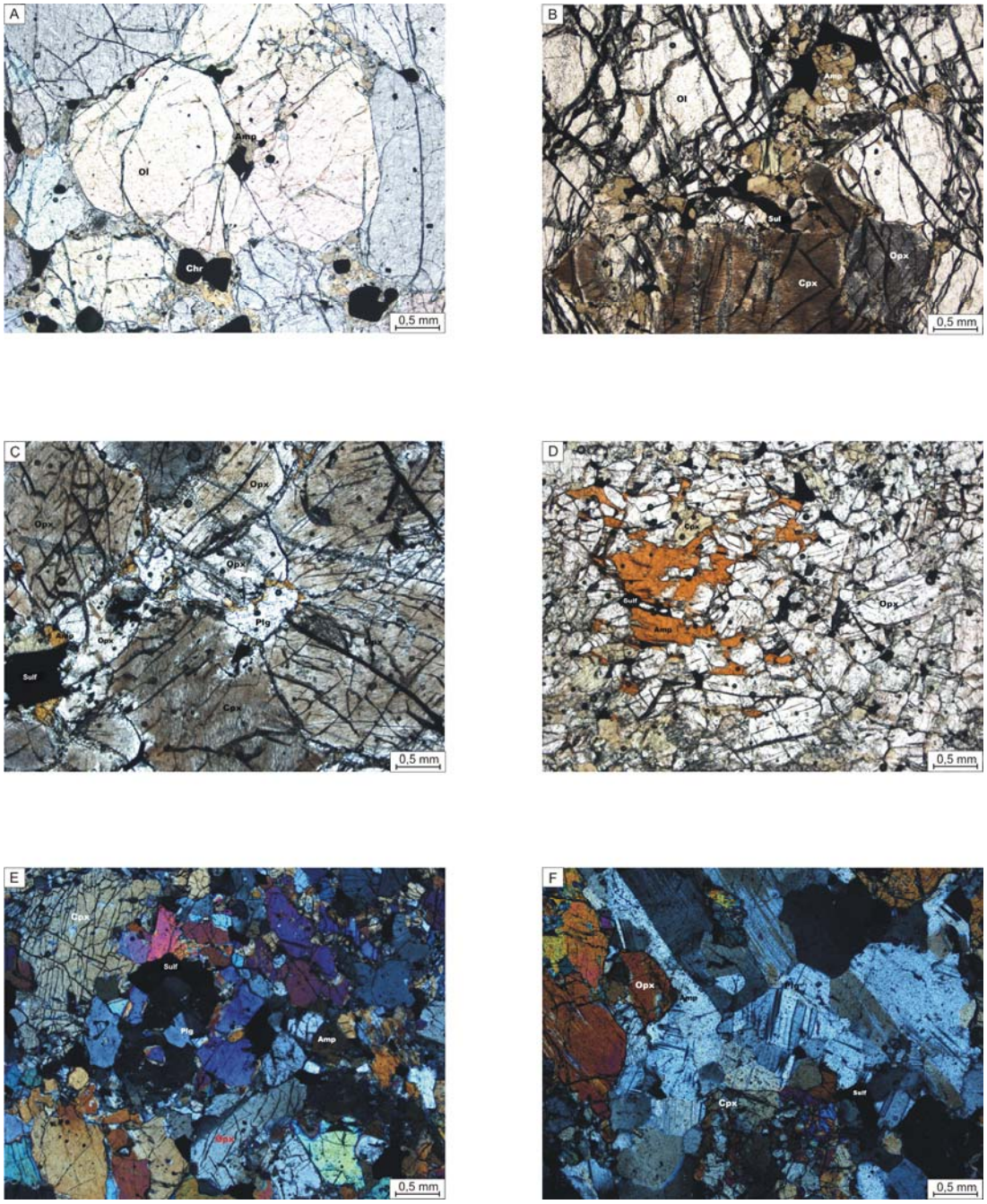

Figure 4.13 – Photomicrographs of rock types from the Fazenda Mirabela Complex. (A) Mesocumulate dunite. Olivines with borders of amphibole, prismatic chromites and sulphides traces. Observation under plane polarized light (PPL). (B) Mesocumulate serpentinized harzburgite. Interstitial sulfides to olivines, clinopyroxene and orthopyroxene cumulates. PPL. (C) Mesocumulate olivine orthopyroxenite with interstitial sulfides, amphiboles and plagioclases. PPL. (D) Mesocumulate orthopyroxenite with interstitials amphiboles and sulfides. PPL. (E) Mesocumulate websterite with interstitials sulfides. Observation under cross polarized light (XPL). (F) Mesocumulate gabbronorite. Medium-grained plagioclase, orthopyroxene and clinopyroxene. Interstitial amphiboles and traces of sulfides. XPL.

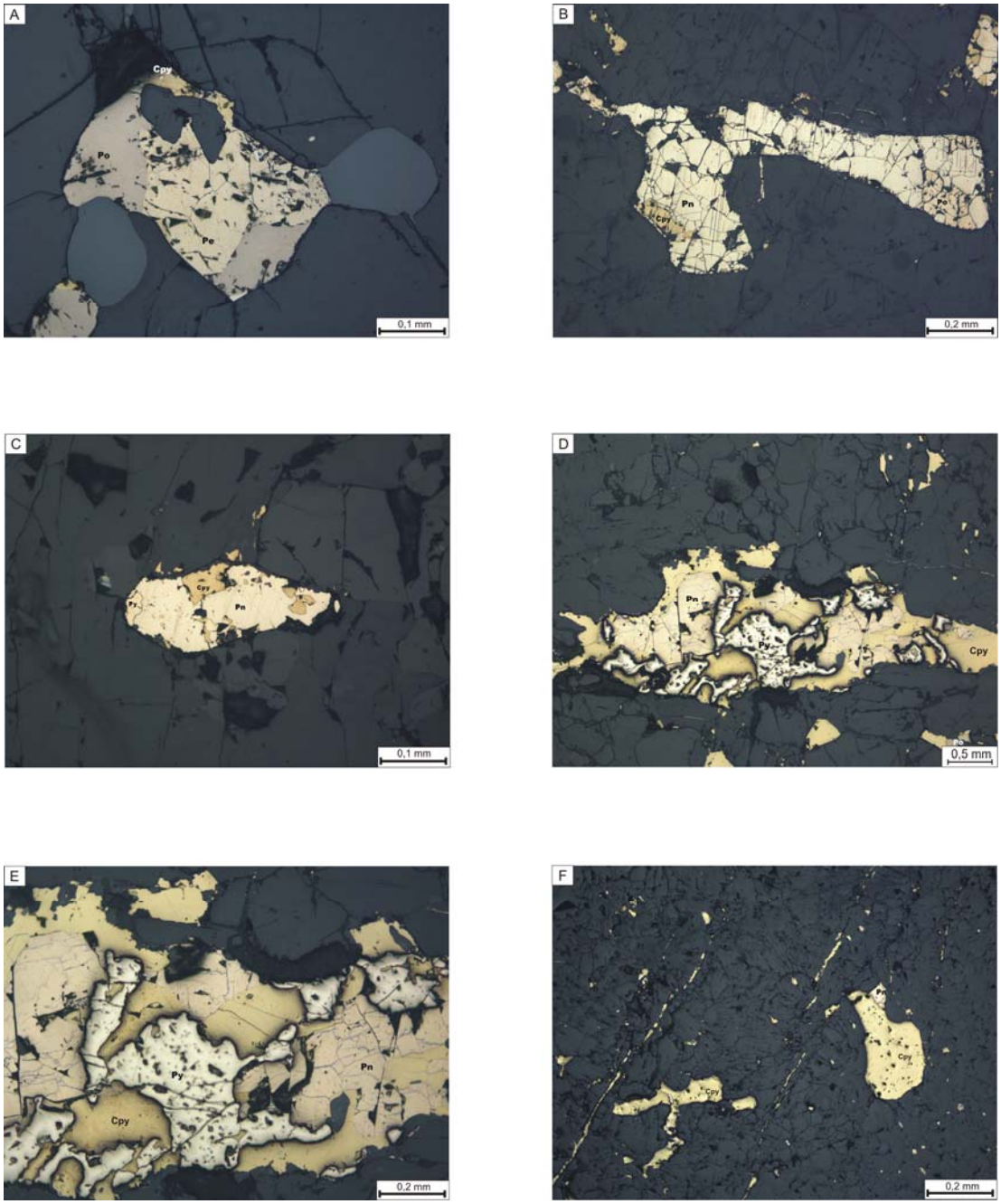

Figure 4.14 - Photomicrographs of sulfides from the Fazenda Mirabela Complex. Observation under Reflected Light and PPL. (A) Harzburgite with interstitial sulfides (pentlandite + chalcopyrite + pyrrhotite). (B) Gabbronorite with interstitial sulfides (pentlandite + chalcopyrite + pyrrhotite). (C) Gabbronorite with interstitial sulfides (pentlandite + chalcopyrite + pyrite). (D) (E) Orthopyroxenite with a sulfide vein consisting of pentlandite + chalcopyrite + pyrite. (F) Orthopyroxenite with sulfide veinlets and blebs of pentlandite + chalcopyrite.

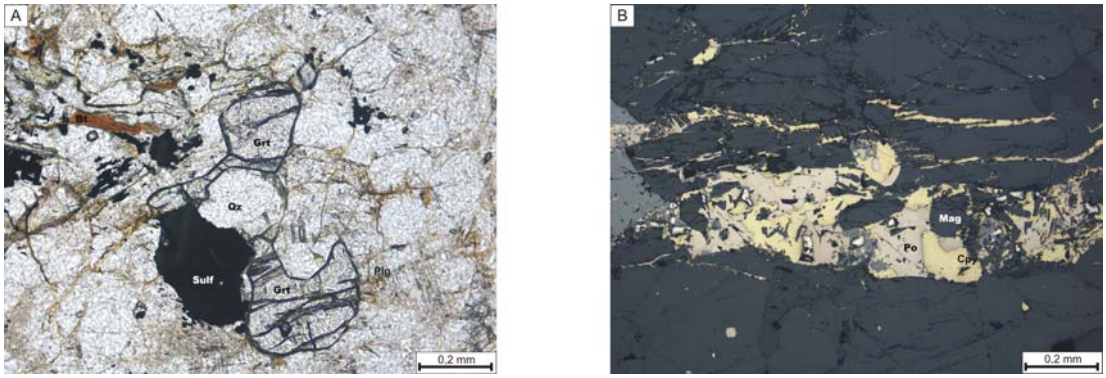

Figure 4.15 - Photomicrographs of the country rocks of Mirabela intrusion. (A) Garnet gneiss with minor sulfides PPL (B) Mafic granulite with veins and blebs of chalcopyrite + pyrrhotite + pyrite. Obsevation under reflected light (PPL).

4.7.3. S isotopes

The sulfur isotopic compositions obtained from sulfides of the Santa Rita and Peri-Peri deposits, as well as sulfides from country rocks, are listed in the Table 4.1 and illustrated in the Figures 4.16 e 4.17. The sulfides were analyzed in a LA-MC-ICPMS and the $\delta^{34}S$ results were related with the Cañon Diablo Troilite (V-CDT).

Sulfide minerals from the Santa Rita deposit are concentrated in a narrow range of values from -1.0 to 0.5 $\delta^{34}S$ ‰ (Figure 4.16). These results correspond to different sulfide minerals (Po, Pn, Cpy, Po) disseminated in mafic-ultramafic rocks. Results are the same for different sulfides and indicate an isotopic composition similar to mantle-derived sulfur. Sulfide minerals from country rocks, including those hosted in graphite-bearing gnaisse (Py and Cpy) and paragranulites (Cpy), have $\delta^{34}S$ ‰ values from 1.5 to 3.0 (Figure 4.16).

Sulfide minerals from the Peri-Peri deposit have $\delta^{34}S$ ‰ values from -2.0 to 1.0 (Figure 4.16). These results correspond to different sulfide minerals (Py, Pn, Cpy, Po) disseminated in mafic-ultramafic rocks. Results are the same for different sulfide minerals and indicate an isotopic composition similar to mantle-derived sulfur. When compared with sulfides from the Santa Rita deposit, sulfides from the Peri-Peri deposit have a broader range of values. Sulfides occurring in veins within host rocks, including gneisses and granulites, located nearby (< 20 meters) the Peri-Peri deposit have $\delta^{34}S$ ‰ values from -0.5 to 1.0. These sulfides consist of associated Pn, Cpy and Py, and are interpreted as primary magmatic sulfides remobilized to the country rocks.

The isotopic composition of sulfide minerals associated with country rocks (1.5 to 3.0 $\delta^{34}S$ ‰) is distictively different from the composition obtained in the sulfide

minerals from the Santa Rita (-1.0 to 0.5 δ^{34}S ‰) and Peri-Peri (-2.0 to 1.0 δ^{34}S ‰) deposits. This feature rules out the possibility that sulfide-bearing country rocks were a significant source of sulfur for the Santa Rita and Peri-Peri Ni-Cu deposit.

The variation of δ^{34}S ‰ values in sulfides throughout the stratigraphy of Santa Rita and Peri-Peri deposits is shown in Figure 4.17. The isotopic results in the deposits show that δ^{34}S ‰ values in sulfides are homogeneous and constant throughout the stratigraphy. Sulfides from the Santa Rita deposit have no systematic variation in sulfide isotopic composition with stratigraphy. Sulfides from the Peri-Peri deposit also have no systematic variation in isotopic sulfide composition with stratigraphy, except for higher values close to the country rocks (Figure 4.17). The latter consist of sulfide minerals in veins host in gneiss and granulite of country rocks. Results from the Peri-Peri deposit suggest that isotopic compositions of Ni-Cu-Fe sulfides (Po, Pn, Cpy, Py) located in nearby country rocks, mainly in veins, result of remobilization of magmatic sulfides, and partial contamination with crustal sulfides from the country rocks (Figure 4.17).

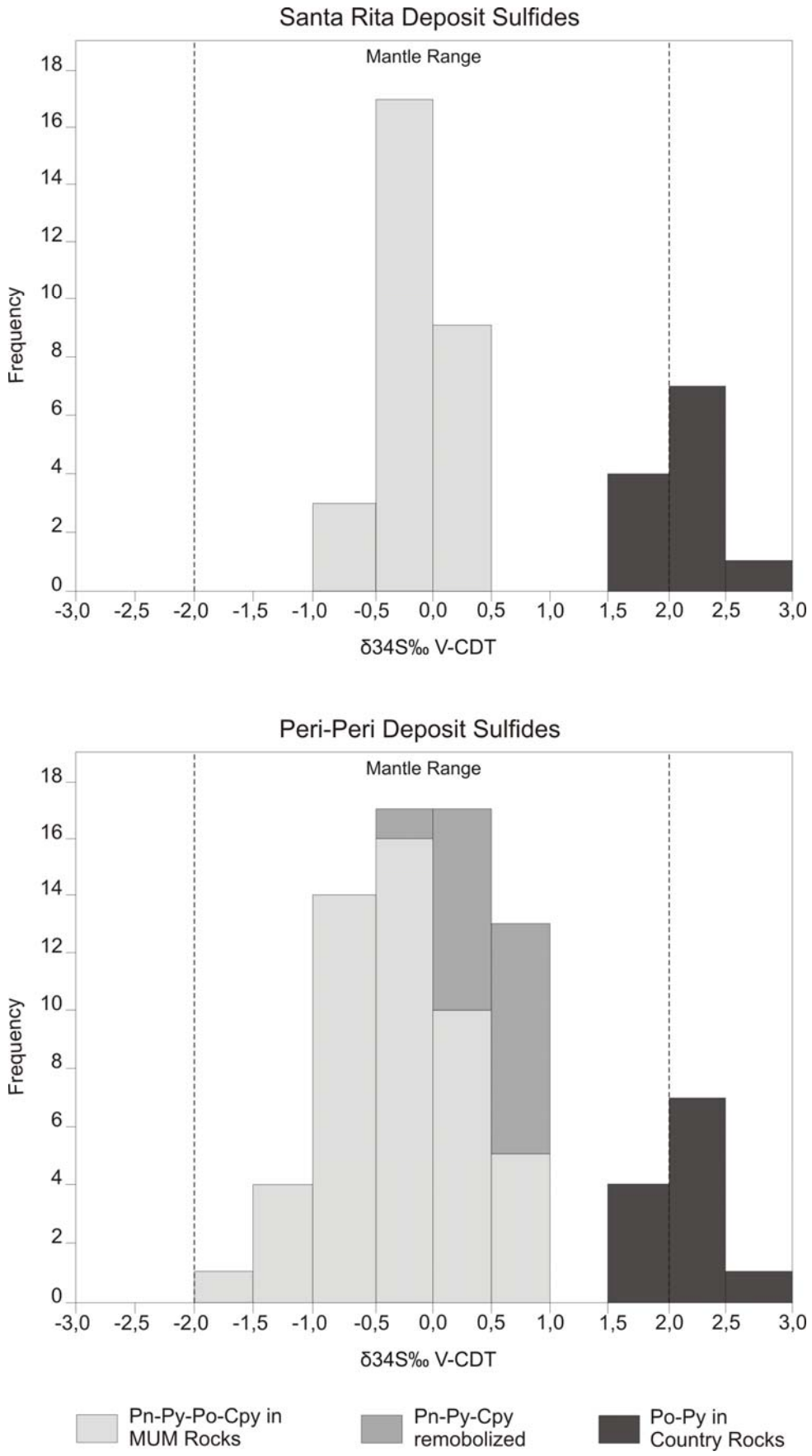

Figure 4.16 - Histogram of δ^{34}S‰ V-CDT values of sulfides from the Santa Rita and Peri-Peri deposits and country rocks.

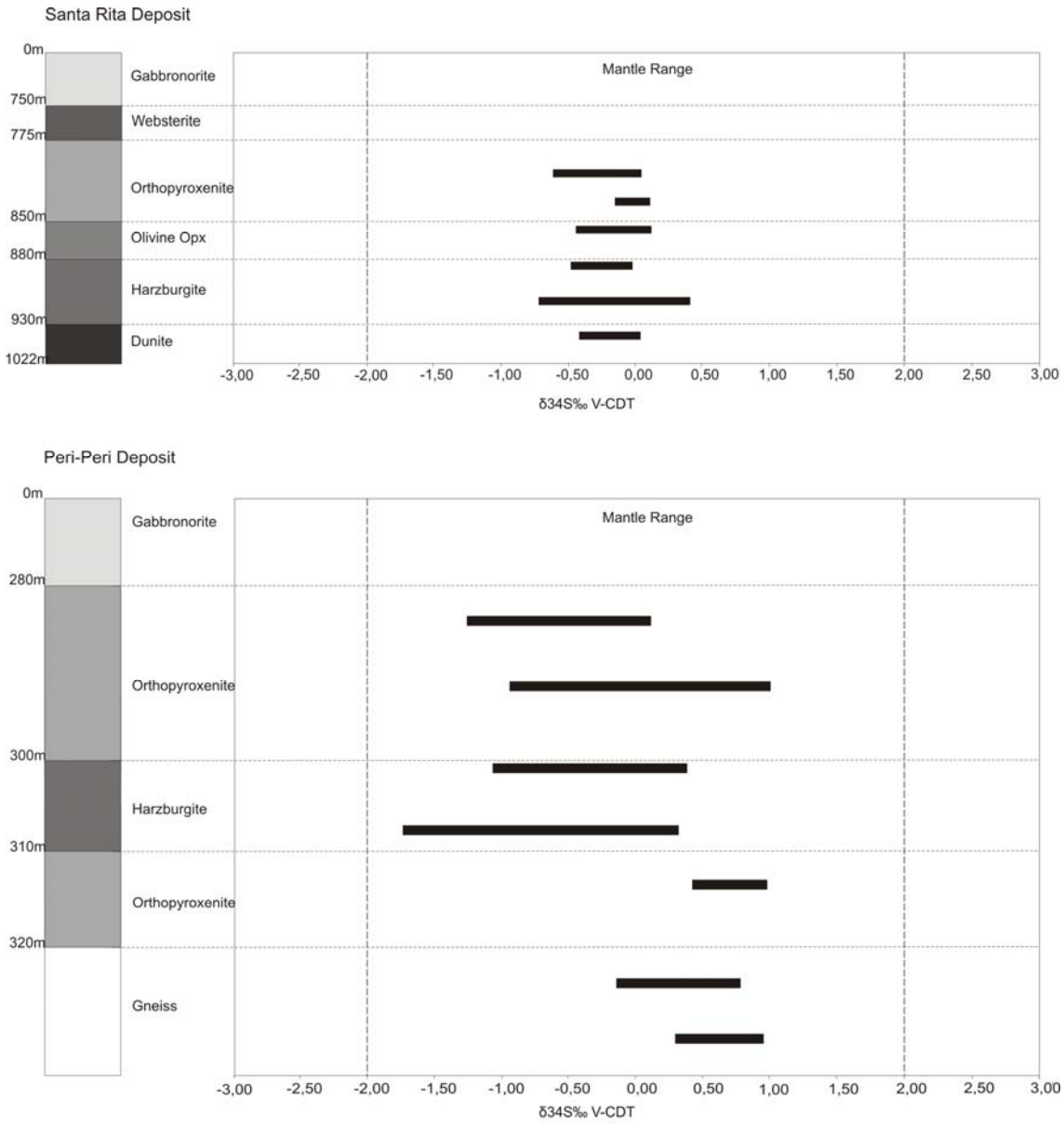

Figure 4.17 – Variation of sulfur isotopic compositions with depth for sulfide minerals of the Santa Rita and Peri-Peri deposits.

Table 4.1 - Representative sulfur isotope data for sulfide minerals of the Fazenda Mirabela Complex.

Sample	Lithology	Mineral	δ34S‰ V-CDT	Depth (m)	Deposit
CFF-12	Dunite	py	-0.16	938.50	Santa-Rita
CFF-12	Dunite	py	-0.39	938.50	Santa-Rita
CFF-12	Dunite	pn	-0.04	938.50	Santa-Rita
CFF-12	Dunite	pn	0.02	938.50	Santa-Rita
CFF-16	Harzburgite	cpy	-0.32	910.60	Santa-Rita
CFF-16	Harzburgite	cpy	-0.69	910.60	Santa-Rita
CFF-16	Harzburgite	pn	0.37	910.60	Santa-Rita
CFF-16	Harzburgite	pn	0.25	910.60	Santa-Rita
CFF-16	Harzburgite	py	0.14	910.60	Santa-Rita
CFF-16	Harzburgite	py	0.38	910.60	Santa-Rita
CFF-20	Harzburgite	pn	-0.04	881.80	Santa-Rita
CFF-20	Harzburgite	pn	-0.08	881.80	Santa-Rita
CFF-20	Harzburgite	py	-0.46	881.80	Santa-Rita
CFF-20	Harzburgite	pn	-0.06	881.80	Santa-Rita
CFF-24	Olivine Orthopyroxenite	pn	0.03	852.30	Santa-Rita
CFF-24	Olivine Orthopyroxenite	pn	-0.42	852.30	Santa-Rita
CFF-24	Olivine Orthopyroxenite	cpy	-0.30	852.30	Santa-Rita
CFF-24	Olivine Orthopyroxenite	pn	0.10	852.30	Santa-Rita
CFF-27	Orthopyroxenite	py	0.09	829.70	Santa-Rita
CFF-27	Orthopyroxenite	py	-0.07	829.70	Santa-Rita
CFF-27	Orthopyroxenite	pn	-0.03	829.70	Santa-Rita
CFF-27	Orthopyroxenite	pn	-0.12	829.70	Santa-Rita
CFF-32	Orthopyroxenite	py	-0.08	806.60	Santa-Rita
CFF-32	Orthopyroxenite	py	-0.18	806.60	Santa-Rita
CFF-32	Orthopyroxenite	po	-0.43	806.60	Santa-Rita
CFF-32	Orthopyroxenite	po	-0.58	806.60	Santa-Rita
CFF-32	Orthopyroxenite	po	-0.59	806.60	Santa-Rita
CFF-32	Orthopyroxenite	pn	-0.05	806.60	Santa-Rita
CFF-32	Orthopyroxenite	pn	0.03	806.60	Santa-Rita
MBS-343_01	Mafic Granulite	py	0.60	47.00	Peri-Peri
MBS-343_01	Mafic Granulite	py	0.73	47.00	Peri-Peri
MBS-343_01	Mafic Granulite	cpy	-0.13	47.00	Peri-Peri
MBS-343_01	Mafic Granulite	cpy	0.27	47.00	Peri-Peri
MBS-343_01	Mafic Granulite	py	0.43	47.00	Peri-Peri
MBS-343_01	Mafic Granulite	py	0.37	47.00	Peri-Peri
MBS-343_01	Mafic Granulite	cpy	0.69	47.00	Peri-Peri
MBS-343_01	Mafic Granulite	cpy	0.58	47.00	Peri-Peri
MBS-391_01	Gneiss	py	0.43	195.40	Peri-Peri
MBS-391_01	Gneiss	py	0.39	195.40	Peri-Peri
MBS-391_01	Gneiss	cpy	0.49	195.40	Peri-Peri
MBS-391_01	Gneiss	cpy	0.76	195.40	Peri-Peri
MBS-391_01	Gneiss	py	0.56	195.40	Peri-Peri
MBS-391_01	Gneiss	py	0.90	195.40	Peri-Peri
MBS-391_01	Gneiss	pn	0.59	195.40	Peri-Peri
MBS-391_01	Gneiss	pn	0.31	195.40	Peri-Peri
MBS-401_03	Orthopyroxenite	py	0.46	314.70	Peri-Peri
MBS-401_03	Orthopyroxenite	py	0.54	314.70	Peri-Peri
MBS-401_03	Orthopyroxenite	pn	0.58	314.70	Peri-Peri
MBS-401_03	Orthopyroxenite	pn	0.49	314.70	Peri-Peri
MBS-401_03	Orthopyroxenite	py	0.43	314.70	Peri-Peri
MBS-401_03	Orthopyroxenite	py	0.58	314.70	Peri-Peri
MBS-401_03	Orthopyroxenite	pn	0.91	314.70	Peri-Peri
MBS-401_03	Orthopyroxenite	pn	0.43	314.70	Peri-Peri
MBS-401_04	Harzburgite	pn	-0.65	308.70	Peri-Peri
MBS-401_04	Harzburgite	pn	-0.37	308.70	Peri-Peri
MBS-401_04	Harzburgite	cpy	-1.72	308.70	Peri-Peri
MBS-401_04	Harzburgite	cpy	-0.63	308.70	Peri-Peri
MBS-401_04	Harzburgite	py	-0.92	308.70	Peri-Peri
MBS-401_04	Harzburgite	py	-0.48	308.70	Peri-Peri
MBS-401_04	Harzburgite	cpy	-0.90	308.70	Peri-Peri
MBS-401_04	Harzburgite	cpy	0.26	308.70	Peri-Peri
MBS-401_06	Harzburgite	pn	-0.73	301.95	Peri-Peri

Cont. Table 4.1 - Representative sulfur isotope data for sulfide minerals of the Fazenda Mirabela Complex.

Sample	Lithology	Mineral	δ34S‰ V-CDT	Depth (m)	Deposit
MBS-401_06	Harzburgite	pn	-0.44	301.95	Peri-Peri
MBS-401_06	Harzburgite	py	0.32	301.95	Peri-Peri
MBS-401_06	Harzburgite	py	-1.05	301.95	Peri-Peri
MBS-401_06	Harzburgite	po	-0.66	301.95	Peri-Peri
MBS-401_06	Harzburgite	po	-0.97	301.95	Peri-Peri
MBS-401_08	Orthopyroxenite	py	0.40	292.90	Peri-Peri
MBS-401_08	Orthopyroxenite	py	-0.42	292.90	Peri-Peri
MBS-401_08	Orthopyroxenite	po	-0.34	292.90	Peri-Peri
MBS-401_08	Orthopyroxenite	po	-0.46	292.90	Peri-Peri
MBS-401_08	Orthopyroxenite	pn	-0.20	292.90	Peri-Peri
MBS-401_08	Orthopyroxenite	pn	-0.19	292.90	Peri-Peri
MBS-401_08	Orthopyroxenite	cpy	0.95	292.90	Peri-Peri
MBS-401_08	Orthopyroxenite	cpy	0.44	292.90	Peri-Peri
MBS-401_08	Orthopyroxenite	po	-0.06	292.90	Peri-Peri
MBS-401_08	Orthopyroxenite	po	-0.39	292.90	Peri-Peri
MBS-401_08	Orthopyroxenite	pn	-0.15	292.90	Peri-Peri
MBS-401_08	Orthopyroxenite	pn	-0.51	292.90	Peri-Peri
MBS-401_08	Orthopyroxenite	po	-0.93	292.90	Peri-Peri
MBS-401_08	Orthopyroxenite	po	-0.71	292.90	Peri-Peri
MBS-401_08	Orthopyroxenite	cpy	-0.23	292.90	Peri-Peri
MBS-401_08	Orthopyroxenite	py	0.19	292.90	Peri-Peri
MBS-401_08	Orthopyroxenite	py	-0.04	292.90	Peri-Peri
MBS-401_10	Orthopyroxenite	po	-1.01	285.60	Peri-Peri
MBS-401_10	Orthopyroxenite	po	-1.24	285.60	Peri-Peri
MBS-401_10	Orthopyroxenite	cpy	-1.03	285.60	Peri-Peri
MBS-401_10	Orthopyroxenite	cpy	-0.83	285.60	Peri-Peri
MBS-401_10	Orthopyroxenite	pn	-0.80	285.60	Peri-Peri
MBS-401_10	Orthopyroxenite	pn	-0.64	285.60	Peri-Peri
MBS-401_10	Orthopyroxenite	cpy	-0.34	285.60	Peri-Peri
MBS-401_10	Orthopyroxenite	cpy	-0.57	285.60	Peri-Peri
MBS-401_10	Orthopyroxenite	py	0.05	285.60	Peri-Peri
MBS-401_10	Orthopyroxenite	pn	-0.18	285.60	Peri-Peri
MBS-401_10	Orthopyroxenite	pn	-0.14	285.60	Peri-Peri
MIR-001_01	Graphite Gneiss	po	1.67	322.90	Country Rocks
MIR-001_01	Graphite Gneiss	po	1.89	322.90	Country Rocks
MIR-001_01	Graphite Gneiss	py	1.99	322.90	Country Rocks
MIR-001_01	Graphite Gneiss	py	2.14	322.90	Country Rocks
MIR-003_02	BIF	po	1.92	255.50	Country Rocks
MIR-003_02	BIF	po	2.33	255.50	Country Rocks
MIR-003_02	BIF	po	2.40	255.50	Country Rocks
MIR-003_02	BIF	po	2.11	255.50	Country Rocks
MIR-003_04	Bt-Hbl Gneiss	po	2.16	185.30	Country Rocks
MIR-003_04	Bt-Hbl Gneiss	po	2.14	185.30	Country Rocks
MIR-003_04	Bt-Hbl Gneiss	po	2.53	185.30	Country Rocks
MIR-003_04	Bt-Hbl Gneiss	po	2.40	185.30	Country Rocks

4.7.4. Sm-Nd isotopes

The Sm-Nd isotopic data presented in this work were determined for 15 samples of the Santa Rita and Peri-Peri deposits and summarized in the Table 4.2. The samples selected are different types of mafic-ultramafic rocks with igneous textures and mineralogy (harzburgite, orthopyroxenite, websterite and gabbronorite) and one sample representative of country rocks (garnet gneiss) of the Mirabela Intrusion.

The sample FM-03 is a pegmatoidal gabbronorite occurring as irregular dykes (or pods) at the base of the gabbronorite unit, located in the hanging wall of the Santa Rita deposit. This rock is interpreted as a concentration of trapped intercumulus liquid enriched in volatiles and incompatible elements. This sample was selected for U-Pb age dating of the Mirabela Complex (see Chapter 5). The ε Nd(t) results were calculated based on zircon U-Pb ages described in Chapter 5. The U-Pb isotopic studies defined a crystallization age of 1990 Ma for the Mirabela Complex and of 2542 Ma for the country rocks of the mafic-ultramafic intrusion.

Table 4.2 – Sm-Nd isotopic data for Fazenda Mirabela Complex and country rock, and Palestina Intrusion.

Sample	Lithology	Deposit	Sm (ppm)	Nd (ppm)	$^{147}Sm/^{144}Nd$	$^{143}Nd/^{144}Nd$	ε Nd (0)	T1 (Ma)	ε (T1)
CFF-20	Harzburgite	Santa Rita	0,138	0,516	0,1620	0,511953+/-82	-13,36	1990	-4,52
CFF-27	Orthopyroxenite	Santa Rita	0,202	0,763	0,1598	0,511996+/-22	-12,52	1990	-3,11
CFF-32	Orthopyroxenite	Santa Rita	0,217	0,861	0,1526	0,511856+/-14	-15,25	1990	-4,01
CFF-40	Websterite	Santa Rita	0,721	2,090	0,2086	0,512546+/-18	-1,79	1990	-4,86
CFF-41	Websterite	Santa Rita	0,700	2,181	0,1940	0,512464+/-26	-3,39	1990	-2,72
CFF-48	Gabbronorite	Santa Rita	0,428	1,444	0,1793	0,512159+/-14	-9,34	1990	-4,92
CFF-61	Gabbronorite	Santa Rita	0,610	2,334	0,1579	0,511782+/-11	-16,70	1990	-6,82
FM-03	Pegm. Gabbronorite	Santa Rita	1,034	4,382	0,1426	0,511658+/-5	-19,12	1990	-5,32
FM-06	Gabbronorite	Santa Rita	0,631	2,475	0,1541	0,511728+/-12	-17,75	1990	-6,90
MBS-497/01	Garnet Gneiss	Country Rock	2,406	12,801	0,1136	0,511054+/-10	-30,90	2542	-3,75
MBS-401/03	Orthopyroxenite	Peri-Peri	0,991	4,137	0,1448	0,511714+/-36	-18,02	1990	-4,79
MBS-401/06	Harzburgite	Peri-Peri	0,580	2,451	0,1431	0,511668+/-9	-18,92	1990	-5,25
MBS-401/08	Orthopyroxenite	Peri-Peri	0,425	1,730	0,1487	0,511619+/-14	-19,88	1990	-7,65
MBS-401/10	Orthopyroxenite	Peri-Peri	1,046	4,167	0,1517	0,511681+/-15	-18,67	1990	-7,21
MBS-401/17	Websterite	Peri-Peri	0,975	4,258	0,1385	0,511608+/-24	-20,09	1990	-5,25
MBS-401/20	Gabbronorite	Peri-Peri	1,300	5,414	0,1451	0,511875+/-65	-14,88	1990	-1,71
MBS-401/28	Gabbronorite	Peri-Peri	0,808	3,282	0,1487	0,511908+/-18	-14,24	1990	-1,98
MBP-019/01	Orthopyroxenite	Palestina	0,964	4,051	0,1438	0,511654+/-20	-19,19	2070	-5,16

The mafic-ultramafic rocks of the Mirabela Complex have $^{147}Sm/^{144}Nd$ ratios between 0.1385 and 0.2086, whereas the garnet gneiss have $^{147}Sm/^{144}Nd$ ratio of 0.1136. The ε Nd values for samples of the Mirabela Complex are variable and systematically negative.

The Figure 4.18 shows the ε Nd(t) values and $^{147}Sm/^{144}Nd$ ratios evolution for the Santa Rita and Peri-Peri stratigraphic profiles. The results of the ε Nd(t) are negative with a variation of -7.65 to -1.71, suggesting that the magma was contaminated with

older crustal rocks. The small variation in Sm-Nd ratios is consistent with the mafic-ultramafic rocks hosting both deposits being associated with the same parental magma.

The Figure 4.19 presents the ε Nd(t) isotopic evolution during the geological time for the Fazenda Mirabela Intrusion and the country rock garnet gneiss. Combined crystallization age (Chapter 5) and isotopic compositions are consistent with the crystallization of the Fazenda Mirabela Intrusion from an undepleted mantle-derived magma that was contaminated with older crustal material during ascent and emplacement.

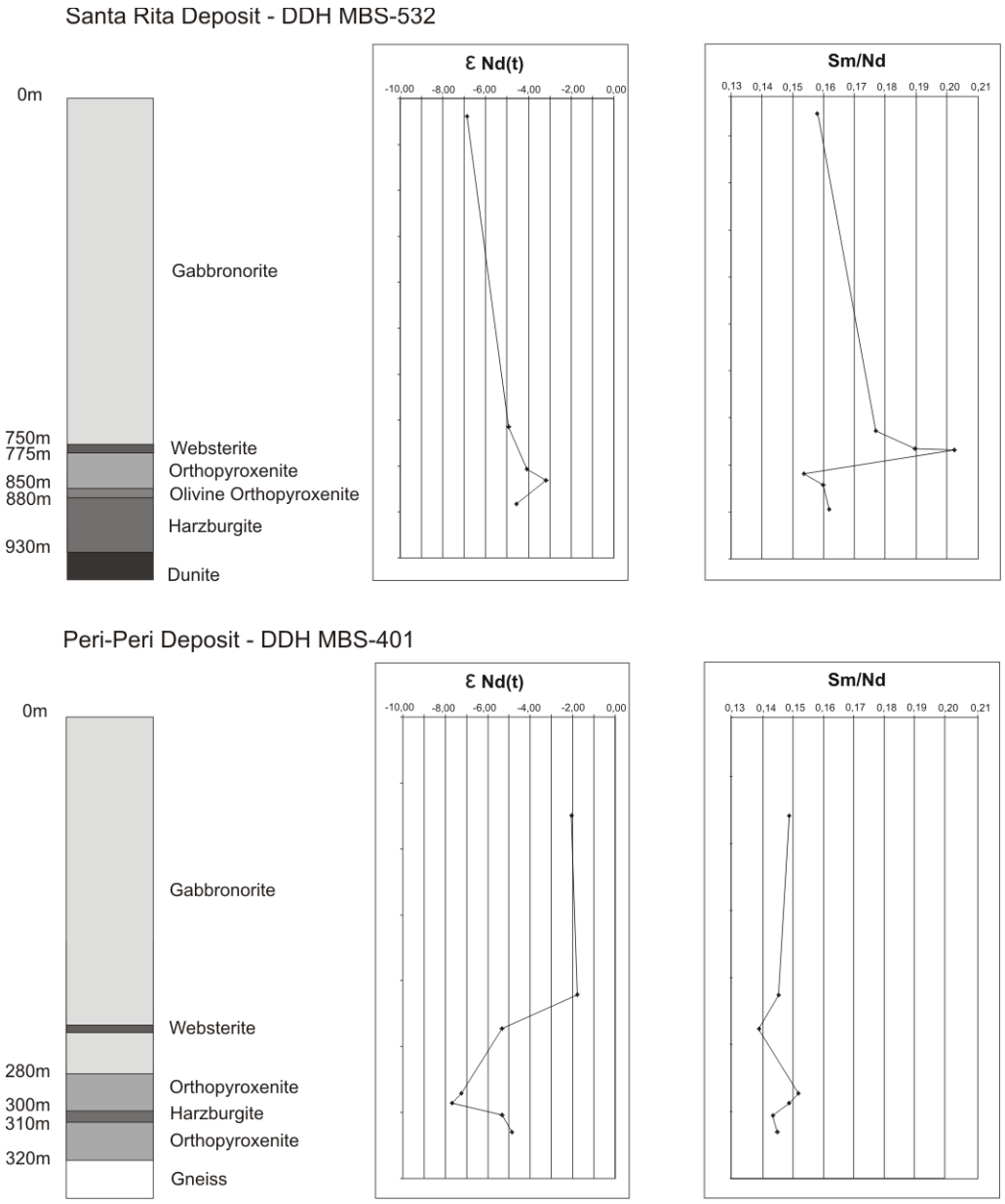

Figure 4.18 – Plot of ε Nd (T) and Sm-Nd throught the stratigraphy for the Santa Rita and Peri-Peri deposits.

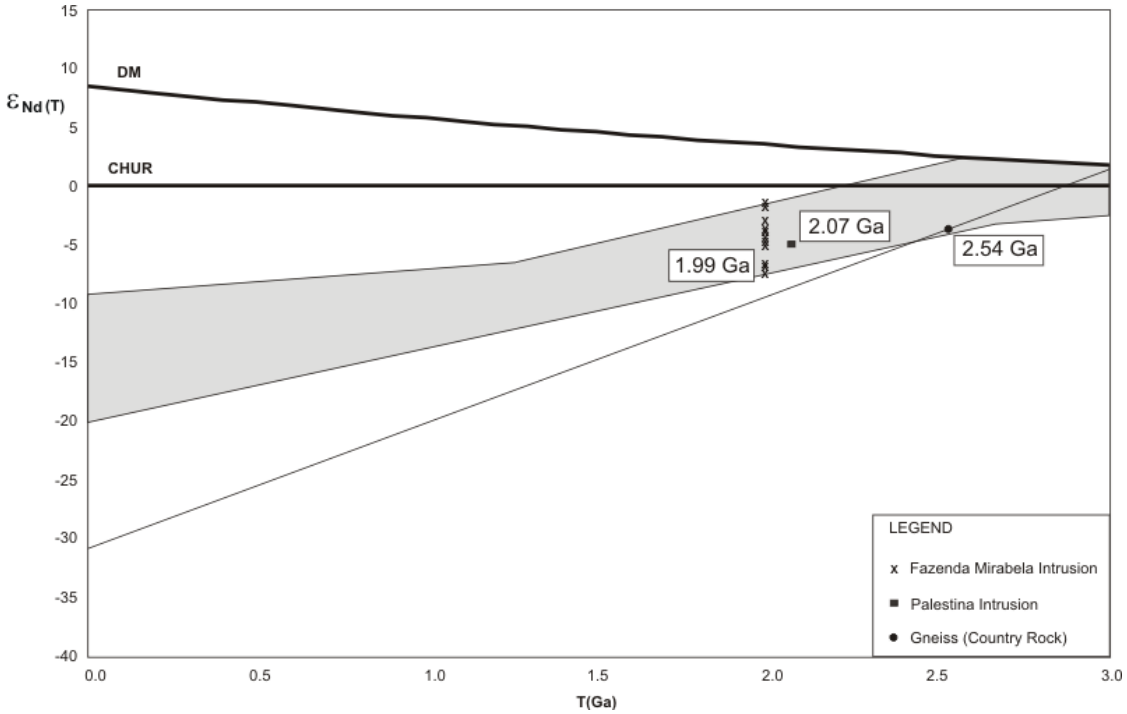

Figure 4.19 – ε Nd isotopic evolution diagram (modified from De Paolo 1988) comparing isotopic compositions versus time for Fazenda Mirabela Intrusion and the country rock.

4.8. Discussion

During the Paleoproterozoic Orogeny (2.3-2.0 Ga) the crustal segments Jequié, Gavião, Serrinha Blocks and Itabuna–Salvador–Curaçá Belt collided, resulting in the formation of the Itabuna-Salvador-Curaçá Orogeny. The 1.99 Ga Fazenda Mirabela Complex intruded highly deformed and metamorphosed 2.54 Ga crustal rocks in the final stages of this orogeny. Combined crystallization age (1.99 Ga) and variable but systematically negative ε Nd(t) values are consistent with the crystallization of the Fazenda Mirabela Intrusion from an undepleted mantle-derived magma that was contaminated with older crustal material during ascent and emplacement.

The Mirabela Intrusion has undergone a process of magmatic fractionation responsible for the stratigraphic and mineralogical composition of the body. The mineralogy of the intrusion is characteristic of a mafic-ultramafic layered body, whose stratigraphy is defined from the base to the top in five zones according with lithological and petrographical parameters: Lower Border Group – gabbronorites and orthopyroxenites; Lower Zone – dunites; Intermediate Zone: harzburgites, olivine orthopyroxenites, orthopyroxenites and websterites; Upper Zone: gabbronorites; and Upper Border Group: websterites, orthopyroxenites, harzburgites and gabbronorites.

The sulfide mineralization occurs disseminated throughout the Mirabela Complex, with economic concentrations of Ni-Cu sulfides associated with the transition from ultramafic cumulates to mafic cumulates, at the upper part of the ultramafic zone. The mineral assemblage of the sulfides is characterized by pentlandite, chalcopyrite, pyrite and pyrrhotite.

Several studies suggest that assimilation of crustal sulfur is important, and eventually essential, for the genesis of world-class Ni-Cu sulfide deposits (Barnes & Lightfoot 2005; Ripley & Li 2003). The importance of an external source of sulfur for the origin of magmatic Ni–Cu sulfide mineralizations is indicated by the $\delta^{34}S$ ‰ values for many deposits (Figure 4.20). Isotopic compositions of sulfide minerals from the Santa Rita and Peri-Peri Ni-Cu deposits are bracket between $\delta^{34}S$ ‰ values of -1.72 and +0.95, suggesting that the sulfur was transferred from the mantle by mafic magmas (Figure 4.20). On the other hand, the isotopic composition of sulfide minerals associated with country rocks is distictively different from the composition obtained in the sulfide minerals from the Santa Rita and Peri-Peri deposits. This feature rules out the possibility that sulfide-bearing country rocks were a significant source of sulfur for the Santa Rita and Peri-Peri Ni-Cu deposit. This study provides an additional example of Ni-Cu sulfide deposit where sulfur is considered to be entirely mantle-derived, like the Nebo-Babel Ni–Cu–PGE deposit (Seat et al. 2009), the Platreef PGE–Ni–Cu deposit (Penniston-Dorland et al. 2008) and the Americano do Brasil Ni-Cu deposit (Mota-e-Silva et al. 2010). Evidence for mainly mantle-derived sulfur in Ni–Cu magmatic deposits has implication for mineral exploration, indicating that an external source of sulfur is not fundamental for the origin of world-class deposits.

The Ni-Cu deposits in the world have constraints associated with the contamination of magma by crustal rocks with sulfur enrichment, and mineral assemblages consisted for pentlandite, chalcopyrite and pyrrhotite. The Mirabela Intrusion can be considered an exception between the global layered complexes, because suffered crustal contamination of the mafic-ultramafic magma during the ascension of the body, but there was no assimilation of sulfur from the country rocks. The sulfur has mantle origin and forms a distinct sulfide assemblage, composed for pentlandite, chalcopyrite, pyrrhotite and pyrite.

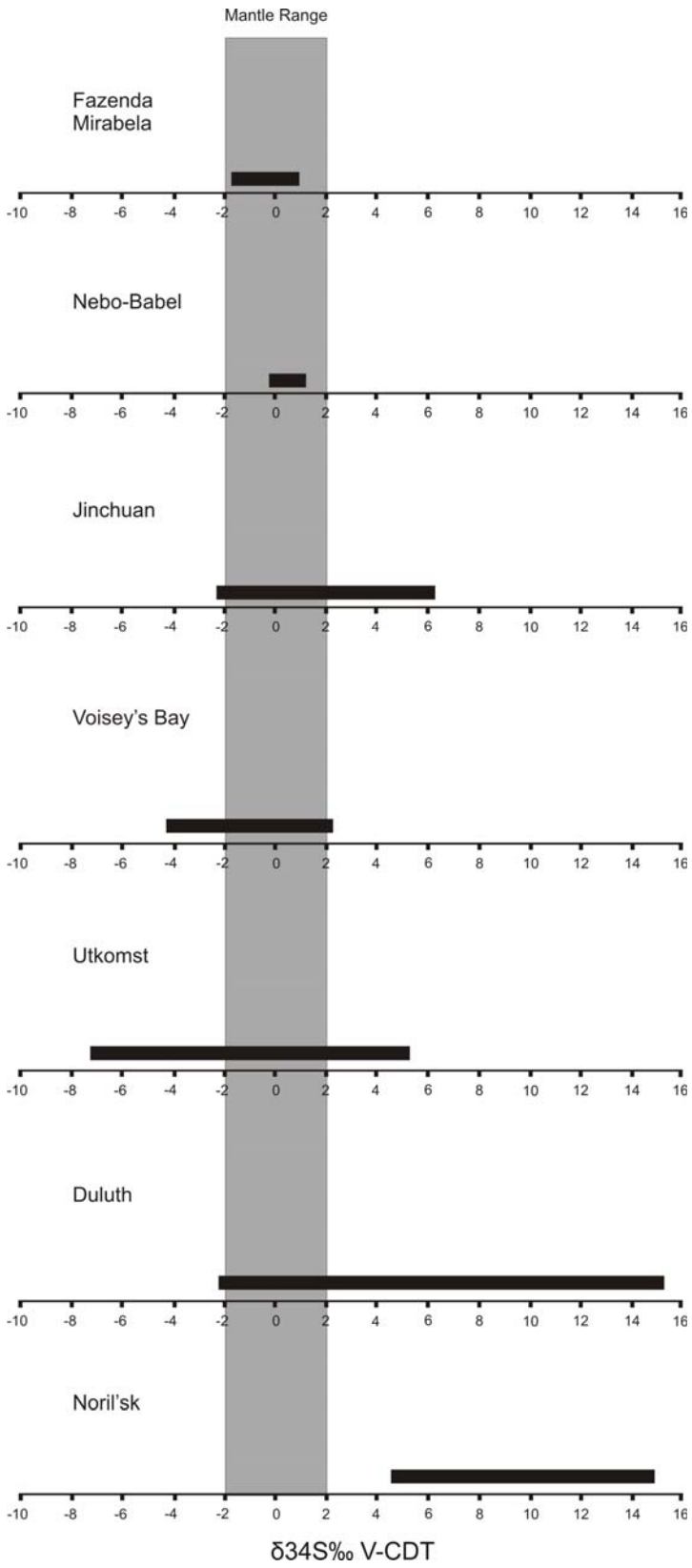

Figure 4.20 – Relation of the $\delta^{34}S$ data for magmatic Ni-Cu-PGE deposits of the world.

4.9. Conclusions

The new isotopic and geochronological data presented in this study, combined with re-interpretation of existing data in the literature and provided by the company Mirabela Mineração do Brasil Ltda, allow some relevant conclusions about the mafic-ultramafic rocks intruded on the south portion of Itabuna-Salvador-Curaçá Belt during the Paleoproterozoic Orogeny (2.3 – 2.0 Ga).

The summary of the conclusions of this study is presented below.

- The Fazenda Mirabela Complex was dated at 1.99 Ga with U-Pb method on zircon grains. The Mirabela Complex intruded Archean granulite facies orthogneisses (charnockites and enderbites) and supracrustal rocks of the Itabuna-Salvador-Curaçá Belt in the final stages of the Paleoproterozoic Orogeny.

- The Mirabela Complex was submitted to a magmatic fractionation process during the cooling phase, responsible for the stratigraphy and mineralogy of the body. The intrusion was subdivided according with lithological and petrographical parameters in five zones: Lower Border Group – gabbronorites and orthopyroxenites; Lower Zone – dunites; Intermediate Zone: harzburgites, olivine orthopyroxenites, orthopyroxenites and websterites; Upper Zone: gabbronorites; and Upper Border Group: websterite, orthopyroxenite, harzburgite and gabbronorite.

- Geochemical analyses in Peri-Peri diamond drill holes defined the distribution of Ni, Cu, Pt and Pd contents associated with mafic-ultramafic horizons with predominance of disseminated sulfides. High sulfur contents are related to an increase of sulfidation and are mainly associated to ultramafic horizons of the intrusion.

- Systematic studies of petrography in drill holes of the Santa Rita and Peri-Peri deposits reported occurrences of polycrystalline aggregates of disseminated Ni-Cu sulfides, associated with a strong lithostratigraphic control, from the harzburgites to websterites in Santa Rita, and the websterites to

harzburgites in Peri-Peri. These results suggest the occurrence of primitive rocks on the top of the magmatic camara. The mineralogical assemblage of the sulfides is composed for pentlandite, chalcopyrite, pyrrhotite and pyrite, disseminated and in economic concentrations of Ni and Cu associated with the transition from ultramafic to mafic cumulates, at the upper part of the ultramafic zone.

¤ The isotopic studies of $\delta^{34}S$ in sulfide minerals (Pn, Cpy, Po, Py) obtained values between -1.0 to 0.5 ‰ $\delta^{34}S$ for Santa Rita and -2.0 to 1.0 ‰ $\delta^{34}S$ for Peri-Peri, results that indicate an isotopic composition similar to mantle-derived sulfur. Sulfide minerals from country rocks, including those hosted in graphite-bearing gnaisses (Py and Cpy) and paragranulites (Cpy), have $\delta^{34}S$ ‰ values from 1.5 to 3.0. Sulfides (Pn, Cpy and Py) occurring in veins within host rocks, including gneisses and granulites, located nearby (< 20 meters) the Peri-Peri deposit have $\delta^{34}S$ ‰ values from -0.5 to 1.0, and are interpreted as primary magmatic sulfides remobilized to the country rocks. The isotopic composition of sulfide minerals of the Santa Rita and Peri-Peri deposits are distictively different from the composition obtained in the sulfide minerals of the country rocks. This feature rules out the possibility that sulfide-bearing country rocks were a significant source of sulfur for the Santa Rita and Peri-Peri Ni-Cu deposits.

¤ The Sm-Nd analyses realized in the rocks of the Santa Rita and Peri-Peri deposits resulted in ε Nd values of -7.65 to -1.71. The Sm-Nd ratios are similar for rocks hosting the Santa Rita and Peri-Peri deposits, suggesting that they were formed by the same parental magma. The U-Pb age and isotopic compositions are consistent with the crystallization of the Fazenda Mirabela Intrusion from an undepleted mantle-derived magma that was contaminated with older crustal material during ascent and emplacement.

The metallogenic potential of Itabuna-Salvador-Curaçá Belt in São Francisco Craton is relevant to occurrences of new Ni-Cu-PGE sulfide deposits, because there are several mafic-ultramafic intrusions along the block, and probably can be associated with

the Paleoproterozoic Orogeny responsible for the mineralized intrusion of the Fazenda Mirabela Complex.

4.10. Acknowledgments

The authors are grateful to CNPq and CAPES for continuous support to field and laboratory work through research grants and schollarships. This study was partially supported by Mirabela Mineração do Brasil Ltda. The company provided field access to the Santa Rita and Peri-Peri deposits, the data base, and permitted geological descriptions and samplings in the diamond drill holes. The geologist Douglas Cook is acknowledged for the greateful assistance during the field work in Fazenda Mirabela Complex. The staff of the Geochronology Laboratory is thanked for the assistance during the isotopic analyses.

4.11. References

Abram, M.B., Silva, M.G. 1992. O corpo máfico-ultramáfico da Fazenda Mirabela, Ipiaú-BA-Química Mineral, Litogeoquímica e Evolução Petrogenética. In: Congresso Brasileiro de Geologia 37˚, São Paulo, Brazil External Abstract SBG.1 pp. 449–450.

Abram, M. B. O corpo máfico-ultramáfico da Fazenda Mirabela, Ipiaú-Ba: caracterização petrográfica, geoquímica, tipológica e implicações metalogenéticas. 1993. 137 f. Dissertação (Mestrado) - Instituto de Geociências, Universidade Federal da Bahia, Salvador, 1993.

Abram, M.B. 1994, O corpo máfico-ultramáfico da Fazenda Mirabela, Ipiaú-BA: caracterização petrográfica, geoquímica, tipologia e implicações metalogenéticas, in Marinho, M.M., ed.: Salvador-Bahia, Sociedade Brasileira de Geologia, Núcleo Bahia-Sergipe, 58p.

Alibert, C.; Barbosa, J. S. F. Ages U-Pb determines a la SHRIMP sur des zircons du Complexe de Jequié, Cráton de São Francisco, Bahia, Brésil. In: Reunion des Sciences de la Terre (RST), 1992. Toulouse. 14 p.

Almeida, F.F.M. 1977. O Cráton do São Francisco. Revista Brasileira de Geociências, 7(4), p349-364.

Barbosa, J.S.F. 1990. The granulites of the Jequié Complex and Atlantic mobile belt, Southern Bahia, Brazil – An expression of archean proterozoic plate convergence. In: Vielzeuf, Ph. Vidal, Process of ARW. ed. Granulites and Crustal Evolution. Clermont Ferrand (France), Springer-Verlag, 585p.

Barbosa, J.S.F. and Sapucaia, N.S. 1996. Os Corpos Máficos-Ultramáficos da Região de Ipiaú-Bahia e suas Encaixantes Granulitizadas. Congresso Brasileiro de Geologia 39˚, Anais, Salvador: SBG, n.6, pp279-285.

Barbosa J.S.F. and Sabaté P. 2002. Geological features and the Paleoproterozoic collision of four Archean crustal segments of the São Francisco Craton, Bahia, Brazil. A synthesis. Anais Academia Brasileira de Ciências, 74:343-359.

Barbosa, J. S. F.; Sabaté, P.; Marinho, M. M. 2003. O Cráton do São Francisco: uma síntese. Revista Brasileira de Geociências, 33: 3-6.

Barbosa, J.S.F and Sabaté, P. 2004. Archaean and Paleoproterozoic crust of the São Francisco Craton, Bahia, Brazil: geodynamic features. Precambrian Research, 133, pp1-47.

Barbosa, J.S.F (Coordenador) Pinho, I.C.A., Sobrinho, V.R.S., Cruz, S.C.P. Companhia de Pesquisa de

Recursos Minerais – CPRM/Serviço Geológico do Brasil. Ipiaú- SD.24-Y-B-II, escala 1:100.000: nota explicativa. Bahia: UFBA/CPRM, 2007.

Barnes, S. J. and Lighfoot, P.C. 2005. Formation of Magmatic Nickel Sulfide Ore Deposits and Processes Affecting Their Copper and Platinum Group Element Contents. In Hedenquist, J.W., Thompson, J.F.H., Goldfarb, R.J. and Richards, J.P. (eds.) Economic Geology 100th Anniversary Volume, p. 179-213.

Barnes, S. J., Osborne, G. A., Cook, D., Barnes, L., Maier, W. D., Godel, B. 2011. The Santa Rita Nickel Sulfide Deposit in the Fazenda Mirabela Intrusion, Bahia, Brazil: Geology, Sulfide Geochemistry, and Genesis. Society of Economic Geologists, Inc. Economic Geology, v. 106, pp. 1083-1110.

Boyd R., Mathiesen C.O. 1979. The nickel mineralization of the Rana mafic intrusion Nordland Norway. Can Min 17: 287-298.

Corrêa-Gomes, L.C.; Oliveira, E.P. Dados Sm-Nd, Ar-Ar e Pb-Pb de Corpos Plutônicos no Sudeste da Bahia, Brasil. Implicações para o Entendimento da Evolução Tectônica no Limite Orógeno Araçuaí/Cráton do São Francisco. Revista Brasileira de Geociências 32(2):185-196, junho de 2002.

Cunha, J.C.; Fróes, R.J.B ; Garrido, I.A. 1991. Projeto Verificações Minerais no Estado da Bahia - Prospecto Fazenda Mirabela. Convênio SME/CBPM, Salvador.

Cunha, J.C.; Fróes, R.J.B., 1992, Complexo máfico-ultramáfico da Fazenda Mirabela (CFM): geologia e mineralização: Congresso Brasileiro de Geologia, 37, São Paulo-SP, v. 2, p. 158-159.

Cunha, J.C.; Garrido, I.V. de A. E Fróes, R.J.B. 1998. Projeto Verificações Minerais no Estado da Bahia - Prospecto Fazenda Mirabela. Salvador, CBPM. Unpublished.

DePaolo, D.J., 1981. A neodymium and strontium isotopic study of the Mesozoic calc-alkaline granitic batholiths of the Sierra Nevada and Peninsular Ranges, California. Journal of Geophysical Research 86, 10470-10488.

DePaolo, D.J. 1988. Neodymium Isotope Geochemistry. Springer-Verlag, Berlin, 181 p.

Eckstrand, O.R. 1996. Magmatic nickel-copper-platinum group elements; in Geology of Canadian Mineral Deposit Types, (ed.) O.R. Eckstrand, W.D. Sinclair, and R.I. Thorpe; Geological Survey of Canada, Geology of Canada, no. 8, p. 583 (also Geological Society of America, The Geology of North America, v. P-1).

Ferreira, M.J., Moraes, A.M.de V. e Fróes, R.J.B. 2000. Projeto Avaliação de Ni-Cu-Platinóides na Faixa Ipiaú. Relatório de Atividades e Técnico Preliminar. Parte II – Programa Secundário de Sondagem. CBPM, Salvador, Bahia. Julho 2000. Unpublished.

Fletcher TA. 1987. Nickel-copper and precious metal mineralization in the Caledonian mafic and ultramafic intrusions of north-east Scotland (abs). In Geoplatinum 87 (eds HM Pritchard, PJ Potts, JFW Bowles, SJ Cribb). Elsevier, p.163.

Fróes, R. J. B. Petrology, geochemistry and Cu-Ni-PGE the Fazenda Mirabela Complex, Bahia. 1993. 175 f. Dissertação (Mestrado) - Toronto University, Canadá, 1993.

Fróes, R.J.B. e Moraes, A.M.de V. Projeto Avaliação de Ni-Cu-Platinóides na Faixa Ipiaú. Relatório de Atividades e Técnico Preliminar. Parte I – Programa Primário de Sondagem. CBPM, Salvador, Bahia. Julho 2000. Unpublished.

Gioia, S.M.C.L., Pimentel, M.M.. 2000. The Sm-Nd isotopic method in the Geochronology Laboratory of the University of Brasília. Anais Academia Brasileira de Ciências 72, 219-245.

Loureiro, H. S. C. (Organizador). Programa levantamentos geológicos básicos do Brasil: Mundo Novo. Folha SC.24-Y-D-IV. Escala 1:100.000. DNPM/CPRM/SUREG-SA, 1991. 196 p.

Melo, R. C. Programa de levantamentos geológicos básicos do Brasil (PLGB): Folha SD.24-Y-D-V, Pintadas, Estado da Bahia. Brasília: Convênio DNPM/CPRM, 1991. 192 p.

Melo, R. C.; Loureiro, H. S. C.; Pereira, L. H. M. Programa levantamentos geológicos básicos do Brasil (PLGB): Folha SC.24-Y-D, Serrinha. Escala 1:250.000. MME/CPRM/SUREG-SA, 1995. 80 p.

Mirabela Nickel Limited. 2007. Santa Rita and Serra Azul Projects. Revised Technical Report. Prepared by RSG Global Consulting Pty Ltd. Bahia, Brazil.

Misi, A. and Silva, M.G. 1992. Algumas feições metalogenéticas relacionadas à evolução geodinâmica do Cráton do São Francisco. In: Congresso Brasileiro de Geologia, 37°, São Paulo, SBG/SP, v.2, p.225-226.

Mota-e-Silva, J., Ferreira Filho, C.F., Buhn, B.M. and Dantas, E.L. 2010. Geology, Petrology and Geochemistry of the "Americano do Brasil" Layered Intrusion and its Ni-Cu Sulfide Deposits, Central Brazil. Mineralium Deposita, v. 46, p. 57-90.

Naldrett, A.J., 2004. Magmatic sulfide deposits: Geology, geochemistry and exploration. Heidelberg,

Berlin, Springer Verlag, 728 p.

Penniston-Dorland, S.C. Wing, B.A. Nex, P.A.M. Kinnaird, J.A. Farquhar, J. Brown, M. Sharman, E.R. Multiple sulfur isotopes reveal a magmatic origin for the Platreef platinum group element deposit, Bushveld Complex, South Africa. Geology; December 2008; v. 36; n°. 12; p. 979-982; Geological Society of America.

Peucat, J.J., Figueiredo Barbosa, J.S., de Araújo Pinho, I.C., Paquette, J.L., Martin, H., Fanning, M., de Menezes Leal, A.B., Cruz, S. Geochronology of granulites from the south Itabuna-Salvador-Curaçá Block, São Francisco Craton (Brazil): Nd isotopes and U-Pb zircon ages, Journal of South American Earth Sciences 2011, doi: 10.1016/j.jsames.2011.03.009.

Ripley, E.M.. Li, C. 2003. Sulfur isotopic exchange and metal enrichment in the formation of magmatic Cu-Ni-(PGE) deposits. Economic Geology 98:635-641.

Sato, K. Evolução crustal da plataforma Sul Americana com base na geoquímica isotópica Sm-Nd. 1998. 297 f. Tese (Doutorado) - Instituto de Geociências, Universidade de São Paulo, 1998.

Seat, Z. Beresford, S.W. Grguric, B. A. Mary Gee, M.A. Grassineau, N.V. Reevaluation of the Role of External Sulfur Addition in the Genesis of Ni-Cu-PGE Deposits: Evidence from the Nebo-Babel Ni-Cu-PGE Deposit, West Musgrave, Western Australia. 2009 Society of Economic Geologists Inc. Economic Geology, v. 104, pp. 521-538.

Silva et al, L. C. U–Pb SHRIMP ages in the Itabuna-Caraíba TTG high - grade Complex: the first window beyond the Paleoproterozoic overprint of the eastern Jequié Craton, NE Brazil. In: International Symposium on Granites and Associated Mineralization. Abstracts. Salvador, 1997. p. 282-283.

Silva, M. G. da; Barbosa, J.S.F., and Misi, A. 1992. A faixa Aratuípe-Nova Canaã: um trend de corpos máficos e ultramáficos de grande potencial metalogenético no cinturão granulítico Jequié-Itabuna (BA). In: Congresso Brasileiro de Geologia 37°, São Paulo, v2, p. 227.

Teixeira, L. R. O Complexo Caraíba e a Suíte São José do Jacuípe no Cinturão Salvador-Curaçá (Bahia, Brasil): petrologia, geoquímica e potencial metalogenético. 243 f. Tese (Doutorado) - Instituto de Geociências, Universidade Federal da Bahia, Salvador, 1997.

Thompson, J.F.H.; Naldrett A.J. 1984. Sulfide-silicate reactions as a guide to Ni-Cu-Co mineralization in central Maine. In Sulfide deposits in mafic and ultramafic rocks (eds. DL Buchanan, MJ Jones). Inst Mining Metall Special Publication, pp. 103-113.

Whitney D.L., Evans B.W. 2010 Abbreviations for names of rock-forming minerals. American Mineralogist 95: 185-187.

Whitney, J. A. and Naldrett, A. J. (eds), 1989. Ore deposits associated with magmas. Society of Economic Geology, Reviews in Economic Geology, vol. 4, 250 p.

Wilson, N. Combined Sm-Nd, Pb/Pb and Rb-Sr geochronology and isotope geochemistry in polymetamorphic precambrian terrains: examples from Bahia, Brazil and Channel Island, U.K. 150 f. MSC - Oxford University, 1987.

5. GEOCRONOLOGIA

Análises U-Pb foram realizadas em amostras do Complexo Fazenda Mirabela e a respectiva rocha encaixante (granada gnaisse), e na Intrusão Palestina (Anexo 4). Os resultados analíticos em zircões estão apresentados na Tabela 5.1 e nos diagramas de concórdia (Figuras 5.1 e 5.2).

Tabela 5.1 – Dados geocronológicos U-Pb para o Complexo Fazenda Mirabela e rocha encaixante (granada gnaisse), e Intrusão Palestina.

Amostra	Litologia	Depósito	Idade U-Pb (Ma)
FM-03	Gabronorito Pegmatóide	Santa Rita	1990 ±28
MBS-497/01	Granada Gnaisse	Rocha Encaixante - Peri-Peri	2542 ±15
MBP-019/01	Ortopiroxenito	Palestina	2079 ±14

Complexo Fazenda Mirabela

A amostra FM-03 corresponde a um gabronorito pegmatóide do depósito Santa Rita. A datação geocronológica desta rocha obteve idade de 1990 ±28 Ma (Figura 5.1), correspondente à idade de cristalização do magma original da Intrusão Mirabela, sugerindo uma associação tectônica da Intrusão Mirabela à fase final da Orogênese Paleoproterozóica (2.3-2.0 Ga).

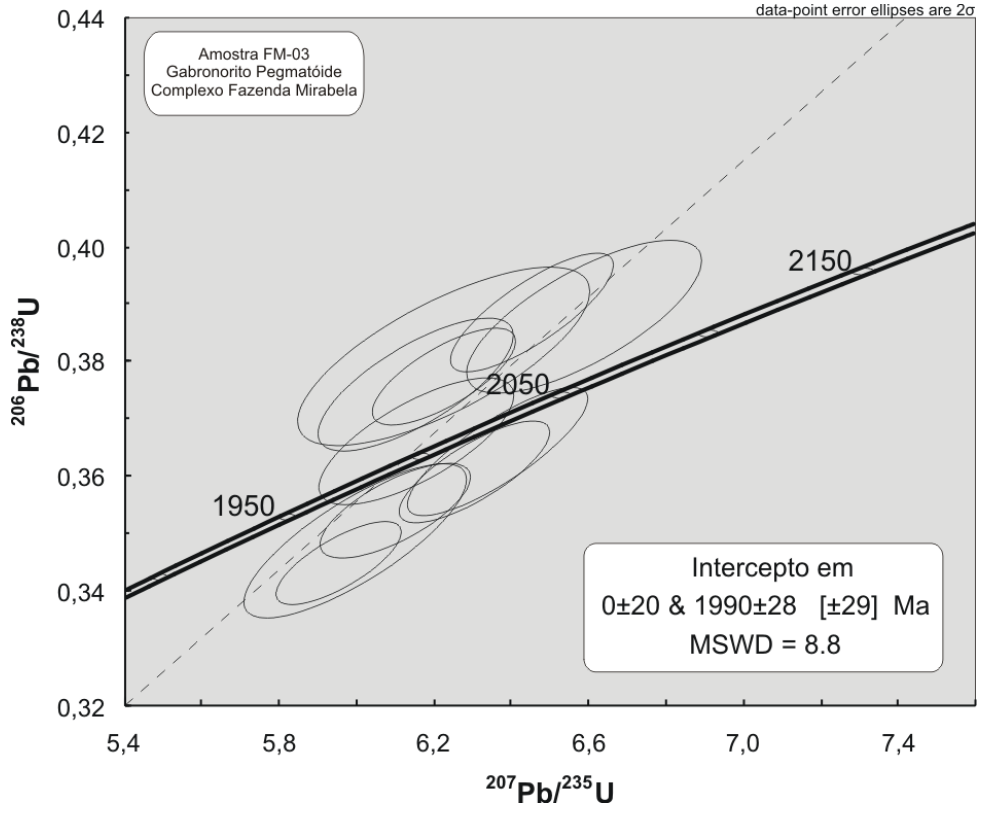

Figura 5.1 - Diagrama de concórdia para análises U-Pb em zircões de um gabronorito pegmatóide do Complexo Fazenda Mirabela (Amostra FM-03).

Rocha Encaixante

As rochas encaixantes à Intrusão Mirabela correspondem às sucessões de ortognaisses e rochas supracrustais granulitizadas de idade Arqueana. A datação geocronológica da rocha encaixante foi representada pela amostra MBS-497/01, um granada gnaisse obtido em um furo de sondagem diamantada. Os dados U-Pb para esta rocha encaixante obtiveram a idade de 2542 ±15 Ma (Figura 5.2), correspondente à idade de cristalização do protolito do granada gnaisse e anterior a Orogênese Paleoproterozóica.

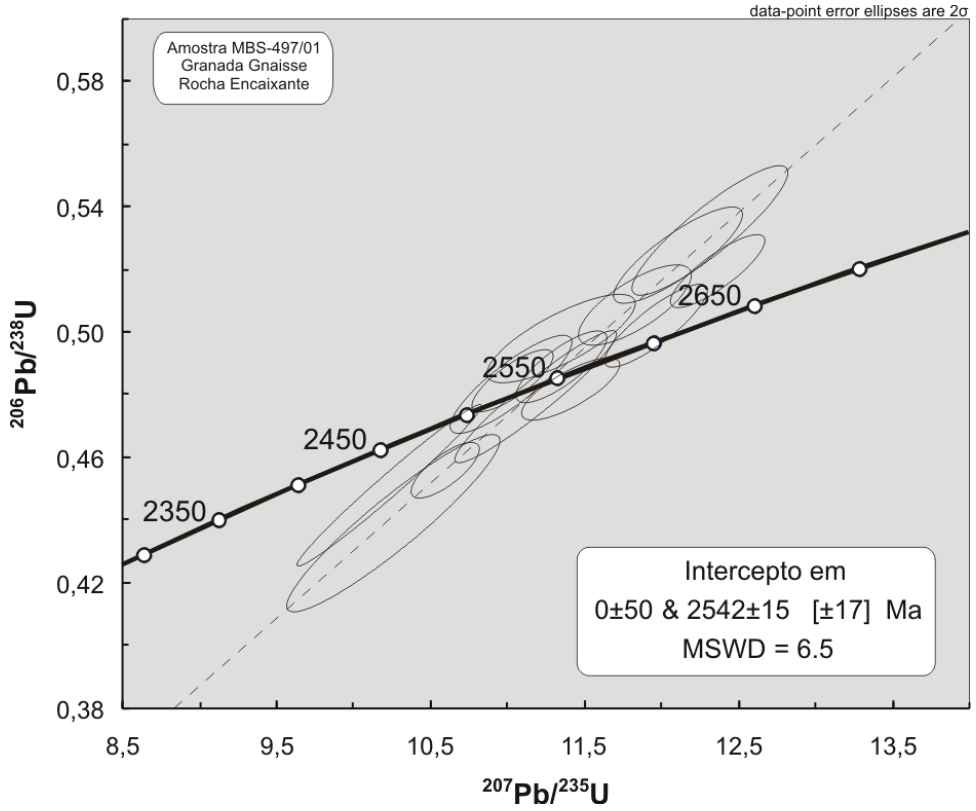

Figura 5.2 - Diagrama de concórdia para análises U-Pb em zircões de um granada gnaisse encaixante do Complexo Fazenda Mirabela (Amostra MBS-497/01).

Intrusão Palestina

A Intrusão Palestina está alojada a sul do Complexo Fazenda Mirabela, ao longo de um lineamento estrutural que se estende por mais de 100 km adjacente à margem oeste do Cinturão Itabuna-Salvador-Curaçá.

A amostra MBP-019/01 corresponde a um ortopiroxenito da Intrusão Palestina cuja análise U-Pb em zircões obteve a idade de 2079 ±14 Ma (Figura 5.3). Este dado é correspondente à idade de cristalização do corpo máfico-ultramáfico, correlaciona a Intrusão Palestina à fase final da Orogênese Paleoproterozóica.

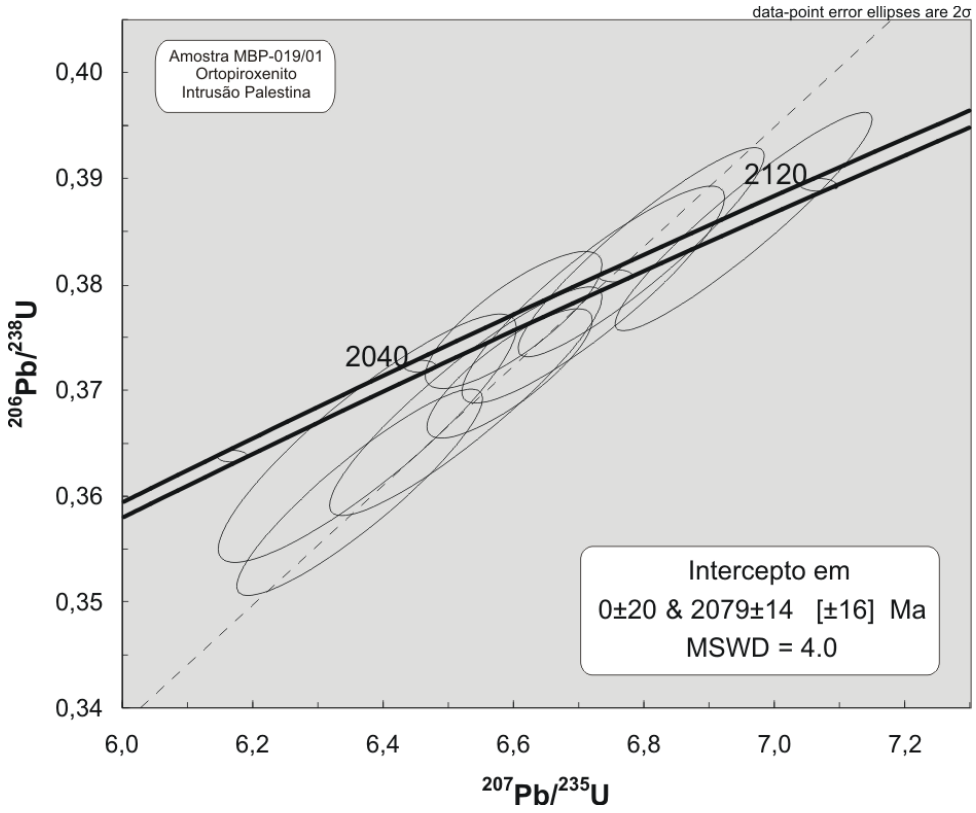

Figura 5.3 - Diagrama de concórdia para análises U-Pb em zircões de um ortopiroxenito da Intrusão Palestina (Amostra MBP-019/01).

Discussão

Embora as idades de cristalização dos dois corpos máfico-ultramáficos datados sejam relativamente próximas, elas são distintas permitindo definir um intervalo de tempo para o posicionamento deste magmatismo máfico-ultramáfico (ca 1960-2100 Ma). As idades de cristalização obtidas no Complexo Mirabela e na Intrusão Palestina indicam que o magmatismo máfico-ultramáfico com mineralizações de Ni-Cu sulfetado associado do sudeste da Bahia é tardio com relação à Orogênese Paleoproterozóica (ca 2.0-2.3 Ga; Barbosa & Sabaté 2002). Os resultados geocronológicos são consistentes com o forte contraste na deformação e recristalização metamórfica dos complexos máfico-ultramáficos e suas encaixantes gnáissicas e granulíticas, corroborando interpretações anteriormente apresentadas (Silva et al. 1992). A idade de 2542 ± 15 Ma obtida em granada gnaisse encaixante do Complexo Mirabela, indica a existência de rochas arqueanas cristalizadas antes do evento metamórfico de alto grau Paleoproterozóico. Este resultado é consistente com estudo recente desenvolvido na parte sul da faixa Itabuna-Salvador-Curaçá, que indicam uma extensão significativa de terrenos arqueanos nesta região (Peaucat et al. 2011).

6. CONCLUSÕES

O presente trabalho realizou a contextualização do Complexo Máfico-Ultramáfico Fazenda Mirabela, desenvolvendo o estudo da gênese e evolução das mineralizações de Ni-Cu-EGP e relações estratigráficas com a intrusão.

Os trabalhos de campo, os estudos petrográficos, a interpretação dos resultados geoquímicos dos furos de sonda e os novos dados isotópicos $\delta^{34}S$, Sm-Nd e U-Pb propiciaram a elaboração de relevantes conclusões sobre as rochas máficas-ultramáficas intrusivas na porção sul do Cinturão Itabuna-Salvador-Curaçá.

O sumário das conclusões deste trabalho é apresentado a seguir.

- O Complexo Fazenda Mirabela foi datado em 1.99 Ga com o método U-Pb em zircões. O Complexo Mirabela é intrusivo em rochas Arqueanas granulíticas ortognáissicas (charnoquitos e enderbitos) e supracrustais do Cinturão Itabuna-Salvador-Curaçá durante os estágios finais da Orogênese Paleoproterozóica. A idade U-Pb de 2.07 Ga, obtida para a Intrusão Palestina, a correlaciona à Orogenia Paleoproterozóica geradora do Complexo Fazenda Mirabela. A datação de 2.54 Ga em um granada gnaisse constatou a idade Arqueana das rochas encaixantes às intrusões máficas-ultramáficas.

- O Complexo Acamadado Fazenda Mirabela foi submetido a um processo de fracionamento magmático durante a fase de resfriamento, responsável pela estratigrafia e mineralogia do corpo. A intrusão foi subdividida de acordo com parâmetros litológicos e petrográficos em cinco zonas: Grupo de Borda Inferior - gabronoritos e ortopiroxenitos; Zona Inferior - dunitos; Zona Intermediária – harzburgitos, olivina ortopiroxenitos, ortopiroxenitos e websteritos; Zona Superior - gabronoritos; e Grupo de Borda Superior - websteritos, ortopiroxenitos, harzburgitos e gabronoritos.

- Análises geoquímicas em furos de sondagem do depósito Peri-Peri mostram a distribuição dos conteúdos de Ni, Cu, Pt e Pd associada aos horizontes máficos-ultramáficos com predominância de sulfetos disseminados. Conteúdos elevados de enxofre estão relacionados a um aumento de sulfetação e são associados principalmente aos horizontes ultramáficos da intrusão.

¤ Estudos sistemáticos de petrografia em furos de sondagem dos depósitos Santa Rita e Peri-Peri descrevem ocorrências de agregados policristalinos de sulfetos de Ni-Cu disseminados, associados a um forte controle litoestratigráfico, dos harzburgitos até os websteritos em Santa Rita, e websteritos aos harzburgitos em Peri-Peri. Estes resultados sugerem a ocorrência de rochas mais primitivas no topo da câmara magmática (Peri-Peri). A assembléia mineralógica dos sulfetos é composta por pentlandita, calcopirita, pirrotita e pirita, disseminadas e em concentrações econômicas de Ni e Cu associadas com a transição dos cumulatos ultramáficos a máficos, na porção superior da zona ultramáfica.

¤ Os estudos isotópicos de $\delta^{34}S$ em sulfetos (Pn, Cpy, Po, Py) obtiveram valores entre -1.0 a 0.5 ‰ $\delta^{34}S$ para Santa Rita e -2.0 a 1.0 ‰ $\delta^{34}S$ para Peri-Peri, resultados que indicam composições isotópicas similares ao enxofre de origem mantélica. Sulfetos de rochas encaixantes, incluindo sulfetos alojados em grafita-gnaisses (Py e Cpy) e paragranulitos (Cpy), têm valores $\delta^{34}S$ ‰ de 1.5 a 3.0. Sulfetos (Pn, Cpy e Py) em veios nas rochas encaixantes, incluindo gnaisses e granulitos, localizados próximos (< 20 metros) ao depósito Peri-Peri têm valores $\delta^{34}S$ ‰ de -0.5 a 1.0, e são interpretados como sulfetos magmáticos primários remobilizados. As composições isotópicas dos sulfetos dos depósitos Santa Rita e Peri-Peri são distintamente diferentes das composições obtidas dos sulfetos das rochas encaixantes. Esta feição inviabiliza a possibilidade das rochas encaixantes serem a fonte de enxofre dos sulfetos dos depósitos de Ni-Cu Santa Rita e Peri-Peri.

¤ As análises Sm-Nd realizadas nas rochas dos depósitos Santa Rita e Peri-Peri resultaram em valores ε Nd(t) de -7.65 a -1.71, dados consistentes com a contaminação do magma por rochas crustais encaixantes durante a ascensão da intrusão. As razões Sm-Nd entre 0.1385 e 0.2086 sugerem um pulso magmático que aloja os depósitos Santa Rita e Peri-Peri. As idades U-Pb e as composições isotópicas são consistentes com a cristalização da Intrusão Fazenda Mirabela apartir de um magma mantélico enriquecido contaminado com material crustal durante ascensão e alojamento.

- As datações geocronológicas U-Pb em zircões para o Complexo Mirabela (1990 ±28 Ma) e Intrusão Palestina (2079 ±14 Ma) definiram um intervalo de tempo para o posicionamento deste magmatismo máfico-ultramáfico (ca 1960-2100 Ma), sugerindo uma associação tectônica à fase final da Orogênese Paleoproterozóica (2.3-2.0 Ga). Enquanto que a datação da rocha encaixante ao Complexo Mirabela (2541 ±15 Ma) confirmou a existência de rochas arqueanas cristalizadas anteriores ao evento Paleoproterozóico.

Os principais depósitos de Ni-Cu mundiais têm condicionantes associados à contaminação dos magmas por rochas crustais encaixantes com assimilação de enxofre, e assembléia mineralógica constituída por pentlandita, calcopirita e pirrotita. A Intrusão Mirabela é distinta destes depósitos mundiais, pois sofreu contaminação crustal do magma máfico-ultramáfico durante a ascensão do corpo, mas não houve assimilação de enxofre proveniente das rochas encaixantes, o enxofre responsável pelos sulfetos tem origem mantélica e forma uma assembléia sulfetada distinta da tradicional, composta por pentlandita, calcopirita, pirrotita e pirita.

Os processos de resfriamento e fracionamento magmático do Complexo Mirabela foram responsáveis pelo empilhamento estratigráfico, associado às concentrações econômicas de sulfetos de Ni-Cu-EGP em dois horizontes ultramáficos, os depósitos Santa Rita e Peri-Peri, na base e no topo da intrusão, respectivamente.

O potencial metalogenético do Cinturão Itabuna-Salvador-Curaçá no Cráton do São Francisco é relevante para ocorrências de novos depósitos de sulfetos de Ni-Cu-EGP, visto que ocorrem várias intrusões máficas-ultramáficas ao longo do bloco, e provavelmente podem estar associadas ao mesmo evento orogênico responsável pela intrusão do Complexo Mirabela.

Este estudo pode ser considerado como um guia exploratório para caracterização de novos depósitos sulfetados de Ni-Cu-EGP com potenciais econômicos, de forma que se faz necessário o incentivo e a realização de mais estudos ao longo das intrusões máficas-ultramáficas no Cinturão Itabuna-Salvador-Curaçá.

7. REFERÊNCIAS BIBLIOGRÁFICAS

Abram, M.B., Silva, M.G. 1992. O corpo máfico-ultramáfico da Fazenda Mirabela, Ipiaú-BA-Química Mineral, Litogeoquímica e Evolução Petrogenética. In: Congresso Brasileiro de Geologia 37˚, São Paulo, Brazil External Abstract SBG.1 pp. 449–450.

Abram, M. B. O corpo máfico-ultramáfico da Fazenda Mirabela, Ipiaú-Ba: caracterização petrográfica, geoquímica, tipológica e implicações metalogenéticas. 1993. 137 f. Dissertação (Mestrado) - Instituto de Geociências, Universidade Federal da Bahia, Salvador, 1993.

Alibert, C.; Barbosa, J. S. F. Ages U-Pb determines a la SHRIMP sur des zircons du Complexe de Jequié, Cráton de São Francisco, Bahia, Brésil. In: Reunion des Sciences de la Terre (RST), 1992. Toulouse. 14 p.

Almeida, F.F.M. 1977. O Cráton do São Francisco. Revista Brasileira de Geociências, 7(4), p349-364.

Armstrong, R.; Wilson, 2000. A.H. A SHRIMP U-Pb study of zircons from the layered sequence of the Great Dyke, Zimbabwe, and a granitoid anatectic dyke. Earth and Planetary Science Letters 180, 1-12.

Barbosa, J.S.F. 1990. The granulites of the Jequié Complex and Atlantic mobile belt, Southern Bahia, Brazil – An expression of archean proterozoic plate convergence. In: Vielzeuf, Ph. Vidal, Process of ARW. ed. Granulites and Crustal Evolution. Clermont Ferrand (France), Springer-Verlag, 585p.

Barbosa J.S.F. and Sabaté P. 2002. Geological features and the Paleoproterozoic collision of four Archean crustal segments of the São Francisco Craton, Bahia, Brazil. A synthesis. Anais Academia Brasileira de Ciências, 74:343-359.

Barbosa, J. S. F.; Sabaté, P.; Marinho, M. M. 2003. O Cráton do São Francisco: uma síntese. Revista Brasileira de Geociências, 33: 3-6.

Barbosa, J.S.F and Sabaté, P. 2004. Archaean and Paleoproterozoic crust of the São Francisco Craton, Bahia, Brazil: geodynamic features. Precambrian Research, 133, pp1-47.

Barbosa, J.S.F (Coordenador) Pinho, I.C.A., Sobrinho, V.R.S., Cruz, S.C.P. Companhia de Pesquisa de Recursos Minerais – CPRM/Serviço Geológico do Brasil. Ipiaú- SD.24-Y-B-II, escala 1:100.000: nota explicativa. Bahia: UFBA/CPRM, 2007.

Barnes, S. J., Osborne, G. A., Cook, D., Barnes, L., Maier, W. D., Godel, B. 2011. The Santa Rita Nickel

Sulfide Deposit in the Fazenda Mirabela Intrusion, Bahia, Brazil: Geology, Sulfide Geochemistry, and Genesis. Society of Economic Geologists, Inc. Economic Geology, v. 106, pp. 1083-1110.

Corrêa-Gomes, L.C.; Oliveira, E.P. Dados Sm-Nd, Ar-Ar e Pb-Pb de Corpos Plutônicos no Sudeste da Bahia, Brasil. Implicações para o Entendimento da Evolução Tectônica no Limite Orógeno Araçuaí/Cráton do São Francisco. Revista Brasileira de Geociências 32(2):185-196, junho de 2002.

Cunha, J.C.; Fróes, R.J.B., 1992, Complexo máfico-ultramáfico da Fazenda Mirabela (CFM): geologia e mineralização: Congresso Brasileiro de Geologia, 37, São Paulo-SP, v. 2, p. 158-159.

DePaolo, D.J. 1988. Neodymium Isotope Geochemistry. Springer-Verlag, Berlin, 181 p.

Faure, G. 1986. Principles of Isotope Geology. John Wiley and Sons, New York, USA, 475 p.

Gioia, S.M.C.L., Pimentel, M.M.. 2000. The Sm-Nd isotopic method in the Geochronology Laboratory of the University of Brasília. Anais Academia Brasileira de Ciências 72, 219-245.

Keays, R.R., 1995. The role of komatiitic and picritic magmatism and S-saturation in the formation of ore deposits. Lithos 34: 1–18.

Li C, Naldrett A J, Ripely E M. 2001. Critical factors for the formation of a nickel-copper deposit in an evolved magma system: lessons from a comparison of the Pants Lake and Voisey's Bay sulfide occurrences in Labrador, Canada. Mineralium Deposita, 36: 85−92.

Loureiro, H. S. C. (Organizador). Programa levantamentos geológicos básicos do Brasil: Mundo Novo. Folha SC.24-Y-D-IV. Escala 1:100.000. DNPM/CPRM/SUREG-SA, 1991. 196 p.

Melo, R. C. Programa de levantamentos geológicos básicos do Brasil (PLGB): Folha SD.24-Y-D-V, Pintadas, Estado da Bahia. Brasília: Convênio DNPM/CPRM, 1991. 192 p.

Melo, R. C.; Loureiro, H. S. C.; Pereira, L. H. M. Programa levantamentos geológicos básicos do Brasil (PLGB): Folha SC.24-Y-D, Serrinha. Escala 1:250.000. MME/CPRM/SUREG-SA, 1995. 80 p.

Misi, A. and Silva, M.G. 1992. Algumas feições metalogenéticas relacionadas à evolução geodinâmica do Cráton do São Francisco. In: Congresso Brasileiro de Geologia, 37˚, São Paulo, SBG/SP, v.2, p.225-226.

Mota-e-Silva, J., Ferreira Filho, C.F., Buhn, B.M. and Dantas, E.L. 2010. Geology, Petrology and Geochemistry of the "Americano do Brasil" Layered Intrusion and its Ni-Cu Sulfide Deposits, Central Brazil. Mineralium Deposita, v. 46, p. 57-90.

Naldrett, A.J. 1966. The role of sulphurization in the gneiss of iron-nickel sulphide deposit of the porcupine district, Ontario. Transactions LXIX, 147-155.

Naldrett, A.J., 2004. Magmatic sulfide deposits: Geology, geochemistry and exploration. Heidelberg, Berlin, Springer Verlag, 728 p.

Peucat, J.J., Figueiredo Barbosa, J.S., de Araújo Pinho, I.C., Paquette, J.L., Martin, H., Fanning, M., de Menezes Leal, A.B., Cruz, S. Geochronology of granulites from the south Itabuna-Salvador-Curaçá Block, São Francisco Craton (Brazil): Nd isotopes and U-Pb zircon ages, Journal of South American Earth Sciences 2011, doi: 10.1016/j.jsames.2011.03.009.

Sato, K. Evolução crustal da plataforma Sul Americana com base na geoquímica isotópica Sm-Nd. 297 f. Tese (Doutorado) - Instituto de Geociências, Universidade de São Paulo, 1998.

Seat, Z. Beresford, S.W. Grguric, B. A. Mary Gee, M.A. Grassineau, N.V. Reevaluation of the Role of External Sulfur Addition in the Genesis of Ni-Cu-PGE Deposits: Evidence from the Nebo-Babel Ni-Cu-PGE Deposit, West Musgrave, Western Australia. 2009 Society of Economic Geologists Inc. Economic Geology, v. 104, pp. 521-538.

Silva, M. G. da; Barbosa, J.S.F., Misi, A. 1992. A faixa Aratuípe-Nova Canaã: um trend de corpos máficos e ultramáficos de grande potencial metalogenético no cinturão granulítico Jequié-Itabuna (BA). In: Congresso Brasileiro De Geologia, 37, São Paulo,Boletim Resumos Expandidos v2, p. 227.

Silva et al, L. C. U–Pb SHRIMP ages in the Itabuna-Caraíba TTG high - grade Complex: the first window beyond the Paleoproterozoic overprint of the eastern Jequié Craton, NE Brazil. In: International Symposium on Granites and Associated Mineralization. Abstracts. Salvador, 1997. p. 282-283.

Teixeira, L. R. O Complexo Caraíba e a Suíte São José do Jacuípe no Cinturão Salvador-Curaçá (Bahia, Brasil): petrologia, geoquímica e potencial metalogenético. 243 f. Tese (Doutorado) - Instituto de Geociências, Universidade Federal da Bahia, Salvador, 1997.

Whitney, J. A. and Naldrett, A. J. (eds), 1989. Ore deposits associated with magmas. Society of Economic Geology, Reviews in Economic Geology, vol. 4, 250 p.

Whitney D.L., Evans B.W. 2010 Abbreviations for names of rock-forming minerals. American Mineralogist 95: 185-187.

Wilson, N. Combined Sm-Nd, Pb/Pb and Rb-Sr geochronology and isotope geochemistry in polymetamorphic precambrian terrains: examples from Bahia, Brazil and Channel Island, U.K. 150 f. MSC - Oxford University, 1987.

ANEXOS

ANEXO 1

- Tabela de análises geoquímicas dos furos de sondagens MBS-401 e MBS-391

DH_Hole	DH_From	DH_To	Rock_Type	Ag_ppm	Al_ppm	Ars_ppm	Au_ppb	Ba_ppm	Be_ppm	Bi_ppm	Ca_ppm	Cd_ppm	Co_ppm	Cr_ppm	Cu_ppm
MBS-401	212	213	gabb	0.25	88200	2.5	0.5	110	0.25	1	84600	0.25	51	465	92
MBS-401	213	214	gabb	0.25	84900	2.5	0.5	130	0.25	1	84600	0.25	52	509	94
MBS-401	214	215	gabb	0.25	81300	2.5	0.5	100	0.25	1	82400	0.7	51	493	95
MBS-401	215	216	gabb	0.25	80000	2.5	1	90	0.25	1	86100	0.5	54	508	105
MBS-401	216	217	gabb	0.25	70500	2.5	3	100	0.25	1	88500	0.25	57	605	122
MBS-401	217	218	gabb	0.25	56500	2.5	2	70	0.25	1	88700	0.25	64	707	182
MBS-401	218	219	gabb	0.25	48600	8	2	80	0.25	1	91400	0.5	71	1310	237
MBS-401	219	220	gabb	0.25	48500	11	2	70	0.25	1	91600	0.25	67	1450	227
MBS-401	220	221	gabb	0.25	49800	2.5	2	70	0.25	1	93100	0.25	69	1570	205
MBS-401	221	222	gabb	0.25	49200	9	1	80	0.25	1	91200	0.9	68	1620	194
MBS-401	222	223	gabb	0.25	50200	2.5	1	70	0.25	1	90100	0.25	67	1630	194
MBS-401	223	224	gabb	0.25	52000	2.5	3	80	0.25	1	84800	1	71	1660	279
MBS-401	224	225	gabb	0.25	49500	2.5	2	100	0.25	1	80400	0.25	67	1690	209
MBS-401	225	226	gabb	0.25	47200	2.5	2	80	0.25	1	48700	0.7	81	1450	225
MBS-401	226	227	gabb	0.25	43400	2.5	2	100	0.25	1	42900	0.25	91	1400	401
MBS-401	227	228	gabb	0.25	48200	2.5	2	120	0.25	1	41800	1	84	1450	350
MBS-401	228	229	gabb	0.25	47400	2.5	6	140	0.25	1	41700	0.25	85	1610	237
MBS-401	229	230	gabb	0.25	41200	2.5	4	100	0.25	1	45200	0.25	92	1610	517
MBS-401	230	231	gabb	0.5	31200	2.5	6	120	0.25	1	32700	0.25	119	1500	1040
MBS-401	231	232	gabb	0.25	34600	2.5	15	100	0.25	1	33200	0.25	119	1530	1230
MBS-401	232	233	gabb	0.25	44600	2.5	11	240	0.6	1	26100	0.5	101	1420	1370
MBS-401	233	234	gabb	0.5	41500	2.5	15	120	0.25	1	33600	0.25	131	1920	1810
MBS-401	234	235	gabb	0.25	38600	2.5	8	70	0.25	1	38700	0.6	101	1870	856
MBS-401	235	236	gabb	0.25	37700	2.5	9	90	0.25	1	35700	0.25	98	1880	774
MBS-401	236	237	gabb	0.25	38900	2.5	5	90	0.25	1	34800	0.25	88	1920	348
MBS-401	237	238	gabb	0.25	37600	9	6	80	0.25	1	34500	0.5	92	1920	434
MBS-401	238	239	gabb	0.25	37800	2.5	5	70	0.25	1	34500	0.5	92	1910	362
MBS-401	239	240	gabb	0.25	39500	11	5	170	0.25	1	33500	0.25	85	1880	336
MBS-401	240	241	gabb	0.25	36300	2.5	4	90	0.25	1	36500	0.25	91	2120	229
MBS-401	241	242	gabb	0.25	33000	7	1	70	0.25	1	33400	0.25	75	1820	171
MBS-401	242	243	gabb	0.5	34500	2.5	0.5	70	0.25	1	35700	0.25	75	1810	164
MBS-401	243	244	gabb	0.25	33900	2.5	1	60	0.25	1	35100	0.25	78	1890	189
MBS-401	244	245	gabb	0.25	35600	2.5	1	60	0.25	1	37000	0.25	80	1830	213
MBS-401	245	246	gabb	0.25	34200	2.5	1	60	0.25	1	35000	0.25	78	1850	178
MBS-401	246	247	gabb	0.5	34200	2.5	1	60	0.25	1	34700	0.25	79	1860	195

DH_Hole	DH_From	DH_To	Rock_Type	Fe_pct	K_ppm	Mg_pct	Mn_ppm	Mo_ppm	Na_ppm	Ni_ppm	P_ppm	Pd_ppb	Pt_ppb	Pb_ppm	S_pct	Sb_ppm
MBS-401	212	213	gabb	5.56	3200	5.92	1030	0.5	15900	262	170	0.5	0.3	4	0.1	5
MBS-401	213	214	gabb	5.65	3000	6.11	1050	0.5	15200	279	160	0.5	0.3	1	0.1	6
MBS-401	214	215	gabb	5.5	2800	6.11	1030	0.5	14800	285	140	1	0.3	1	0.09	2.5
MBS-401	215	216	gabb	5.8	2700	6.54	1095	1	14300	303	140	0.5	0.3	3	0.1	6
MBS-401	216	217	gabb	6.18	2500	7.14	1170	0.5	13000	337	120	2	2	1	0.12	2.5
MBS-401	217	218	gabb	6.57	2000	7.9	1260	0.5	10700	448	130	0.5	0.3	1	0.18	10
MBS-401	218	219	gabb	7.08	2200	8.7	1350	0.5	9300	627	130	0.5	0.5	1	0.19	2.5
MBS-401	219	220	gabb	7.12	1900	8.68	1370	0.5	9300	642	120	0.5	0.3	1	0.18	2.5
MBS-401	220	221	gabb	7.26	2000	8.81	1390	0.5	9600	612	130	0.5	0.3	1	0.17	2.5
MBS-401	221	222	gabb	7.19	2100	8.71	1360	0.5	9500	586	150	0.5	0.3	1	0.16	8
MBS-401	222	223	gabb	7.13	1700	8.93	1375	0.5	9600	612	110	0.5	0.3	1	0.15	2.5
MBS-401	223	224	gabb	7.34	2100	9.11	1370	0.5	10200	745	150	0.5	0.3	4	0.22	2.5
MBS-401	224	225	gabb	7.05	2700	8.56	1305	1	10100	659	200	0.5	0.3	1	0.16	7
MBS-401	225	226	gabb	7.66	2300	10.9	1350	1	9400	790	170	1	0.5	1	0.13	2.5
MBS-401	226	227	gabb	8.06	2200	11.25	1385	0.5	8600	1210	150	1	1.3	4	0.28	2.5
MBS-401	227	228	gabb	7.7	3100	11.2	1335	0.5	10200	1000	160	1	0.9	1	0.21	5
MBS-401	228	229	gabb	8.03	3700	11.9	1405	1	9600	891	160	1	0.6	1	0.15	2.5
MBS-401	229	230	gabb	8.35	2400	12.05	1405	0.5	8600	1720	160	2	2.9	1	0.35	5
MBS-401	230	231	gabb	9.55	2700	12.9	1500	0.5	6500	3430	230	7	7.3	1	0.75	5
MBS-401	231	232	gabb	9.3	2100	12.3	1420	1	7600	3610	180	8	12.5	6	0.78	6
MBS-401	232	233	gabb	7.02	15000	8.59	1030	1	9900	3540	170	7	9.8	13	0.78	2.5
MBS-401	233	234	gabb	9.09	5800	11.55	1305	2	9200	4770	170	7	10.8	8	1.09	2.5
MBS-401	234	235	gabb	8.4	1900	12.15	1330	0.5	7500	2540	150	4	7	1	0.56	2.5
MBS-401	235	236	gabb	8.35	2100	11.9	1315	0.5	7300	2540	150	4	6.2	1	0.55	9
MBS-401	236	237	gabb	8	2300	12.25	1315	0.5	8000	1350	160	1	1.9	8	0.22	2.5
MBS-401	237	238	gabb	8.15	2000	12.3	1330	0.5	7300	1580	140	2	5.6	1	0.29	2.5
MBS-401	238	239	gabb	8.07	1900	12.45	1325	0.5	7400	1450	140	3	4.5	1	0.24	2.5
MBS-401	239	240	gabb	8.25	4300	11.75	1350	0.5	9000	1340	210	2	5.1	1	0.22	2.5
MBS-401	240	241	gabb	8.19	2200	13	1395	1	7200	1160	220	1	4.7	1	0.18	2.5
MBS-401	241	242	gabb	7.26	2000	12.6	1240	1	6600	942	170	1	2.8	1	0.15	2.5
MBS-401	242	243	gabb	7.13	2000	12.4	1230	0.5	7000	912	230	1	0.7	1	0.14	2.5
MBS-401	243	244	gabb	7.18	1700	12.55	1230	1	6700	990	180	1	1.1	1	0.16	2.5
MBS-401	244	245	gabb	7.48	1700	13.2	1300	0.5	7200	1030	150	1	1.7	1	0.18	2.5
MBS-401	245	246	gabb	7.39	1500	13.05	1290	1	6800	982	110	1	1.1	1	0.15	2.5
MBS-401	246	247	gabb	7.13	2100	12.55	1245	1	7500	976	170	1	1.1	4	0.15	2.5

DH_Hole	DH_From	DH_To	Rock_Type	Sr_ppm	Ti_ppm	V_ppm	W_ppm	Zn_ppm
MBS-401	212	213	gabb	240	1900	147	5	54
MBS-401	213	214	gabb	232	1800	149	5	54
MBS-401	214	215	gabb	224	1700	143	5	52
MBS-401	215	216	gabb	216	1700	155	5	54
MBS-401	216	217	gabb	187	1800	170	5	55
MBS-401	217	218	gabb	144	1800	182	5	57
MBS-401	218	219	gabb	118	2100	199	5	63
MBS-401	219	220	gabb	120	1900	198	5	63
MBS-401	220	221	gabb	124	2000	204	5	64
MBS-401	221	222	gabb	124	2100	201	5	65
MBS-401	222	223	gabb	127	1800	194	5	64
MBS-401	223	224	gabb	133	1900	188	5	68
MBS-401	224	225	gabb	128	2400	178	5	68
MBS-401	225	226	gabb	119	1500	135	5	77
MBS-401	226	227	gabb	115	1300	128	5	78
MBS-401	227	228	gabb	126	1600	119	5	84
MBS-401	228	229	gabb	114	2000	129	5	89
MBS-401	229	230	gabb	104	1500	129	5	82
MBS-401	230	231	gabb	79	1600	126	5	90
MBS-401	231	232	gabb	89	1600	120	5	95
MBS-401	232	233	gabb	100	1600	91	5	72
MBS-401	233	234	gabb	93	1900	114	5	87
MBS-401	234	235	gabb	94	1300	117	5	79
MBS-401	235	236	gabb	92	1300	114	5	78
MBS-401	236	237	gabb	98	1400	117	5	82
MBS-401	237	238	gabb	93	1200	111	5	78
MBS-401	238	239	gabb	93	1300	110	5	78
MBS-401	239	240	gabb	98	2200	123	5	99
MBS-401	240	241	gabb	89	1600	138	5	83
MBS-401	241	242	gabb	85	1400	122	5	72
MBS-401	242	243	gabb	90	1400	127	5	70
MBS-401	243	244	gabb	91	1300	131	5	70
MBS-401	244	245	gabb	93	1400	135	5	72
MBS-401	245	246	gabb	85	1300	132	5	71
MBS-401	246	247	gabb	85	1600	134	5	72

DH_Hole	DH_From	DH_To	Rock_Type	Ag_ppm	Al_ppm	Ars_ppm	Au_ppb	Ba_ppm	Be_ppm	Bi_ppm	Ca_ppm	Cd_ppm	Co_ppm	Cr_ppm	Cu_ppm
MBS-401	247	248	gabb	0.8	39800	2.5	1	130	0.25	1	34400	0.25	73	1690	218
MBS-401	248	249	gabb	0.25	33700	2.5	1	80	0.25	1	34800	0.6	76	1820	237
MBS-401	249	250	gabb	0.25	55100	2.5	0.5	210	1.1	1	13000	0.25	23	590	40
MBS-401	250	251	vein	0.25	35300	2.5	4	250	0.25	1	29800	0.25	74	1740	365
MBS-401	251	252	vein	0.25	76500	2.5	2	230	1.3	1	8600	0.25	9	132	36
MBS-401	252	253	opx	0.25	28600	2.5	3	50	0.25	1	32000	0.25	88	1920	320
MBS-401	253	254	opx	0.25	28600	2.5	4	70	0.25	1	30400	0.25	82	1810	305
MBS-401	254	255	opx	0.25	36200	2.5	3	240	0.25	1	31000	0.25	78	1870	250
MBS-401	255	256	opx	0.25	28000	2.5	4	100	0.25	1	33800	0.25	90	1970	427
MBS-401	256	257	opx	0.25	28900	2.5	1	50	0.25	1	34100	0.25	85	2120	206
MBS-401	257	258	opx	0.25	29600	17	0.5	50	0.25	1	33600	0.25	84	2080	196
MBS-401	258	259	opx	0.25	30800	2.5	0.5	60	0.25	1	34000	0.25	83	2110	227
MBS-401	259	260	opx	0.25	36600	2.5	0.5	140	0.25	1	33000	0.25	78	1980	199
MBS-401	260	261	opx	0.25	56100	2.5	0.5	200	0.9	1	32000	0.25	58	1440	164
MBS-401	261	262	opx	0.25	30500	2.5	2	60	0.25	1	33000	0.25	85	1950	267
MBS-401	262	263	opx	0.25	29300	2.5	1	80	0.25	1	33200	0.25	80	1970	170
MBS-401	263	264	opx	0.25	30300	5	1	90	0.25	1	34500	0.7	84	1970	147
MBS-401	264	265	opx	0.5	29700	2.5	0.5	50	0.25	1	33900	0.25	81	2110	162
MBS-401	265	266	opx	0.9	28400	11	1	50	0.25	1	32600	0.25	84	2000	235
MBS-401	266	267	opx	0.7	32100	2.5	0.5	60	0.25	1	32100	0.25	79	2000	195
MBS-401	267	268	opx	0.25	40400	2.5	2	50	1.7	1	19800	0.25	55	1340	205
MBS-401	268	269	opx	0.25	43500	2.5	2	50	3.8	1	23500	0.25	56	1420	229
MBS-401	269	270	opx	0.25	28500	2.5	2	50	0.25	1	30600	0.25	88	2110	369
MBS-401	270	271	opx	0.25	29300	2.5	4	50	0.25	1	31200	0.25	94	2120	433
MBS-401	271	272	opx	0.25	46000	2.5	8	180	0.5	1	17000	0.25	79	1250	645
MBS-401	272	273	opx	0.25	29400	15	14	40	0.25	1	27500	0.25	116	1970	1170
MBS-401	273	274	opx	0.8	27900	2.5	28	50	0.25	1	29700	0.25	144	2050	2470
MBS-401	274	275	opx	0.8	30000	2.5	25	50	0.25	1	31900	0.25	157	1970	2150
MBS-401	275	276	opx	0.7	28500	2.5	19	50	0.25	1	30700	0.25	137	1930	1540
MBS-401	276	277	opx	0.25	29000	8	14	50	0.25	1	31500	0.25	130	1950	1495
MBS-401	277	278	opx	0.25	35900	2.5	28	60	0.5	1	32600	0.25	96	1780	629
MBS-401	278	279	opx	1.5	32800	2.5	2	50	0.25	1	32700	0.25	84	1730	292
MBS-401	279	280	opx	0.7	31000	2.5	2	50	0.25	1	34700	0.25	85	1850	259
MBS-401	280	281	opx	0.25	36500	12	5	50	1	1	32800	0.25	85	1880	412
MBS-401	281	282	opx	0.25	30100	2.5	6	50	0.25	2	35600	0.25	88	1830	420

DH_Hole	DH_From	DH_To	Rock_Type	Fe_pct	K_ppm	Mg_pct	Mn_ppm	Mo_ppm	Na_ppm	Ni_ppm	P_ppm	Pd_ppb	Pt_ppb	Pb_ppm	S_pct	Sb_ppm
MBS-401	247	248	gabb	6.74	5400	11.25	1140	1	9300	917	270	1	1.1	3	0.16	2.5
MBS-401	248	249	gabb	7.16	2500	12.2	1250	0.5	7100	1010	160	1	1.7	1	0.16	2.5
MBS-401	249	250	gabb	2.5	31400	3.47	499	1	16300	301	80	0.5	0.5	30	0.03	2.5
MBS-401	250	251	vein	6.42	8800	11.35	1100	0.5	7400	1410	140	1	2.8	25	0.25	2.5
MBS-401	251	252	vein	1.71	34400	1.35	186	2	26400	120	170	0.5	0.3	40	0.05	2.5
MBS-401	252	253	opx	7.31	1300	13.5	1285	2	5500	1420	150	1	2.6	4	0.23	2.5
MBS-401	253	254	opx	7.05	1800	12.8	1225	1	5600	1380	140	1	3.1	1	0.21	2.5
MBS-401	254	255	opx	7.32	6000	12.1	1240	0.5	8700	1230	250	1	1.8	4	0.16	2.5
MBS-401	255	256	opx	7.84	2200	13.75	1325	1	5300	1620	150	2	2.3	5	0.3	2.5
MBS-401	256	257	opx	7.67	1200	14.15	1335	2	5200	1070	130	1	0.9	1	0.16	2.5
MBS-401	257	258	opx	7.7	1500	14	1340	0.5	5500	1050	170	0.5	0.7	4	0.14	2.5
MBS-401	258	259	opx	7.59	1800	13.9	1340	0.5	5900	1060	200	1	0.7	1	0.13	2.5
MBS-401	259	260	opx	7.35	5000	12.8	1300	1	8400	946	160	0.5	0.6	2	0.12	2.5
MBS-401	260	261	opx	5.3	8800	9.11	914	0.5	16900	715	170	0.5	0.5	10	0.1	2.5
MBS-401	261	262	opx	7.53	2000	13.6	1315	0.5	5900	1240	180	2	1.7	1	0.2	2.5
MBS-401	262	263	opx	7.29	1400	13.55	1290	0.5	5400	989	170	1	3.4	2	0.14	2.5
MBS-401	263	264	opx	7.53	1700	13.9	1335	0.5	5900	938	160	1	0.6	4	0.12	2.5
MBS-401	264	265	opx	7.53	2000	13.9	1335	0.5	5500	981	150	0.5	0.6	1	0.13	2.5
MBS-401	265	266	opx	7.26	1300	13.45	1275	0.5	5100	1160	150	1	1.3	3	0.18	2.5
MBS-401	266	267	opx	7.14	2900	13.05	1250	2	6700	1020	200	1	0.9	5	0.13	2.5
MBS-401	267	268	opx	5.43	12700	8.63	987	1	12500	757	140	1	0.6	25	0.11	2.5
MBS-401	268	269	opx	5.06	7700	8.76	891	1	15100	845	110	1	1.4	13	0.11	2.5
MBS-401	269	270	opx	7.49	1700	13.8	1300	0.5	5400	1450	150	2	2.3	1	0.22	2.5
MBS-401	270	271	opx	7.79	1500	14.15	1335	2	5400	1780	160	2	2.7	1	0.31	2.5
MBS-401	271	272	opx	5.57	27000	9.24	862	2	9500	2300	170	4	5.9	28	0.38	2.5
MBS-401	272	273	opx	7.76	3400	13.2	1250	1	5900	4010	150	6	10.5	9	0.75	2.5
MBS-401	273	274	opx	8.5	1500	13.6	1285	1	5100	6300	120	10	21.3	5	1.31	2.5
MBS-401	274	275	opx	9.09	1600	14.6	1380	3	5500	6400	150	11	15.3	7	1.38	2.5
MBS-401	275	276	opx	8.46	1600	13.9	1315	0.5	5300	5400	200	8	16.1	6	1.08	2.5
MBS-401	276	277	opx	8.43	1300	14.15	1340	0.5	5100	4700	150	7	11	8	0.95	2.5
MBS-401	277	278	opx	7.7	4600	13.55	1270	1	7500	2350	190	5	6.2	1	0.43	2.5
MBS-401	278	279	opx	7.37	2000	13.55	1295	1	7000	1250	140	1	1.3	1	0.16	2.5
MBS-401	279	280	opx	7.75	1900	14.4	1365	2	6000	1250	180	1	1.5	1	0.17	5
MBS-401	280	281	opx	7.1	8300	12.4	1225	0.5	8600	1680	140	2	2.4	11	0.28	2.5
MBS-401	281	282	opx	7.71	1600	14.2	1345	0.5	5600	1500	160	2	2	3	0.24	2.5

DH_Hole	DH_From	DH_To	Rock_Type	Sr_ppm	Ti_ppm	V_ppm	W_ppm	Zn_ppm
MBS-401	247	248	gabb	101	2100	130	5	72
MBS-401	248	249	gabb	85	1600	123	5	73
MBS-401	249	250	gabb	80	1000	34	5	44
MBS-401	250	251	vein	87	1600	100	5	128
MBS-401	251	252	vein	107	1500	9	5	49
MBS-401	252	253	opx	66	1500	113	5	69
MBS-401	253	254	opx	69	1600	112	5	68
MBS-401	254	255	opx	93	1800	108	5	82
MBS-401	255	256	opx	63	1500	118	5	76
MBS-401	256	257	opx	63	1400	126	5	75
MBS-401	257	258	opx	66	1500	124	10	75
MBS-401	258	259	opx	71	1600	124	5	74
MBS-401	259	260	opx	93	1800	118	5	83
MBS-401	260	261	opx	179	1600	87	5	60
MBS-401	261	262	opx	70	1500	119	5	74
MBS-401	262	263	opx	67	1300	120	5	70
MBS-401	263	264	opx	68	1500	124	5	71
MBS-401	264	265	opx	63	1500	126	5	76
MBS-401	265	266	opx	63	1300	120	5	70
MBS-401	266	267	opx	72	1700	120	5	72
MBS-401	267	268	opx	41	1800	83	5	67
MBS-401	268	269	opx	65	1400	80	5	58
MBS-401	269	270	opx	64	1500	116	5	74
MBS-401	270	271	opx	66	1400	121	5	75
MBS-401	271	272	opx	79	1100	63	5	54
MBS-401	272	273	opx	56	1400	107	5	71
MBS-401	273	274	opx	62	1500	116	5	71
MBS-401	274	275	opx	68	1500	125	5	78
MBS-401	275	276	opx	63	1500	121	5	73
MBS-401	276	277	opx	66	1400	120	10	73
MBS-401	277	278	opx	72	2100	134	10	72
MBS-401	278	279	opx	72	1400	117	5	70
MBS-401	279	280	opx	67	1600	125	10	74
MBS-401	280	281	opx	60	1700	112	5	69
MBS-401	281	282	opx	68	1500	126	5	71

DH_Hole	DH_From	DH_To	Rock_Type	Ag_ppm	Al_ppm	Ars_ppm	Au_ppb	Ba_ppm	Be_ppm	Bi_ppm	Ca_ppm	Cd_ppm	Co_ppm	Cr_ppm	Cu_ppm
MBS-401	282	283	opx	0.8	30600	2.5	25	50	0.25	3	38100	0.25	116	1860	1835
MBS-401	283	284	opx	0.5	41200	2.5	26	40	0.8	1	31900	0.25	93	1690	990
MBS-401	284	285	opx	0.6	33700	2.5	34	60	0.25	2	38800	0.25	177	1780	2210
MBS-401	285	286	opx	0.25	31800	2.5	38	50	0.25	1	36800	0.25	119	1830	1905
MBS-401	286	287	opx	0.25	58800	7	14	30	2	1	21500	0.25	89	740	1160
MBS-401	287	288	opx	0.25	39400	2.5	16	50	0.6	1	29800	0.25	102	1690	916
MBS-401	288	289	opx	0.25	36700	2.5	26	60	0.8	1	32600	0.25	140	1720	1615
MBS-401	289	290	opx	0.25	30700	2.5	74	60	0.25	1	30100	0.25	162	1910	1430
MBS-401	290	291	opx	0.7	19100	2.5	112	30	0.25	1	20400	0.25	225	2430	2690
MBS-401	291	292	opx	1.2	22100	2.5	127	40	0.25	1	23200	0.25	147	2410	3410
MBS-401	292	293	opx	0.5	22100	2.5	100	30	0.25	1	23600	0.25	130	2450	1175
MBS-401	293	294	opx	0.25	23300	2.5	76	30	0.25	1	21900	0.25	100	3960	775
MBS-401	294	295	opx	1.1	21300	2.5	171	30	0.25	1	20700	0.25	152	3440	3560
MBS-401	295	296	opx	1.2	28600	2.5	151	30	0.25	3	17000	0.25	141	3740	3770
MBS-401	296	297	opx	1	23600	7	158	30	0.25	1	15300	0.25	229	7220	3180
MBS-401	297	298	opx	0.7	21700	2.5	199	10	0.25	1	15000	0.25	269	10000	2240
MBS-401	298	299	opx	0.7	21100	6	179	20	0.25	1	18200	0.25	187	10000	2030
MBS-401	299	300	opx	1	25500	2.5	161	40	0.25	1	25900	0.25	174	4970	2920
MBS-401	300	301	opx	0.25	31000	2.5	141	30	0.25	1	17700	0.25	151	10000	1130
MBS-401	301	302	opx	0.6	30300	2.5	150	30	0.5	1	11400	0.25	188	10000	2370
MBS-401	302	303	opx	0.5	21500	2.5	232	20	0.25	1	19600	0.5	196	9510	1710
MBS-401	303	304	opx	0.7	21800	2.5	194	40	0.25	1	19100	0.25	154	3280	1630
MBS-401	304	305	opx	0.25	33200	2.5	217	50	0.25	1	24600	0.6	176	10000	1120
MBS-401	305	306	opx	1.8	32700	2.5	275	40	0.9	1	27700	0.25	141	5450	5850
MBS-401	306	307	opx	1	33200	2.5	219	30	0.25	1	25900	0.25	148	10000	1855
MBS-401	307	308	opx	0.25	30200	2.5	153	50	0.25	4	27700	0.25	166	10000	1080
MBS-401	308	309	opx	0.25	27100	2.5	261	40	0.25	3	27600	0.6	135	10000	1120
MBS-401	309	310	opx	0.5	27600	2.5	318	40	0.25	1	25900	0.25	127	10000	1400
MBS-401	310	311	opx	0.25	30000	2.5	156	40	0.25	1	25300	0.25	118	10000	738
MBS-401	311	312	opx	0.7	24900	2.5	267	30	0.25	1	23200	0.25	115	9690	2230
MBS-401	312	313	opx	0.25	38600	2.5	84	60	0.25	1	35900	0.25	175	2000	1560
MBS-401	313	314	opx	0.25	39400	2.5	75	50	0.25	1	37700	0.25	246	1890	1035
MBS-401	314	315	opx	0.6	32100	2.5	95	50	0.25	1	31400	0.25	250	2110	2110
MBS-401	315	316	opx	1.1	28800	2.5	224	60	0.25	2	26900	0.25	153	2910	3910
MBS-401	316	317	opx	0.25	29500	12	54	60	0.25	1	26300	0.25	181	1940	1240

DH_Hole	DH_From	DH_To	Rock_Type	Fe_pct	K_ppm	Mg_pct	Mn_ppm	Mo_ppm	Na_ppm	Ni_ppm	P_ppm	Pd_ppb	Pt_ppb	Pb_ppm	S_pct	Sb_ppm
MBS-401	282	283	opx	8.37	1400	13.9	1335	1	5600	4190	140	11	18.4	3	0.88	2.5
MBS-401	283	284	opx	6.8	9900	11.05	1160	1	10700	3120	100	9	6.4	5	0.6	2.5
MBS-401	284	285	opx	9.17	2300	13.35	1295	0.5	7000	8500	200	37	19.8	11	1.87	2.5
MBS-401	285	286	opx	8.34	3900	13.5	1320	0.5	6000	4560	150	18	23.1	1	0.94	2.5
MBS-401	286	287	opx	4.28	13700	4.79	593	4	22400	3280	80	11	5.4	24	0.92	2.5
MBS-401	287	288	opx	7.55	7900	11.5	1275	1	9700	3760	160	13	16.3	14	0.71	2.5
MBS-401	288	289	opx	8.31	6700	11.7	1200	1	8500	7000	200	34	30	8	1.41	2.5
MBS-401	289	290	opx	8.76	4100	13.35	1265	2	6300	8300	190	46	72.4	12	1.59	2.5
MBS-401	290	291	opx	9.49	800	16.15	1230	0.5	2700	13700	110	124	125	5	2.79	2.5
MBS-401	291	292	opx	8.66	1000	15.9	1290	0.5	3400	6700	140	76	51.4	5	1.61	2.5
MBS-401	292	293	opx	8.18	1200	16.65	1335	1	3200	4680	110	30	77.4	1	0.86	2.5
MBS-401	293	294	opx	7.94	6500	17	1395	0.5	2700	2540	90	34	85.5	2	0.29	2.5
MBS-401	294	295	opx	8.56	1600	15.9	1275	0.5	3400	7700	80	93	137	2	1.74	2.5
MBS-401	295	296	opx	8.2	6000	13.5	1175	2	6000	7400	90	135	195	10	1.78	2.5
MBS-401	296	297	opx	9.66	4500	13.95	1235	2	3500	12500	60	235	235	3	2.82	2.5
MBS-401	297	298	opx	10.75	400	16.55	1145	2	1700	15700	60	232	366	3	2.99	5
MBS-401	298	299	opx	9.4	600	17.5	1270	1	2300	9300	80	211	445	2	1.79	2.5
MBS-401	299	300	opx	9.1	1700	15.75	1300	1	4400	8400	120	262	350	8	1.8	2.5
MBS-401	300	301	opx	8.69	8700	13.05	1200	2	4900	7900	80	389	386	6	1.31	2.5
MBS-401	301	302	opx	9.1	8900	12.35	972	4	3400	11000	100	220	529	7	2.19	2.5
MBS-401	302	303	opx	9.26	700	16.25	1255	1	2600	10700	90	164	319	1	2.02	2.5
MBS-401	303	304	opx	8.54	3300	16	1265	1	3400	7500	100	157	350	7	1.44	2.5
MBS-401	304	305	opx	9.07	4100	13.15	1180	3	5700	9400	140	560	608	12	1.67	2.5
MBS-401	305	306	opx	8.62	4900	12.4	1170	1	7500	7000	110	256	822	14	1.96	5
MBS-401	306	307	opx	9.58	3100	14.25	1220	2	3400	6600	90	702	827	1	1.24	5
MBS-401	307	308	opx	9.09	1900	15.65	1280	1	4800	8400	110	517	677	2	1.6	2.5
MBS-401	308	309	opx	8.66	1400	15.3	1180	1	3600	4960	100	895	833	5	0.85	9
MBS-401	309	310	opx	8.11	1400	14	1195	1	4100	5240	110	511	792	9	0.96	2.5
MBS-401	310	311	opx	7.88	2100	14.05	1145	1	4200	4130	120	489	434	1	0.67	2.5
MBS-401	311	312	opx	7.75	1300	13.85	1175	1	3600	4320	100	536	716	1	0.9	2.5
MBS-401	312	313	opx	8.29	1900	11.15	1125	1	7600	10200	140	252	245	13	2.02	2.5
MBS-401	313	314	opx	9.36	1500	10.85	1135	0.5	7700	15800	150	188	244	20	3.1	2.5
MBS-401	314	315	opx	9.97	1700	11.8	1150	1	6200	16000	150	188	184	15	3.3	2.5
MBS-401	315	316	opx	8.95	2900	12.6	1145	0.5	5300	8300	200	177	166	15	2.04	2.5
MBS-401	316	317	opx	8.39	4600	10.6	1090	2	6000	10800	120	115	207	12	2.14	2.5

DH_Hole	DH_From	DH_To	Rock_Type	Sr_ppm	Ti_ppm	V_ppm	W_ppm	Zn_ppm
MBS-401	282	283	opx	69	1600	129	5	70
MBS-401	283	284	opx	59	1400	98	5	69
MBS-401	284	285	opx	76	1900	137	5	70
MBS-401	285	286	opx	61	1900	128	5	75
MBS-401	286	287	opx	61	1100	48	5	44
MBS-401	287	288	opx	66	1800	106	5	78
MBS-401	288	289	opx	68	1900	115	5	73
MBS-401	289	290	opx	61	1900	118	10	71
MBS-401	290	291	opx	31	1400	92	5	71
MBS-401	291	292	opx	42	1500	105	10	68
MBS-401	292	293	opx	38	1300	106	5	70
MBS-401	293	294	opx	27	1500	106	5	93
MBS-401	294	295	opx	34	1200	98	5	72
MBS-401	295	296	opx	39	1600	88	5	86
MBS-401	296	297	opx	28	1300	106	5	84
MBS-401	297	298	opx	24	1200	167	5	155
MBS-401	298	299	opx	26	1200	134	5	89
MBS-401	299	300	opx	49	1500	121	5	66
MBS-401	300	301	opx	29	1600	145	5	127
MBS-401	301	302	opx	27	1800	145	5	145
MBS-401	302	303	opx	33	1300	129	5	79
MBS-401	303	304	opx	30	1200	95	5	65
MBS-401	304	305	opx	58	1800	164	5	88
MBS-401	305	306	opx	49	1400	119	10	91
MBS-401	306	307	opx	39	1800	217	5	132
MBS-401	307	308	opx	53	1800	174	5	104
MBS-401	308	309	opx	38	1500	178	10	98
MBS-401	309	310	opx	53	1600	143	5	80
MBS-401	310	311	opx	49	1500	147	10	85
MBS-401	311	312	opx	44	1300	127	5	76
MBS-401	312	313	opx	99	1500	109	5	60
MBS-401	313	314	opx	104	1700	119	5	65
MBS-401	314	315	opx	82	1800	118	5	71
MBS-401	315	316	opx	62	1800	119	10	76
MBS-401	316	317	opx	63	1500	101	5	66

DH_Hole	DH_From	DH_To	Rock_Type	Ag_ppm	Al_ppm	Ars_ppm	Au_ppb	Ba_ppm	Be_ppm	Bi_ppm	Ca_ppm	Cd_ppm	Co_ppm	Cr_ppm	Cu_ppm
MBS-401	317	318	opx	0.5	34000	2.5	43	60	0.6	1	52100	0.25	105	2260	475
MBS-401	318	319	opx	0.25	50900	2.5	43	130	0.25	1	48600	0.25	79	1650	412
MBS-401	319	320	base	0.25	69900	2.5	10	400	0.9	1	15800	0.25	25	300	270
MBS-401	320	321	base	0.25	69700	2.5	1	460	0.9	1	7300	0.25	2	26	7
MBS-401	321	322	base	0.25	70300	2.5	1	450	0.5	1	7200	0.25	1	27	7
MBS-401	322	323	base	0.25	75100	2.5	222	240	2.1	1	45800	0.25	24	66	98
MBS-401	323	324	base	0.25	76700	2.5	9	40	1.8	1	77000	0.6	51	106	172
MBS-401	324	325	base	0.6	80500	2.5	9	40	2.8	1	65800	0.7	43	116	158

DH_Hole	DH_From	DH_To	Rock_Type	Fe_pct	K_ppm	Mg_pct	Mn_ppm	Mo_ppm	Na_ppm	Ni_ppm	P_ppm	Pd_ppb	Pt_ppb	Pb_ppm	S_pct	Sb_ppm
MBS-401	317	318	opx	7.43	2800	11.4	1260	0.5	7100	3660	150	67	59.6	10	0.7	2.5
MBS-401	318	319	opx	6.29	8800	9.02	1055	1	11800	2350	220	37	74.5	8	0.48	2.5
MBS-401	319	320	base	2	27600	1.59	442	1	26300	1150	160	13	300	33	0.26	2.5
MBS-401	320	321	base	0.71	32500	0.12	363	1	30000	32	200	1	1.1	31	0.01	2.5
MBS-401	321	322	base	0.93	32200	0.16	327	1	29400	23	190	1	0.8	28	0.01	2.5
MBS-401	322	323	base	4.54	6700	1.69	891	1	22200	236	370	185	154	15	0.15	2.5
MBS-401	323	324	base	9.19	2200	3.61	1715	2	16800	170	510	2	3.2	9	0.21	2.5
MBS-401	324	325	base	8.36	3400	3.4	1675	2	19700	114	1710	1	2	10	0.19	2.5

DH_Hole	DH_From	DH_To	Rock_Type	Sr_ppm	Ti_ppm	V_ppm	W_ppm	Zn_ppm
MBS-401	317	318	opx	70	2100	143	5	67
MBS-401	318	319	opx	114	2100	130	5	60
MBS-401	319	320	base	155	700	24	5	33
MBS-401	320	321	base	140	300	2	5	14
MBS-401	321	322	base	131	500	5	5	15
MBS-401	322	323	base	145	3700	138	5	73
MBS-401	323	324	base	120	6800	276	5	125
MBS-401	324	325	base	118	6400	245	10	145

DH_Hole	DH_From	DH_To	Rock_Type	Ag_ppm	Al_ppm	Ars_ppm	Au_ppb	Ba_ppm	Be_ppm	Bi_ppm	Ca_ppm	Cd_ppm	Co_ppm	Cr_ppm	Cu_ppm
MBS-391	148	149	gabb	0.25	67900	2.5	2	130	0.25	1	89600	0.25	61	600	152
MBS-391	149	150	gabb	0.25	61300	2.5	1	120	0.25	1	87900	0.25	63	785	156
MBS-391	150	151	gabb	0.25	61500	2.5	1	100	0.25	1	88500	0.25	64	928	211
MBS-391	151	152	gabb	0.25	63100	2.5	1	110	0.25	1	87600	0.25	65	983	183
MBS-391	152	153	gabb	0.25	63900	2.5	1	120	0.25	1	88000	0.25	63	914	163
MBS-391	153	154	gabb	0.25	60000	2.5	1	130	0.25	1	85000	0.25	63	963	214
MBS-391	154	155	gabb	0.25	65200	2.5	1	150	0.5	1	80800	0.25	58	803	262
MBS-391	155	156	gabb	0.25	56400	2.5	1	120	0.25	1	82800	0.25	79	1300	635
MBS-391	156	157	gabb	0.25	48400	2.5	2	100	0.25	1	75600	0.25	88	1590	780
MBS-391	157	158	gabb	0.25	55700	2.5	1	100	0.25	1	83400	0.25	69	1480	284
MBS-391	158	159	gabb	0.25	53600	2.5	2	140	0.25	1	70900	0.25	88	1550	643
MBS-391	159	160	gabb	0.25	55300	5	5	550	0.5	1	29900	0.25	91	1130	950
MBS-391	160	161	gabb	0.25	41000	2.5	15	190	0.5	1	32800	0.25	109	1810	1270
MBS-391	161	162	gabb	0.25	36400	2.5	18	120	0.25	1	35300	0.25	132	1990	1510
MBS-391	162	163	gabb	0.5	37300	2.5	23	90	0.25	1	36100	0.25	118	1880	1360
MBS-391	163	164	gabb	0.25	37800	2.5	12	140	0.25	1	36100	0.25	105	1860	836
MBS-391	164	165	gabb_nor	0.25	39400	2.5	8	80	0.25	1	36400	0.25	99	1890	602
MBS-391	165	166	gabb_nor	0.25	41600	2.5	5	90	0.25	1	39000	0.25	94	1910	393
MBS-391	166	167	gabb_nor	0.5	37100	2.5	7	70	0.25	1	37600	0.25	104	1770	702
MBS-391	167	168	opx	0.25	31000	2.5	7	70	0.25	1	31200	0.25	125	1720	722
MBS-391	168	169	opx	0.25	26400	2.5	9	180	0.25	1	30400	0.25	112	1980	499
MBS-391	169	170	opx	0.25	20500	2.5	2	230	0.25	1	26700	0.25	139	1580	90
MBS-391	170	171	opx	0.25	30100	2.5	6	220	0.25	1	32500	0.25	118	1850	675
MBS-391	171	172	opx	0.25	48600	2.5	6	380	0.8	1	26400	0.25	84	1590	522
MBS-391	172	173	base	0.25	75700	2.5	1	530	0.6	1	7500	0.25	0.5	19	21
MBS-391	173	174	base	0.25	76400	2.5	3	600	0.9	1	9400	0.25	2	18	37
MBS-391	174	175	base	0.25	72300	2.5	2	440	0.7	1	7500	0.25	0.5	18	7
MBS-391	192	193	base	0.25	72400	2.5	6	510	0.5	1	7900	0.25	18	21	288
MBS-391	193	194	base	1	70800	2.5	19	420	0.8	1	7500	0.25	44	25	4270
MBS-391	194	195	base	0.25	71800	2.5	8	370	0.7	1	7200	0.25	20	12	297
MBS-391	195	196	base	0.25	70100	2.5	11	340	0.7	1	7300	0.25	120	20	932

DH_Hole	DH_From	DH_To	Rock_Type	Fe_pct	K_ppm	Mg_pct	Mn_ppm	Mo_ppm	Na_ppm	Ni_ppm	P_ppm	Pd_ppb	Pt_ppb	Pb_ppm	S_pct	Sb_ppm
MBS-391	148	149	gabb	7.3	4100	7.12	1295	0.5	14500	384	270	1	0.5	4	0.15	2.5
MBS-391	149	150	gabb	7.54	3600	7.51	1350	0.5	12600	401	250	0.5	0.3	4	0.14	2.5
MBS-391	150	151	gabb	7.65	3300	7.69	1355	0.5	12700	489	210	0.5	0.3	6	0.19	2.5
MBS-391	151	152	gabb	7.52	3400	7.62	1335	1	13100	469	230	0.5	0.3	6	0.16	2.5
MBS-391	152	153	gabb	7.42	3700	7.46	1320	0.5	13500	449	240	0.5	0.3	6	0.13	2.5
MBS-391	153	154	gabb	7.59	3800	7.25	1320	0.5	12800	537	270	0.5	0.3	6	0.17	2.5
MBS-391	154	155	gabb	7.17	5400	6.23	1225	0.5	14200	553	330	0.5	0.3	10	0.2	2.5
MBS-391	155	156	gabb	7.79	3500	7.58	1295	0.5	11900	1180	230	0.5	0.3	30	0.48	2.5
MBS-391	156	157	gabb	8.12	2900	8.44	1360	1	10000	1540	200	1	0.8	12	0.53	2.5
MBS-391	157	158	gabb	7.74	2900	8.67	1390	0.5	11600	734	200	0.5	0.3	10	0.21	2.5
MBS-391	158	159	gabb	8.19	2800	9.71	1410	0.5	11200	1420	170	1	0.8	7	0.4	2.5
MBS-391	159	160	gabb	6.74	23000	8.61	1035	0.5	11700	2730	580	3	5.5	37	0.57	2.5
MBS-391	160	161	gabb	7.86	6000	11.35	1265	0.5	9600	3360	230	5	13.5	17	0.64	2.5
MBS-391	161	162	gabb	8.59	2400	12.75	1345	1	7600	4570	190	7	20.9	6	0.83	2.5
MBS-391	162	163	gabb	8.32	2400	12.7	1345	0.5	7600	3730	200	8	25.3	3	0.7	2.5
MBS-391	163	164	gabb	8.13	2300	12.6	1365	1	7300	2640	190	5	18.7	7	0.47	2.5
MBS-391	164	165	gabb_nor	7.99	2400	12.6	1360	0.5	7700	1980	200	4	19.4	4	0.36	2.5
MBS-391	165	166	gabb_nor	8.1	2500	13.15	1420	0.5	8300	1530	210	2	8.8	7	0.24	2.5
MBS-391	166	167	gabb_nor	8.22	1900	12.7	1400	1	7400	2310	150	7	11.5	6	0.42	2.5
MBS-391	167	168	opx	8.7	2400	13.65	1400	0.5	5900	3080	140	9	11.2	5	0.5	2.5
MBS-391	168	169	opx	8.93	1200	15.25	1515	1	3800	1780	120	7	3.9	6	0.24	2.5
MBS-391	169	170	opx	9.7	1300	17.85	1460	0.5	2800	1950	130	2	0.9	3	0.07	2.5
MBS-391	170	171	opx	8.67	3100	13.45	1355	0.5	5500	2650	170	4	7.8	6	0.39	2.5
MBS-391	171	172	opx	7.06	19200	9.99	1110	0.5	8500	1920	160	3	6.4	15	0.33	2.5
MBS-391	172	173	base	1.04	48500	0.18	157	0.5	21000	62	140	0.5	0.5	43	0.02	2.5
MBS-391	173	174	base	1	26700	0.17	179	0.5	32900	203	150	1	3.6	53	0.04	2.5
MBS-391	174	175	base	0.82	30800	0.09	203	0.5	29700	35	150	0.5	0.8	44	0.01	2.5
MBS-391	192	193	base	1.57	32700	0.12	322	0.5	27200	1000	160	4	7.9	43	0.27	2.5
MBS-391	193	194	base	2.14	31800	0.1	259	0.5	27500	3230	150	22	31.3	46	1.13	2.5
MBS-391	194	195	base	1.45	30900	0.08	277	0.5	29000	1250	150	7	10.4	44	0.34	2.5
MBS-391	195	196	base	3.42	26900	0.12	334	0.5	27700	8200	140	22	20.6	39	1.74	2.5

DH_Hole	DH_From	DH_To	Rock_Type	Sr_ppm	Ti_ppm	V_ppm	W_ppm	Zn_ppm
MBS-391	148	149	gabb	194	3300	194	5	76
MBS-391	149	150	gabb	167	3200	199	5	78
MBS-391	150	151	gabb	168	3000	199	5	78
MBS-391	151	152	gabb	173	3000	195	5	78
MBS-391	152	153	gabb	179	3200	195	5	79
MBS-391	153	154	gabb	168	3500	206	5	80
MBS-391	154	155	gabb	194	3800	200	5	76
MBS-391	155	156	gabb	157	3100	193	5	79
MBS-391	156	157	gabb	132	2600	189	5	81
MBS-391	157	158	gabb	153	2500	189	5	78
MBS-391	158	159	gabb	146	2100	166	5	83
MBS-391	159	160	gabb	95	1600	95	5	72
MBS-391	160	161	gabb	89	2000	124	5	84
MBS-391	161	162	gabb	92	1400	127	5	82
MBS-391	162	163	gabb	96	1300	125	5	82
MBS-391	163	164	gabb	97	1300	125	5	82
MBS-391	164	165	gabb_nor	100	1200	124	5	81
MBS-391	165	166	gabb_nor	104	1300	133	5	84
MBS-391	166	167	gabb_nor	93	1200	133	5	84
MBS-391	167	168	opx	72	1500	114	5	81
MBS-391	168	169	opx	58	1500	112	5	80
MBS-391	169	170	opx	54	1400	87	5	70
MBS-391	170	171	opx	68	1800	113	5	90
MBS-391	171	172	opx	79	3000	117	5	95
MBS-391	172	173	base	176	400	3	5	22
MBS-391	173	174	base	223	700	3	5	29
MBS-391	174	175	base	150	300	1	5	21
MBS-391	192	193	base	132	600	4	5	17
MBS-391	193	194	base	113	300	3	5	46
MBS-391	194	195	base	111	300	2	5	27
MBS-391	195	196	base	127	500	4	5	25

ANEXO 2

- Tabela de análises isotópicas $\delta^{34}S$

Amostra	Litologia	Mineral	δ34S‰ V-CDT	Profundidade (m)	Depósito
CFF-12	Dunito	pirita	-0.16	938.50	Santa-Rita
CFF-12	Dunito	pirita	-0.39	938.50	Santa-Rita
CFF-12	Dunito	pentlandita	-0.04	938.50	Santa-Rita
CFF-12	Dunito	pentlandita	0.02	938.50	Santa-Rita
CFF-16	Harzburgito	calcopirita	-0.32	910.60	Santa-Rita
CFF-16	Harzburgito	calcopirita	-0.69	910.60	Santa-Rita
CFF-16	Harzburgito	pentlandita	0.37	910.60	Santa-Rita
CFF-16	Harzburgito	pentlandita	0.25	910.60	Santa-Rita
CFF-16	Harzburgito	pirita	0.14	910.60	Santa-Rita
CFF-16	Harzburgito	pirita	0.38	910.60	Santa-Rita
CFF-20	Harzburgito	pentlandita	-0.04	881.80	Santa-Rita
CFF-20	Harzburgito	pentlandita	-0.08	881.80	Santa-Rita
CFF-20	Harzburgito	pirita	-0.46	881.80	Santa-Rita
CFF-20	Harzburgito	pentlandita	-0.06	881.80	Santa-Rita
CFF-24	Olivina Ortopiroxenito	pentlandita	0.03	852.30	Santa-Rita
CFF-24	Olivina Ortopiroxenito	pentlandita	-0.42	852.30	Santa-Rita
CFF-24	Olivina Ortopiroxenito	calcopirita	-0.30	852.30	Santa-Rita
CFF-24	Olivina Ortopiroxenito	pentlandita	0.10	852.30	Santa-Rita
CFF-27	Ortopiroxenito	pirita	0.09	829.70	Santa-Rita
CFF-27	Ortopiroxenito	pirita	-0.07	829.70	Santa-Rita
CFF-27	Ortopiroxenito	pentlandita	-0.03	829.70	Santa-Rita
CFF-27	Ortopiroxenito	pentlandita	-0.12	829.70	Santa-Rita
CFF-32	Ortopiroxenito	pirita	-0.08	806.60	Santa-Rita
CFF-32	Ortopiroxenito	pirita	-0.18	806.60	Santa-Rita
CFF-32	Ortopiroxenito	pirrotita	-0.43	806.60	Santa-Rita
CFF-32	Ortopiroxenito	pirrotita	-0.58	806.60	Santa-Rita
CFF-32	Ortopiroxenito	pirrotita	-0.59	806.60	Santa-Rita
CFF-32	Ortopiroxenito	pentlandita	-0.05	806.60	Santa-Rita
CFF-32	Ortopiroxenito	pentlandita	0.03	806.60	Santa-Rita
MBS-343_01	Granulito Máfico	pirita	0.60	47.00	Peri-Peri
MBS-343_01	Granulito Máfico	pirita	0.73	47.00	Peri-Peri
MBS-343_01	Granulito Máfico	calcopirita	-0.13	47.00	Peri-Peri
MBS-343_01	Granulito Máfico	calcopirita	0.27	47.00	Peri-Peri
MBS-343_01	Granulito Máfico	pirita	0.43	47.00	Peri-Peri
MBS-343_01	Granulito Máfico	pirita	0.37	47.00	Peri-Peri

Amostra	Litologia	Mineral	δ34S‰ V-CDT	Profundidade (m)	Depósito
MBS-343_01	Granulito Máfico	calcopirita	0.69	47.00	Peri-Peri
MBS-343_01	Granulito Máfico	calcopirita	0.58	47.00	Peri-Peri
MBS-391_01	Gnaisse	pirita	0.43	195.40	Peri-Peri
MBS-391_01	Gnaisse	pirita	0.39	195.40	Peri-Peri
MBS-391_01	Gnaisse	calcopirita	0.49	195.40	Peri-Peri
MBS-391_01	Gnaisse	calcopirita	0.76	195.40	Peri-Peri
MBS-391_01	Gnaisse	pirita	0.56	195.40	Peri-Peri
MBS-391_01	Gnaisse	pirita	0.90	195.40	Peri-Peri
MBS-391_01	Gnaisse	pentlandita	0.59	195.40	Peri-Peri
MBS-391_01	Gnaisse	pentlandita	0.31	195.40	Peri-Peri
MBS-401_03	Ortopiroxenito	pirita	0.46	314.70	Peri-Peri
MBS-401_03	Ortopiroxenito	pirita	0.54	314.70	Peri-Peri
MBS-401_03	Ortopiroxenito	pentlandita	0.58	314.70	Peri-Peri
MBS-401_03	Ortopiroxenito	pentlandita	0.49	314.70	Peri-Peri
MBS-401_03	Ortopiroxenito	pirita	0.43	314.70	Peri-Peri
MBS-401_03	Ortopiroxenito	pirita	0.58	314.70	Peri-Peri
MBS-401_03	Ortopiroxenito	pentlandita	0.91	314.70	Peri-Peri
MBS-401_03	Ortopiroxenito	pentlandita	0.43	314.70	Peri-Peri
MBS-401_04	Harzburgito	pentlandita	-0.65	308.70	Peri-Peri
MBS-401_04	Harzburgito	pentlandita	-0.37	308.70	Peri-Peri
MBS-401_04	Harzburgito	calcopirita	-1.72	308.70	Peri-Peri
MBS-401_04	Harzburgito	calcopirita	-0.63	308.70	Peri-Peri
MBS-401_04	Harzburgito	pirita	-0.92	308.70	Peri-Peri
MBS-401_04	Harzburgito	pirita	-0.48	308.70	Peri-Peri
MBS-401_04	Harzburgito	calcopirita	-0.90	308.70	Peri-Peri
MBS-401_04	Harzburgito	calcopirita	0.26	308.70	Peri-Peri
MBS-401_06	Harzburgito	pentlandita	-0.73	301.95	Peri-Peri
MBS-401_06	Harzburgito	pentlandita	-0.44	301.95	Peri-Peri
MBS-401_06	Harzburgito	pirita	0.32	301.95	Peri-Peri
MBS-401_06	Harzburgito	pirita	-1.05	301.95	Peri-Peri
MBS-401_06	Harzburgito	pirrotita	-0.66	301.95	Peri-Peri
MBS-401_06	Harzburgito	pirrotita	-0.97	301.95	Peri-Peri
MBS-401_08	Ortopiroxenito	pirita	0.40	292.90	Peri-Peri
MBS-401_08	Ortopiroxenito	pirita	-0.42	292.90	Peri-Peri
MBS-401_08	Ortopiroxenito	pirrotita	-0.34	292.90	Peri-Peri

Amostra	Litologia	Mineral	δ34S‰ V-CDT	Profundidade (m)	Depósito
MBS-401_08	Ortopiroxenito	pirrotita	-0.46	292.90	Peri-Peri
MBS-401_08	Ortopiroxenito	pentlandita	-0.20	292.90	Peri-Peri
MBS-401_08	Ortopiroxenito	pentlandita	-0.19	292.90	Peri-Peri
MBS-401_08	Ortopiroxenito	calcopirita	0.95	292.90	Peri-Peri
MBS-401_08	Ortopiroxenito	calcopirita	0.44	292.90	Peri-Peri
MBS-401_08	Ortopiroxenito	pirrotita	-0.06	292.90	Peri-Peri
MBS-401_08	Ortopiroxenito	pirrotita	-0.39	292.90	Peri-Peri
MBS-401_08	Ortopiroxenito	pentlandita	-0.15	292.90	Peri-Peri
MBS-401_08	Ortopiroxenito	pentlandita	-0.51	292.90	Peri-Peri
MBS-401_08	Ortopiroxenito	pirrotita	-0.93	292.90	Peri-Peri
MBS-401_08	Ortopiroxenito	pirrotita	-0.71	292.90	Peri-Peri
MBS-401_08	Ortopiroxenito	calcopirita	-0.23	292.90	Peri-Peri
MBS-401_08	Ortopiroxenito	pirita	0.19	292.90	Peri-Peri
MBS-401_08	Ortopiroxenito	pirita	-0.04	292.90	Peri-Peri
MBS-401_10	Ortopiroxenito	pirrotita	-1.01	285.60	Peri-Peri
MBS-401_10	Ortopiroxenito	pirrotita	-1.24	285.60	Peri-Peri
MBS-401_10	Ortopiroxenito	calcopirita	-1.03	285.60	Peri-Peri
MBS-401_10	Ortopiroxenito	calcopirita	-0.83	285.60	Peri-Peri
MBS-401_10	Ortopiroxenito	pentlandita	-0.80	285.60	Peri-Peri
MBS-401_10	Ortopiroxenito	pentlandita	-0.64	285.60	Peri-Peri
MBS-401_10	Ortopiroxenito	calcopirita	-0.34	285.60	Peri-Peri
MBS-401_10	Ortopiroxenito	calcopirita	-0.57	285.60	Peri-Peri
MBS-401_10	Ortopiroxenito	pirita	0.05	285.60	Peri-Peri
MBS-401_10	Ortopiroxenito	pentlandita	-0.18	285.60	Peri-Peri
MBS-401_10	Ortopiroxenito	pentlandita	-0.14	285.60	Peri-Peri
MIR-001_01	Grafita Gnaisse	pirrotita	1.67	322.90	Rochas Encaixantes
MIR-001_01	Grafita Gnaisse	pirrotita	1.89	322.90	Rochas Encaixantes
MIR-001_01	Grafita Gnaisse	pirita	1.99	322.90	Rochas Encaixantes
MIR-001_01	Grafita Gnaisse	pirita	2.14	322.90	Rochas Encaixantes
MIR-003_02	BIF	pirrotita	1.92	255.50	Rochas Encaixantes
MIR-003_02	BIF	pirrotita	2.33	255.50	Rochas Encaixantes
MIR-003_02	BIF	pirrotita	2.40	255.50	Rochas Encaixantes
MIR-003_02	BIF	pirrotita	2.11	255.50	Rochas Encaixantes
MIR-003_04	Bt-Hbl Gnaisse	pirrotita	2.16	185.30	Rochas Encaixantes
MIR-003_04	Bt-Hbl Gnaisse	pirrotita	2.14	185.30	Rochas Encaixantes

Amostra	Litologia	Mineral	δ34S‰ V-CDT	Profundidade (m)	Depósito
MIR-003_04	Bt-Hbl Gnaisse	pirrotita	2.53	185.30	Rochas Encaixantes
MIR-003_04	Bt-Hbl Gnaisse	pirrotita	2.40	185.30	Rochas Encaixantes

ANEXO 3

- Tabela de análises isotópicas Sm-Nd

Amostra	Litologia	Depósito	Sm (ppm)	Nd (ppm)	$^{147}Sm/^{144}Nd$	$^{143}Nd/^{144}Nd$	ε Nd (0)	T1 (Ma)	ε (T1)
CFF-20	Harzburgito	Santa Rita	0,138	0,516	0,1620	0,511953+/-82	-13,36	1990	-4,52
CFF-27	Ortopiroxenito	Santa Rita	0,202	0,763	0,1598	0,511996+/-22	-12,52	1990	-3,11
CFF-32	Ortopiroxenito	Santa Rita	0,217	0,861	0,1526	0,511856+/-14	-15,25	1990	-4,01
CFF-40	Websterito	Santa Rita	0,721	2,090	0,2086	0,512546+/-18	-1,79	1990	-4,86
CFF-41	Websterito	Santa Rita	0,700	2,181	0,1940	0,512464+/-26	-3,39	1990	-2,72
CFF-48	Gabronorito	Santa Rita	0,428	1,444	0,1793	0,512159+/-14	-9,34	1990	-4,92
CFF-61	Gabronorito	Santa Rita	0,610	2,334	0,1579	0,511782+/-11	-16,70	1990	-6,82
FM-03	Gabronorito Pegmatóide	Santa Rita	1,034	4,382	0,1426	0,511658+/-5	-19,12	1990	-5,32
FM-06	Gabronorito	Santa Rita	0,631	2,475	0,1541	0,511728+/-12	-17,75	1990	-6,90
MBS-497/01	Granada Gnaisse	Rocha Encaixante	2,406	12,801	0,1136	0,511054+/-10	-30,90	2542	-3,75
MBS-401/03	Ortopiroxenito	Peri-Peri	0,991	4,137	0,1448	0,511714+/-36	-18,02	1990	-4,79
MBS-401/06	Harzburgito	Peri-Peri	0,580	2,451	0,1431	0,511668+/-9	-18,92	1990	-5,25
MBS-401/08	Ortopiroxenito	Peri-Peri	0,425	1,730	0,1487	0,511619+/-14	-19,88	1990	-7,65
MBS-401/10	Ortopiroxenito	Peri-Peri	1,046	4,167	0,1517	0,511681+/-15	-18,67	1990	-7,21
MBS-401/17	Websterito	Peri-Peri	0,975	4,258	0,1385	0,511608+/-24	-20,09	1990	-5,25
MBS-401/20	Gabronorito	Peri-Peri	1,300	5,414	0,1451	0,511875+/-65	-14,88	1990	-1,71
MBS-401/28	Gabronorito	Peri-Peri	0,808	3,282	0,1487	0,511908+/-18	-14,24	1990	-1,98
MBP-019/01	Ortopiroxenito	Palestina	0,964	4,051	0,1438	0,511654+/-20	-19,19	2070	-5,16

ANEXO 4

- Tabelas de análises geocronológicas U/Pb em zircões

Dados LA-ICP-MS para a amostra FM-03 – Complexo Fazenda Mirabela

Sample	f(206)%	Th/U	6/4 ratio	7/6 ratio	1s(%)	7/5 ratio	1s(%)	6/8 ratio	1s(%)	Rho	7/6 age	1s(%)	7/5 age	1s(%)	6/8 age	1s(%)	Conc (%)
003 Z01	0.019554	0.130759	76483.75	0.124297	0.693078	6.593009	1.138936	0.3847	0.903602	0.774519	2018.805	12.23401	2058.413	9.992178	2098.201	16.16598	103.9328
004 Z02	0.021699	0.280698	79647.15	0.121414	0.812604	6.635761	1.22624	0.396387	0.918136	0.728318	1977.115	14.40289	2064.114	10.76317	2152.38	16.78291	108.8647
005 Z03	0.015788	0.24686	94215.21	0.11923	1.084943	6.462138	1.6379	0.393088	1.227035	0.738097	1944.713	19.39775	2040.76	14.40225	2137.135	22.31961	109.8946
006 Z04	0.047561	0.216625	31516.98	0.120635	1.533948	6.338829	2.211755	0.381095	1.592623	0.742872	1965.641	27.1075	2023.841	19.21469	2081.396	28.28098	105.8889
009 Z05	0.0245	0.294706	60676.5	0.124429	0.623499	6.757369	0.990432	0.393873	0.769359	0.748463	2020.683	11.00802	2080.158	8.7227	2140.763	14.0028	105.9425
010 Z06	0.008763	0.26525	446081.7	0.118433	0.872678	6.485678	1.24622	0.397175	0.889662	0.69052	1932.714	15.62477	2043.958	10.9635	2156.018	16.30326	111.5539
021 Z12	0.003352	0.626421	512486.2	0.326565	3.623243	7.050789	6.062024	0.156591	4.859903	0.801131	3601.034	54.51526	2117.856	52.52494	937.8036	42.27875	26.04262
023 Z14	0.051164	0.215398	30014.74	0.123335	1.209394	5.84278	1.891631	0.343583	1.454522	0.761519	2005.023	21.47101	1952.779	16.40036	1903.885	23.97761	94.95578
039 Z24	0.033288	0.222699	46081.66	0.12514	0.70672	5.956711	1.108137	0.345229	0.853247	0.747187	2030.784	12.45664	1969.545	9.589011	1911.778	14.10502	94.13986
029 Z18	0.070428	0.208639	21725.46	0.124653	1.169807	5.99963	1.955313	0.349075	1.565677	0.795312	2023.879	20.57842	1975.79	16.87646	1930.181	26.08137	95.3704
024 Z15	0.041411	0.110354	36853.36	0.120954	1.497333	5.890753	2.12935	0.353222	1.513349	0.726466	1970.351	26.45172	1959.872	18.31715	1949.966	25.42491	98.96543
034 Z21	0.052676	0.215732	33391.26	0.124925	0.887164	6.102897	1.299599	0.354312	0.949182	0.710802	2027.73	15.62577	1990.661	11.27525	1955.158	15.99651	96.42104
033 Z20	0.054749	0.292417	27735.1	0.126694	0.761687	6.307188	1.258093	0.361059	1.000766	0.780669	2052.596	13.38769	2019.453	10.96682	1987.193	17.1007	96.81364
036 Z23	0.035195	0.229199	43138.78	0.12115	1.596524	6.037562	2.285387	0.361441	1.635268	0.745301	1973.226	28.44897	1981.278	19.90806	1989.003	27.98635	100.7996
030 Z19	0.015975	0.246935	94985.91	0.119282	1.460643	5.959097	2.079189	0.36233	1.479712	0.717668	1945.496	26.1125	1969.894	18.07804	1993.208	25.36981	102.4524
027 Z16	0.086061	0.182485	17602.86	0.126658	0.820516	6.366973	1.494762	0.364585	1.248352	0.827583	2052.096	14.41744	2027.727	13.03334	2003.87	21.48342	97.64992
035 Z22	0.032222	0.1923	46970.94	0.121888	1.130319	6.157251	1.668809	0.366374	1.227722	0.724341	1984.045	20.1161	1998.402	14.5773	2012.316	21.22136	101.4249
041 Z26	0.020942	0.262883	71813.01	0.118664	1.106448	6.155567	1.672471	0.376225	1.254166	0.739345	1936.203	19.8021	1998.163	14.60873	2058.627	22.10201	106.3229
040 Z25	0.013529	0.262378	105831	0.119627	0.799701	6.228437	1.21079	0.377613	0.909115	0.729974	1950.664	14.28787	2008.451	10.59335	2065.124	16.06412	105.8678
018 Z11	0.002863	0.30442	523591.8	0.118517	1.831151	6.228043	2.472288	0.381127	1.661053	0.728242	1933.986	32.78072	2008.396	21.63017	2081.545	29.54865	107.6298
017 Z10	0.002956	0.307554	504935.8	0.123183	1.25485	6.590242	1.878149	0.388015	1.397424	0.735519	2002.839	22.28365	2058.043	16.55791	2113.614	25.18259	105.5309
022 Z13	0.005832	0.33638	284676.9	0.120436	0.772623	6.455388	1.331005	0.388744	1.083739	0.802347	1962.694	13.72059	2039.841	11.63512	2117.002	19.52775	107.862
011 Z07	0.007241	0.26898	203832.6	0.116931	1.225166	6.529605	1.701131	0.405	1.180176	0.680599	1909.838	21.99549	2049.899	14.97899	2192.02	21.93025	114.7752
015 Z08	0.010369	0.294496	142008.5	0.117908	1.141911	6.640278	1.384711	0.408452	0.78324	0.532128	1924.76	20.46448	2064.714	12.21986	2207.842	14.64239	114.7074
028 Z17	0.007805	0.222364	210484.5	0.123779	0.799734	6.975463	1.248184	0.408717	0.958325	0.749871	2011.407	14.18763	2108.311	11.08474	2209.055	17.92382	109.8263
016 Z09	0.007637	0.217159	136830.8	0.116087	1.109317	6.573725	1.527604	0.410702	1.050233	0.670555	1896.817	19.94659	2055.831	13.46303	2218.13	19.7104	116.9396

Dados LA-ICP-MS para a amostra MBS-497-01 – Rocha Encaixante ao Complexo Mirabela

Sample	f(206)%	Th/U	6/4 ratio	7/6 ratio	1s(%)	7/5 ratio	1s(%)	6/8 ratio	1s(%)	Rho	7/6 age	1s(Ma)	7/5 age	1s(Ma)	6/8 age	1s(Ma)	Conc (%)
032-Z24.dyn	0.000822	0.036439	1792596	0.123201	0.669328	6.911074	1.102382	0.406847	0.875927	0.860897	2003.088	11.88559	2100.08	9.7785	2200.49	16.3294	109.8549
028-Z20.dyn	0.001395	0.073828	1058480	0.128161	1.423344	7.134204	1.978466	0.403727	1.374197	0.859356	2072.905	25.07351	2128.322	17.61931	2186.176	25.4784	105.4644
025-Z17.dyn	0.014123	0.045699	105124.6	0.132821	0.821926	7.251494	1.183696	0.395969	0.851806	0.69414	2135.588	14.37732	2142.859	10.56246	2150.451	15.57558	100.696
035-Z25.dyn	0.346307	0.600789	4509.111	0.175566	1.945949	7.674484	4.513024	0.317036	4.071936	0.901801	2611.422	32.40058	2193.619	40.5418	1775.235	63.18727	67.97964
010-Z06.dyn	0.101364	0.17494	14917.04	0.158768	0.523283	8.052508	1.85332	0.367846	1.777911	0.958344	2442.584	8.859362	2236.931	16.7395	2019.259	30.82176	82.66896
038-Z28.dyn	0.005967	0.060707	243187.8	0.170213	1.606393	10.10019	2.427898	0.430363	1.820492	0.887609	2559.742	26.8813	2443.989	22.43156	2307.353	35.30982	90.14006
030-Z22.dyn	0.035705	0.102596	40403.94	0.169241	1.01542	10.247	2.785949	0.439126	2.594309	0.930402	2550.154	17.00795	2457.33	25.77289	2346.725	51.03052	92.02289
009-Z05.dyn	0.186366	1.340554	7683.222	0.165127	0.598708	10.24873	2.455336	0.450142	2.381223	0.969456	2508.852	10.06913	2457.486	22.71472	2395.884	47.64938	95.49719
016-Z10.dyn	1.284165	0.080655	1110.911	0.168726	0.447156	10.59862	0.874613	0.455582	0.751664	0.837655	2545.044	7.493471	2488.588	8.115004	2420.02	15.16603	95.08757
027-Z19.dyn	0.839698	0.022931	1666.649	0.165266	0.721215	11.01554	1.48824	0.483417	1.301809	0.868802	2510.259	12.12777	2524.446	13.85369	2542.132	27.34792	101.2697
026-Z18.dyn	0.024999	0.039565	55943.1	0.165123	0.541262	11.02907	0.986673	0.484429	0.82496	0.816319	2508.806	9.103035	2525.589	9.185654	2546.529	17.3549	101.5036
012-Z08.dyn	0.011211	0.0854	125196.4	0.169229	0.797757	11.18166	1.961957	0.479215	1.792445	0.95295	2550.03	13.36234	2538.388	18.28602	2523.847	37.43375	98.97325
006-Z04.dyn	0.001383	0.038847	1001875	0.16511	1.411365	11.34055	1.780376	0.498149	1.085259	0.772107	2508.674	23.73689	2551.546	16.61274	2605.837	23.26248	103.8731
020-Z14.dyn	0.003519	0.054228	396239.8	0.168436	0.577646	11.34801	1.070782	0.488635	0.901609	0.826231	2542.157	9.682979	2552.16	9.992028	2564.768	19.078	100.8894
022-Z16.dyn	0.000838	0.048742	1672530	0.171758	0.862268	11.40794	1.176322	0.481713	0.800142	0.774271	2574.851	14.40789	2557.076	10.98155	2534.722	16.76909	98.44151
029-Z21.dyn	0.001151	0.033304	1194892	0.168615	0.853395	11.82655	1.309758	0.5087	0.99357	0.741661	2543.938	14.30282	2590.768	12.26222	2651.077	21.59611	104.2115
015-Z9.dyn	0.298827	0.12676	4622.977	0.172931	0.523441	11.96733	1.172117	0.501907	1.048746	0.886686	2586.213	8.736677	2601.851	10.98367	2621.988	22.59275	101.3833
041-Z31.dyn	0.01589	1.488251	84595.1	0.162084	0.868388	12.07252	1.693527	0.540201	1.453939	0.853315	2477.522	14.65039	2610.055	15.88037	2784.289	32.87321	112.382
037-Z27.dyn	0.001403	0.037053	969370.9	0.167434	0.799687	12.10527	1.437696	0.524361	1.194767	0.821989	2532.151	13.41824	2612.595	13.48421	2717.649	26.4938	107.3257
005-Z03.dyn	0.684455	0.146431	1975.067	0.167733	0.725895	12.31109	1.720417	0.532326	1.559779	0.903515	2535.144	12.17646	2628.418	16.15647	2751.245	34.93073	108.5242
011-Z07.dyn	0.158063	0.017041	8632.137	0.172516	0.518197	12.3551	1.019602	0.519417	0.8781	0.846105	2582.2	8.65253	2631.77	9.577668	2696.709	19.35092	104.4345
042-Z32.dyn	0.000822	0.037189	1641896	0.169812	1.144313	12.52903	1.39031	0.535115	0.789625	0.699283	2555.794	19.15628	2644.908	13.07351	2762.967	17.74375	108.106
040-Z30.dyn	0.01365	0.471007	99962.27	0.181159	0.801445	12.97257	1.520979	0.519355	1.292696	0.842922	2663.51	13.2781	2677.662	14.33847	2696.444	28.48522	101.2365
018-Z12.dyn	0.003834	0.075106	352143.7	0.176964	0.769828	13.03104	1.334164	0.534064	1.08966	0.877894	2624.62	12.80162	2681.903	12.58138	2758.553	24.45451	105.1029
031-Z23.dyn	0.260079	0.065586	5172.584	0.181127	0.50003	13.4625	0.999486	0.539064	0.865415	0.850672	2663.219	8.284581	2712.656	9.446893	2779.53	19.54007	104.3673
039-Z29.dyn	0.001959	0.485718	675098.7	0.179914	0.520786	13.95802	0.987337	0.562675	0.838818	0.831723	2652.079	8.637586	2746.863	9.355026	2877.672	19.4704	108.5063
019-Z13.dyn	0.011102	0.07899	120120.6	0.190352	0.548792	14.46312	1.039409	0.551065	0.882722	0.833303	2745.208	9.023072	2780.583	9.871457	2829.599	20.21692	103.0741
017-Z11.dyn	0.19139	0.207862	6831.258	0.187539	1.02617	14.9438	1.531884	0.577922	1.137384	0.729328	2720.696	16.91033	2811.667	14.5789	2940.265	26.854	108.0703
021-Z15.dyn	0.230978	0.109276	5322.611	0.204217	0.702256	18.52851	4.722413	0.658032	4.669906	0.988873	2860.201	11.42667	3017.592	45.49517	3259.509	119.4759	113.9609
036-Z26.dyn	0.006431	0.064552	203851.9	0.236323	1.396227	18.71433	1.612708	0.574338	0.80708	0.470018	3095.372	22.26554	3027.208	15.54454	2925.607	18.98036	94.5155
003-Z01.dyn	2.888869	0.271153	599.1824	0.151637	1.05044	2.991716	1.855525	0.143091	1.529558	0.818772	2364.469	17.9275	1405.515	14.12074	862.1202	12.34289	36.46147
004-Z02.dyn	2.9627	0.172561	549.6837	0.154265	0.609875	5.279986	1.851229	0.248236	1.747885	0.942726	2393.744	10.37707	1865.632	15.8039	1429.374	22.40782	59.71291

Dados LA-ICP-MS para a amostra MBP-019-01 – Intrusão Palestina

Sample	f(206)%	Th/U	6/4 ratio	7/6 ratio	1s(%)	7/5 ratio	1s(%)	6/8 ratio	1s(%)	Rho	7/6 age	1s(%)	7/5 age	1s(%)	6/8 age	1s(%)	Conc (%)
003 Z01	0.039021	1.011901	39097.11	0.128621	0.561476	6.274183	1.076156	0.353788	0.917713	0.838666	2079.216	9.850709	2014.857	9.381453	1952.659	15.44779	93.91325
004 Z02	0.002601	0.63969	545470.9	0.203036	1.382543	6.774021	2.154245	0.241976	1.65203	0.761156	2850.76	22.33834	2082.335	18.88344	1396.96	20.71611	49.00309
005 Z03	0.00896	2.807382	168565.6	0.121954	1.061786	6.214505	1.56863	0.369581	1.154647	0.723191	1985.008	18.89432	2006.492	13.71988	2027.428	20.0858	102.137
006 Z04	0.022536	0.386302	67174.16	0.122474	1.509717	6.178885	2.153498	0.365902	1.535333	0.729765	1992.576	26.59988	2001.466	18.64805	2010.09	26.46503	100.879
009 Z05	0.117728	0.995084	13049.02	0.130939	1.026493	6.18536	2.200095	0.342607	1.943662	0.881846	2110.591	17.89616	2002.382	19.05055	1899.198	31.93166	89.98416
010 Z06	0.014514	0.542775	101053.2	0.125671	0.764441	6.393021	1.389678	0.368952	1.160533	0.825669	2038.27	13.51964	2031.311	12.20193	2024.467	20.16309	99.32278
012 PAD1	0.036046	0.384732	48868.99	0.061195	1.570358	0.942574	2.180192	0.111711	1.512353	0.723664	646.1087	33.73912	674.2284	10.74144	682.6762	9.796591	105.6597
042 PAD1	0.036161	0.394342	48495.01	0.063132	1.216426	1.043083	1.427423	0.119831	0.74689	0.706075	712.6806	25.85003	725.4506	7.399723	729.589	5.152176	102.3725
027 Z16	0.09235	0.889018	16448.59	0.128089	0.48931	6.364066	1.209443	0.360348	1.105021	0.908439	2071.907	8.595409	2027.326	10.55778	1983.824	18.85935	95.7487
018 Z11	0.02255	0.265137	67158.81	0.121724	1.512401	6.132275	2.236746	0.36538	1.647931	0.747813	1981.647	26.92347	1994.852	19.5272	2007.624	28.42812	101.3109
041 Z26	0.049104	0.668709	30836.91	0.126535	0.651904	6.37597	1.465289	0.365455	1.311641	0.890527	2050.382	11.4685	2028.966	12.7804	2007.977	22.60171	97.93183
034 Z21	0.080026	0.867704	18218.34	0.128302	0.52523	6.526941	1.307709	0.368956	1.196638	0.910756	2074.838	9.221351	2049.539	11.44936	2024.487	20.7737	97.57324
028 Z17	0.043816	0.697812	33794.71	0.128705	0.406507	6.594034	0.78547	0.371582	0.671804	0.826505	2080.36	7.13756	2058.55	6.901786	2036.838	11.72704	97.90796
035 Z22	0.065007	0.496046	23158.98	0.128102	0.800877	6.611871	1.620683	0.374341	1.408059	0.864015	2072.087	14.04211	2060.932	14.19456	2049.796	24.69236	98.92424
023 Z14	0.029645	0.843627	50758.15	0.124166	0.443185	6.42621	1.087628	0.375362	0.993239	0.905643	2016.941	7.857262	2035.859	9.556484	2054.58	17.4745	101.8662
033 Z20	0.040175	0.529895	37420.33	0.127102	0.457696	6.600307	0.838684	0.376625	0.702502	0.809395	2058.277	8.054044	2059.388	7.368593	2060.499	12.38273	100.108
021 Z12	0.050785	0.28923	29555.23	0.128636	0.526854	6.722499	1.224091	0.379023	1.104348	0.895838	2079.419	9.24498	2075.583	10.7625	2071.72	19.54703	99.62979
039 Z24	0.019484	0.269411	77014.49	0.124688	0.513649	6.526775	1.142285	0.37964	1.020284	0.884526	2024.374	9.098739	2049.517	10.05759	2074.601	18.09862	102.4811
022 Z13	0.028012	0.748365	46149.59	0.128682	0.421239	6.795912	1.134188	0.383028	1.053062	0.922976	2080.039	7.414511	2085.19	10.03912	2090.411	18.80059	100.4987
040 Z25	0.018266	0.923976	89280.99	0.130673	0.388774	6.953246	1.158321	0.385922	1.090929	0.937892	2107.032	6.806442	2105.478	10.23086	2103.889	19.55672	99.85084
016 Z09	0.013735	0.771786	94737.11	0.12177	0.784909	6.486814	1.308827	0.386358	1.047352	0.786754	1982.32	13.9717	2044.112	11.51454	2105.917	18.81593	106.235
024 Z15	0.009667	0.267826	154540.8	0.123071	0.450908	6.556116	0.724572	0.386359	0.56712	0.840574	2001.214	7.987043	2053.467	6.363531	2105.918	10.18139	105.232
015 Z08	0.009844	0.566261	151012.7	0.120986	0.510898	6.573286	1.016276	0.394046	0.878522	0.849642	1970.811	9.106425	2055.772	8.956532	2141.567	16.00814	108.6643
036 Z23	0.022658	0.623449	65458.31	0.1264	0.643335	6.927545	1.086055	0.397495	0.875006	0.899159	2048.492	11.36449	2102.192	9.636565	2157.494	16.04392	105.3211
011 Z07	0.012053	0.363736	122637.2	0.123182	1.063355	6.838221	1.722847	0.402621	1.355536	0.778645	2002.813	18.88313	2090.686	15.26168	2181.095	25.08333	108.9016
030 Z19	0.011363	0.329552	130072.4	0.127151	0.585874	7.062106	1.058314	0.402822	0.881351	0.912147	2058.952	10.3371	2119.282	9.413043	2182.021	16.31465	105.9773
017 Z10	0.009653	4.197825	152488.4	0.122944	1.084488	6.931837	1.731968	0.408922	1.350408	0.771303	1999.381	19.26608	2102.741	15.36896	2209.991	25.266	110.5337
029 Z18	0.005046	2.340984	290925	0.129427	0.326128	7.373089	0.622841	0.413166	0.530606	0.797373	2090.193	5.722638	2157.712	5.553702	2229.382	9.993265	106.6591